

2020 • 2021

Faculteit Industriële Ingenieurswetenschappen  
master in de industriële wetenschappen: energie

## Masterthesis

A materials and methods study for the fabrication process of thermal actuator microelectromechanical systems

PROMOTOR :

Prof. dr. ir. Wim DEFERME

COPROMOTOR :

De heer Dieter REENAERS

**Bjarne Nilis**

Scriptie ingediend tot het behalen van de graad van master in de industriële wetenschappen: energie,  
afstudeerrichting elektrotechniek

Gezamenlijke opleiding UHasselt en KU Leuven



**KU LEUVEN**



**KU LEUVEN**

2020 • 2021

Faculteit Industriële Ingenieurswetenschappen  
master in de industriële wetenschappen: energie

## Masterthesis

A materials and methods study for the fabrication process of thermal actuator microelectromechanical systems

PROMOTOR :

Prof. dr. ir. Wim DEFERME

COPROMOTOR :

De heer Dieter REENAERS

**Bjarne Nilis**

Scriptie ingediend tot het behalen van de graad van master in de industriële wetenschappen: energie,  
afstudeerrichting elektrotechniek



**KU LEUVEN**



## Preface

Firstly, I would like to express my gratitude to prof. dr. ir. Wim Deferme for his expertise, fast responses, and his detailed feedback to my questions, ing. Dieter Reenaers for his expertise and assistance in getting the knowhow of the different machines and tools used during the writing of this thesis. Henkel Belgium has also been very informative and generous, thank you.

I would also like to thank everybody working at the IMO-IMOMEC for strictly following the COVID-19 guidelines that were in effect at the time. This allowed everybody, including me, to work on site and obtain the necessary results in the lab to bring this thesis to a good conclusion.

Lastly, I am thanking my family, friends, and girlfriend for supporting me for the past 4 years.



# Table of Contents

|   |           |
|---|-----------|
| Preface .....   | 1         |
| List of figures .....   | 7         |
| List of tables .....  | 9         |
| Abstract .....  | 11        |
| Abstract in het Nederlands .....  | 13        |
| <br>  |           |
| <b>1. Introduction .....</b>  | <b>15</b> |
| 1.1. Situation .....  | 15        |
| 1.2. The problem .....  | 15        |
| 1.3. Reference design .....   | 16        |
| 1.4. Goals .....  | 17        |
| 1.5. Content .....  | 17        |
| <br>  |           |
| <b>2. Literature .....</b>  | <b>19</b> |
| 2.1. MEMS and production techniques .....   | 19        |
| 2.2. Printing MEMS .....  | 21        |
| 2.3. Influence of the screen properties .....                                     | 22        |
| 2.4. Influence of the rheological ink properties .....                            | 23        |
| 2.5. Printing multiple stacked layers .....                                       | 30        |
| 2.6. Printed cantilevers .....  | 31        |
| 2.7. Sacrificial layers and the interaction between the structural material ..... | 31        |
| 2.7.1. Polystyrene sulfonate: polystyrene sulfonic acid (PEDOT:PSS) .....         | 31        |
| 2.7.2. Polymethyl methacrylate (PMMA) .....                                       | 32        |
| 2.7.3. Polyethylene glycol (PEO) .....  | 32        |
| 2.7.4. Polyvinylalcohol (PVA) .....   | 33        |
| 2.7.5. Strontium carbonate (SrCO <sub>3</sub> ) .....                             | 33        |
| 2.7.6. Overview of sacrificial materials .....                                    | 33        |
| 2.8. Characterization and properties of MEMS .....                                | 34        |
| 2.8.1. Dimensions .....   | 34        |
| 2.8.2. Electrical .....   | 34        |

|           |  |           |
|-----------|--|-----------|
| 2.8.3.    | Mechanical.....                                    | 35        |
| 2.8.4.    | Displacement .....                                 | 36        |
| 2.8.5.    | Thermal conductivity.....                          | 36        |
| 2.8.6.    | Thermal expansion.....                             | 37        |
| 2.8.7.    | Thermoelectrical .....                             | 37        |
| 2.9.      | Conclusions from literature .....                  | 38        |
| 2.9.1.    | Structural material.....                           | 38        |
| 2.9.2.    | Sacrificial material.....                          | 38        |
| 2.9.3.    | Characterisation .....                             | 38        |
| <b>3.</b> | <b>Method.....</b>                                 | <b>39</b> |
| 3.1.      | Substrate.....                                     | 39        |
| 3.1.1.    | Glass .....  | 39        |
| 3.2.      | Sacrificial layer .....                            | 39        |
| 3.2.1.    | PEO .....  | 39        |
| 3.2.2.    | PVA.....   | 40        |
| 3.2.3.    | PMMA.....  | 40        |
| 3.3.      | Structural layer .....                             | 40        |
| 3.3.1.    | PVA as a substrate .....                           | 43        |
| 3.3.2.    | PEO as a substrate .....                           | 43        |
| 3.4.      | Freestanding beam .....                            | 43        |
| 3.4.1.    | Printing .....                                     | 43        |
| 3.4.2.    | Removal of the sacrificial layer .....             | 43        |
| 3.4.3.    | Beam characteristics.....                          | 43        |
| 3.5.      | Printed MEMS.....                                  | 43        |
| 3.5.1.    | Printing.....                                      | 43        |
| 3.5.2.    | Characterisation .....                             | 44        |
| <b>4.</b> | <b>Results &amp; discussion.....</b>               | <b>45</b> |
| 4.1.      | Sacrificial layer .....                            | 45        |
| 4.1.1.    | PEO .....  | 45        |
| 4.1.2.    | PVA.....   | 45        |
| 4.1.3.    | PMMA.....  | 49        |
| 4.1.4.    | Overview of results of the sacrificial layer ..... | 50        |

|           |  |           |
|-----------|--|-----------|
| 4.2.      | Structural layer .....                                   | 50        |
| 4.2.1.    | PVA.....   | 56        |
| 4.2.2.    | Overview of results of the structural layer .....        | 57        |
| 4.3.      | Freestanding beam .....                                  | 57        |
| 4.3.1.    | Printing .....   | 57        |
| 4.3.2.    | Removal of the sacrificial layer .....                   | 58        |
| 4.3.3.    | Beam characteristics.....                                | 59        |
| 4.3.4.    | Discussion of the results of the freestanding beam ..... | 61        |
| 4.4.      | Printed MEMS.....  | 62        |
| 4.4.1.    | Printing.....  | 62        |
| 4.4.2.    | Characterisation .....                                   | 62        |
| <b>5.</b> | <b>Conclusion .....</b>                                  | <b>65</b> |
| <b>6.</b> | <b>Recommendations.....</b>                              | <b>67</b> |
| 6.1.      | Recommendations for future research .....                | 67        |
| 6.2.      | Recommendations for industrialisation .....              | 68        |
|           | References.....  | 69        |
|           | Appendices .....   | 75        |





# List of figures

|   |    |
|---|----|
| Figure 1: Reference design of a thermal actuator MEMS.....  | 16 |
| Figure 2: Components of a photolithography system .....   | 19 |
| Figure 3: Photolithography process.....   | 20 |
| Figure 4: Visualisation of blade coating .....  | 21 |
| Figure 5: An example of a screen printed MEMS with sacrificial layer .....  | 21 |
| Figure 6: A visualisation of shear.....   | 24 |
| Figure 7: Relation of viscosity and shear of a typical shear-thinning ink, as shear rises the viscosity decreases, allowing the ink to pass through the screen mesh.....  | 24 |
| Figure 8: Relation between viscosity and wt% of the ink, higher solid contents lead to higher viscosity .....   | 25 |
| Figure 9: Effect of mesh count (TPC) on the thickness of the deposited layer. Higher mesh counts cause thinner layer deposition as does lower solid contents in the ink .....   | 25 |
| Figure 10: Results of thin line printing. Larger screen openings lead to less ink spread.....   | 27 |
| Figure 11: Viscosity in function of shear rate of the four inks. All inks show shear thinning properties which is desired for screen printing .....   | 28 |
| Figure 12: Recovery rates of the inks .....   | 29 |
| Figure 13: Widths and heights of the printed grids and their corresponding inks .....   | 29 |
| Figure 14: Young's modulus in function of the sintering temperature for nanoparticle ink. Young's modulus rises with sintering temperature .....  | 30 |
| Figure 15: Viscosity of PEO gels at 25 °C (PEO 10, PEO 15 and PEO 20 with respectively 1, 1,5 and 2 g PEO in 10ml of distilled water). PEO inks show shear thinning properties which are desirable for screen printing..... | 33 |
| Figure 16: Relation between temperature and conductivity. As temperature rises so does conductivity, this is caused by further sintering of the nanoparticles .....   | 34 |
| Figure 17: Relation between Tensile strength of silver and Temperature. The yield strength gradually decreases as the temperature rises until it reaches 0 at its melting point .....                                       | 36 |
| Figure 18: Visualisation of the thermal network in a porous material.....   | 36 |
| Figure 19: Stirring setup (left) and screen printer (right) .....   | 40 |
| Figure 20: DektakXT profilometer (left) and van der Pauw measurement (right).....   | 41 |
| Figure 21: Design of screen for printing Beams/lines 165 TPC 31 $\mu\text{m}$ (units in mm) (left) and actual screen (right) .....  | 41 |
| Figure 22: Simplified model of the reference design in Inventor. Distance between the two dotted lines is the deflection (units in mm).....   | 42 |
| Figure 23: Printing process of the sample for layer interaction (ECI1011, 165 TPC mesh, wire diameter of 31 $\mu\text{m}$ , squeegee pressure 2 bar, stroke speed 100 mm/s) .....   | 42 |
| Figure 24: Screen design for MEMS designs (units in mm) .....   | 44 |
| Figure 25: Needle of profilometer pushed into PEO layer. The PEO layer cured at 150 °C was proven to be soft and not usable in the printing process .....   | 45 |
| Figure 26: Viscosity of the PVA inks. The PVA 25 wt% ink shows shear thinning properties which is ideal for screen printing .....   | 46 |

|   |    |
|---|----|
| Figure 27: SEM-image of the surface after reducing the roughness at 200 °C of a screen printed sample PVA 25 wt% foil ink. The mesh is imprinted in the sample.....   | 47 |
| Figure 28: PVA 25 wt% foil sample after treatment at 200 °C. It has been discoloured and its solubility in water is affected.....   | 47 |
| Figure 29: PVA 25 wt% foil ink sample of 3, 5 and 9 layers (from top to bottom). The sample of 9 layers stuck to the screen and came loose from the substrate, making it difficult to print a high number of layers.....                                | 47 |
| Figure 30: Profile of PVA foil 25 wt% sample shows that it has detached from the surface when cut by a scalpel.....   | 48 |
| Figure 31: Profile of PVA foil 25 wt% sample after oven treatment shows that the layer affixes itself back onto the substrate after 10 min. at 150 °C in the oven.....  | 48 |
| Figure 32: Rough surface of blade coated samples from PVA web 17 wt% ink, unusable as a substrate.....  | 48 |
| Figure 33: Slump of the inks increases with number of layers printed and smaller screen opening.....  | 51 |
| Figure 34: Slump decreases as line width and screen opening increases.....  | 51 |
| Figure 35: Printed line with 40 µm mesh opening (ECI1011) was not continuous.....   | 52 |
| Figure 36: Temperature of beams in increases with current, however the properties of the beams change as a second measurement reveals lower stable temperatures.....  | 54 |
| Figure 37: FLIR image of ECI1011 beam when a current of 1,5 A is applied suggests heat generates from adhesion applied on the beams.....  | 54 |
| Figure 38: SEM images of the inks before and after a current was applied show that the ECI1011 nanoparticle ink has sintered further. The ME602 microflake ink seems denser due to solvent vaporising.....  | 55 |
| Figure 39: Interface between layer 4, 3 and 2 in the cross-section of sample (ECI1011) at which was prepared at different curing temperatures.....  | 55 |
| Figure 40: Cross-section of silver printed on top of screen printed PVA foil 25 wt% (17.03.A) shows that it causes the silver to form cracks.....   | 56 |
| Figure 41: Comparison of the profiles of a blade coated and screen printed sample. It can clearly be seen that the blade coated sample is favoured as a substrate due to low roughness.....   | 56 |
| Figure 42: Releasing a sample of ME602 in a sonication bath causes curling of the beam.....   | 58 |
| Figure 43: The release of a sample of ME602 in hot water with no deforming of the beam.....   | 58 |
| Figure 44: Bending of beam due to residual stress. The forming of the silver layer at high temperature in the oven causes stress to build up. This stress is released in the form of curling when the print is released from the sacrificial layer..... | 59 |
| Figure 45: The Young's modulus has no direct correlation to beam width for Dupont ME602.....  | 60 |
| Figure 46: The Young's modulus of the printed beams for Dupont ME602 decreases with higher number of layers.....  | 60 |
| Figure 47: Simulated deflection in function of beam length (200 µm width, 100 µm thickness). Both inks can print long enough freestanding structures in comparison to the reference design ..   | 61 |
| Figure 48: Printed mems (left) and heat generation at 4 A (right). The heat generation primarily takes place in the hot arm.....  | 62 |
| Figure 49: Applying a current to the MEMS for the first time will greatly deform it. Afterwards, applying current will lead to a deflection.....  | 63 |
| Figure 50: Flowchart of the automated printing process.....   | 68 |

## List of tables

|   |    |
|---|----|
| Table 1: Dimensions of the reference design .....   | 16 |
| Table 2: Goals for the printed MEMS in comparison to the reference design.....  | 17 |
| Table 3: Selected inks for thin line printing test .....  | 26 |
| Table 4: Change of viscosity after the printing process. Due to solvent evaporating when the ink is exposed to air, the viscosity of the ink rises.....   | 26 |
| Table 5: Properties of four silver pastes .....   | 27 |
| Table 6: Parameters of the screen printer .....   | 27 |
| Table 7: Recovery rate and viscosity of the four different inks corresponding to different shear rates at steps in the printing process .....   | 28 |
| Table 8: Creep compliance $J_c$ , recovery compliance $J_r$ and recovery ratio for the four kinds of pastes.....  | 28 |
| Table 9: Parameters of the substrate that affect slump .....  | 29 |
| Table 10: Cantilever dimensions and properties .....  | 31 |
| Table 11: Properties of the PEDOT ink .....   | 32 |
| Table 12: Overview of the sacrificial materials .....   | 33 |
| Table 13: Measurements of screen printed samples with PVA 25 wt% foil ink. The roughness of these samples is too high. Three measurements with confidence interval of 95% .....   | 46 |
| Table 14: Measurements after treatment to lower the roughness of screen printed samples of PVA 25 wt% foil ink. The treatment at 180 °C has lowered the roughness. However, it seems that the layer thickness was also greatly affected. Three measurements with confidence interval of 95% . | 46 |
| Table 15: Measurements of blade-coated PVA foil 25 wt% samples show very low roughness. Three measurements with confidence interval of 95% .....  | 47 |
| Table 16: ASH and roughness of 27 000 mw PVA 20 wt% blade coated samples with low roughness. Three measurements with confidence interval of 95%.....  | 49 |
| Table 17: Sheet resistance decrease was associated with higher curing temperatures. Eight measurements with confidence interval of 95% .....  | 52 |
| Table 18: In-plane thermal conductivity saw an increase as curing temperature increases .....   | 52 |
| Table 19: Simulated deflection of the MEMS rises with temperature.....  | 53 |



## Abstract

The conventional production process of MEMS, silicon micromachining, is expensive and lengthy. Printing and coating techniques such as screen printing, inkjet printing, and blade coating could be a solution to this problem, reducing costs and turnover time.

In this study, the materials and production process for a thermal actuator MEMS is selected and tested. The structure of the print is as follows: the substrate, the sacrificial layer, and the structural layer. After depositing this layer, the sacrificial material is dissolved and removed to achieve a freestanding structure. PVA, PMMA, and PEO are tested for their usability in the process as a sacrificial material. The main criterium for the sacrificial layer is that it can be dissolved after the production process with no negative impact on the MEMS. For the structural material, a silver nanoparticle and microflake ink are tested.

PVA was selected as a sacrificial material because of its dissolving under 15 min. in water of 85 °C. It was applied using blade coating. For the structural material, screen printing was found most suitable. Both inks are strong enough to support a freestanding actuator up to 9 mm long, however, the nanoparticle ink was brittle and broke down easily. In thermoelectric testing, temperatures >170 °C were achieved for both inks which translates to simulated deflections of up to 224 µm. A proof of concept achieved deflections of 100 µm, however, further optimisation of the process and design is needed due to deformations that occur in the structure.



## Abstract in het Nederlands

Het conventionele productieproces van MEMS, silicium-micromachining, is duur en neemt veel tijd in beslag. Print- en coatingtechnieken zoals zeefdruk, inkjetprinten en bladecoating zouden een oplossing kunnen zijn, door hun lagere kost en doorlooptijd.

In deze studie zullen de materialen en het productieproces voor een thermische actuator MEMS worden geselecteerd en getest. De structuur van de print is als volgt: het substraat, de sacrificiële laag en de structurele laag. Na het afzetten van deze laag wordt het sacrificieel materiaal opgelost. PVA, PMMA en PEO worden getest op hun bruikbaarheid als sacrificieel materiaal. Het belangrijkste criterium voor deze laag is dat deze na het productieproces kan worden opgelost zonder negatieve gevolgen voor de MEMS. Voor het structurele materiaal zijn een zilver nanopartikel en microflake inkt getest.

PVA werd gekozen als sacrificieel materiaal omdat het binnen 15 min. oplost in heet (85 °C) water. Het werd aangebracht met behulp van bladecoating. Voor de structurele laag was zeefdrukken de beste optie. Beide inkten waren sterk genoeg om een vrijstaande actuator van 9 mm lang te printen, de nanodeeltjes-inkt was echter bros en ging gemakkelijk kapot. Bij thermoelektrische testen werden voor beide inkten temperaturen boven 170 °C behaald, wat zich vertaalt in gesimuleerde verplaatsingen tot 224 µm. Een proof of concept behaalde verplaatsingen tot 100 µm. Verdere optimalisatie van het proces en design is vereist omdat de MEMS vervormd tijdens productie en gebruik.





# 1. Introduction

The Institute for Materials Research (IMO) located in Diepenbeek, Belgium is a research institution of Hasselt University. At IMO, research is done to develop and characterise new material systems for the use in printable electronics, bioelectronics etc. This thesis is done under the Functional Material Engineering (FME) group. Within this group, research is being conducted regarding the printability/coating of functional materials.

## 1.1. Situation

Microelectromechanical Systems (MEMS) are miniaturised structures with dimensions ranging from below one micron to several millimetres. These structures can be complex with moving parts and controlled by microelectronics or they can be simple nonmoving objects, here the movement is realised by thermal expansion. The main criterium for a structure to be characterised as a MEMS is that it has at least one element that has some sort of mechanical functionality [1].

Researchers have found that many MEMS sensors and actuators sometimes even outperform macroscale counterparts made using precise machining techniques. On top of this, the available production methods allow to produce the MEMS at a low per-device cost [2]. Unsurprisingly then, the last couple of years have seen a surge in the application of MEMS. Their size and versatility make them perfect for numerous applications in the automotive industry, for medical uses and for smartphones (e.g. gyroscopes) [1].

Today the majority of MEMS are made using normal bulk and surface micromachining technologies [3], [4]. Bulk micromachining means that material is etched away directly into the wafer. This is done by applying a mask to cover up the areas that need to stay intact. Materials used for this are silicon and quartz, which are readily available. Since it is a technology that is compatible with integrated circuits (IC) it is easy to include electronics. Surface micromachining, on the other hand makes use of thin films that are deposited to form the desired structure. After depositing a layer, some parts are selectively removed before depositing a new layer. As this process is also used in IC, it is easy to integrate electronics [5].

Other manufacturing options are thermal oxidation [6], high-aspect-ratio silicon micromachining [7] and screen/inkjet printing. For this master's thesis we will focus on screen/inkjet printing as it could be a great alternative for micromachining techniques.

## 1.2. The problem

The normal bulk and surface micromachining technologies are the standard when it comes to producing MEMS. A major disadvantage of these technologies, however, is the high cost. The infrastructure needed like state-of-the-art clean rooms, is expensive, whereas screen printing techniques are much more affordable. For instance, the cost including production of 6000 units and a 10% overhead per year for infrastructure, for screen printing will be 115.000€ whilst silicon micromachining would cost 1.755.000€ [8].

Another disadvantage is the turnaround time for development due to the slow production process of micromachining. The maximum rate at which material can be removed is 4,1  $\mu\text{m}/\text{min}$ . whereas with screen printing layers of up to 20  $\mu\text{m}$  can be printed within seconds [9]. Since printing is less expensive and more accessible it could be a solution to realise cheaper and faster MEMS production.

For screen printing and inkjet printing it is of great importance that the materials used in the MEMS are compatible with each other. This means that the agent used to remove the sacrificial layer does not react with the structural layer, that the treatments needed for the layers do not damage the other layer and that the layers do not dissolve into each other. This thesis will focus on the characteristics and interactions of different materials.

1.3.Reference design

The Centre for Nano Materials and MEMS of the Nitte Meenakshi institute of Technology has provided a reference design of a MEMS to work towards to. They have done extensive simulations of the device (See appendix A). See Figure 1 for a visualisation of the design. The simulated model is made from silver. It consists of five different components. The anchors are the contact pads where the current is applied. The flexure is the part that allows the device to flex. The cold arm is meant to stay cool during the process whilst the hot arm will heat up and due to thermal expansion create a force that will result in a displacement. Lastly the connector serves as a bridge between the hot and cold arm. In Table 1 the dimensions of the parts are shown.

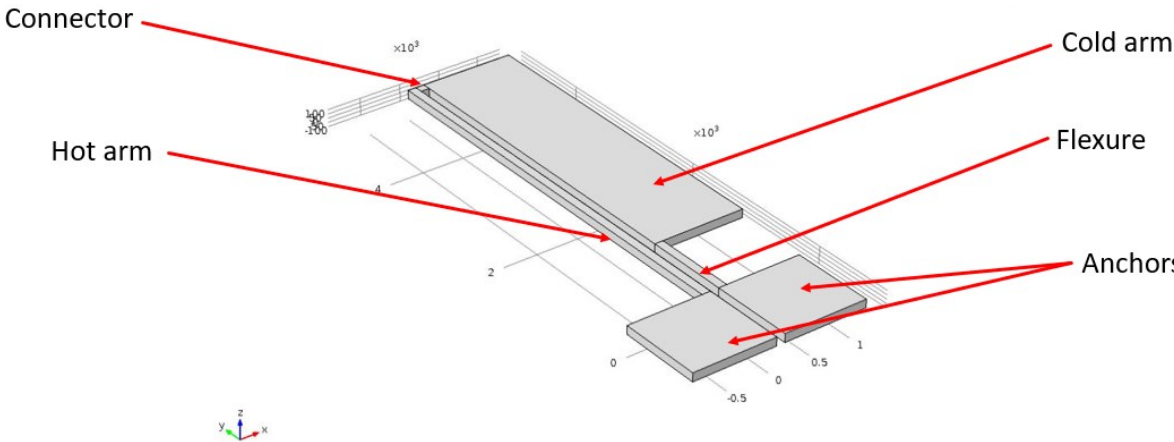


Figure 1: Reference design of a thermal actuator MEMS

Table 1: Dimensions of the reference design

| Components | Dimension (width*depth*height) $\mu\text{m}$ |
|------------|--|
| Anchor     | 1000*1000*100                                |
| Flexure    | 100*1000*100                                 |
| Cold arm   | 1100*4000*100                                |
| Hot arm    | 100*5000*100                                 |
| Connector  | 100*200*100                                  |

## 1.4.Goals

In this master thesis it will be researched which materials can be applied in the fabrication process of printed thermal actuator MEMS and what the possible dimensions are, combinations of materials and curing/sintering treatments to change the structure of the materials. In addition, a MEMS will be made using the process that was developed as a proof of concept.

In order to achieve this goal, an appropriate substrate needs to be selected. The substrate supports the first layer in the stacking process, so it needs to be flat (submicron surface roughness) and rigid to act as a good base. The sacrificial layer also plays a big role in the production process. It needs to be compatible with the structural layer whilst still being easily soluble in water. Curing is also an important factor that needs to be optimised, the structural layer needs to be cured without affecting the sacrificial layer. Lastly the ratios between thickness, length and width are going to be compared in order to find an optimum fitting to the envisioned design.

The main goal of this master's thesis is to optimise the production process of printed MEMS, using this process a printed thermal actuator MEMS will be made which is compared to the reference design. Table 2 shows the goals wished to be achieved.

*Table 2: Goals for the printed MEMS in comparison to the reference design*

| Parameter             | Goal compared to reference design |
|-----------------------|-----------------------------------|
| Actuating range       | 495 $\mu\text{m}\pm 5\%$          |
| Dimensions            | $\pm 10\%$                        |
| Voltage               | 0,6 V $\pm 20\%$                  |
| Operating temperature | <900 °C                           |

## 1.5.Content

In chapter 2: Literature we will take a deeper look at the theory behind printing techniques and the underlying principles. Chapter 3: Method will describe the process of the experiments. The results and discussion of the experiments are narrated in chapter 4: Results and discussion. The last two chapters: Conclusions and Recommendations to future research will conclude this thesis and will touch upon possible experiments to follow up on this research.



## 2. Literature

The purpose of this chapter is to look at the available information about printed MEMS. In 2.1. MEMS and production techniques, the most commonly used techniques are explained. In 2.2. Printing MEMS, printing is explored and the parameters of the process are discussed in further detail in the following two paragraphs. In chapter 2.5. the effect of printing layers on top of each other is analysed. The next paragraph talks about the cantilever structure. This brings us to the use of a sacrificial layer which is described in chapter 2.7. In the last paragraph of this chapter the properties of MEMS themselves and their relation to the process are studied.

### 2.1. MEMS and production techniques

There are multiple production techniques used to produce MEMS, amongst these techniques is photolithography, also known for its use in the production of integrated circuits (IC). Compared to the other production techniques, photolithography is one of the most developed methods for production of MEMS [10]. Photolithography systems contain the following components: a light source, an optical projection system, a mask, and a substrate which is coated with photoresist, as shown in Figure 2.

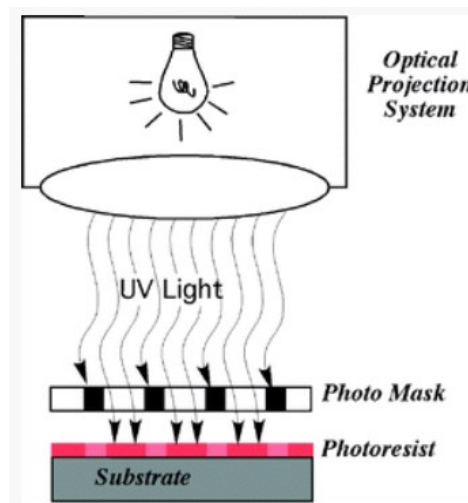


Figure 2: Components of a photolithography system [10, p. 668]

The process can be described in five steps as shown in Figure 3. The first step is to cover the substrate in a layer of photoresist. Secondly the optical projection system exposes the photoresist to UV light for a short amount of time, the photomask will block the light to certain areas. The photoresist that was exposed to UV will then cure, forming the desired pattern in the photoresist. The pattern is then used to either add or remove material by deposition or etching respectively. Lastly the cured photoresist is removed. Theoretically features of up to 20 nm are possible, however, features of 50 nm (see x-ray lithography) are achievable in reality. Contrary to IC fabrication, the requirements of MEMS demand for the ability to print multiple materials like polymers or elastomers to create, for example stretchable channels, or a layer that is removable after the process to make complex freestanding structures [10].

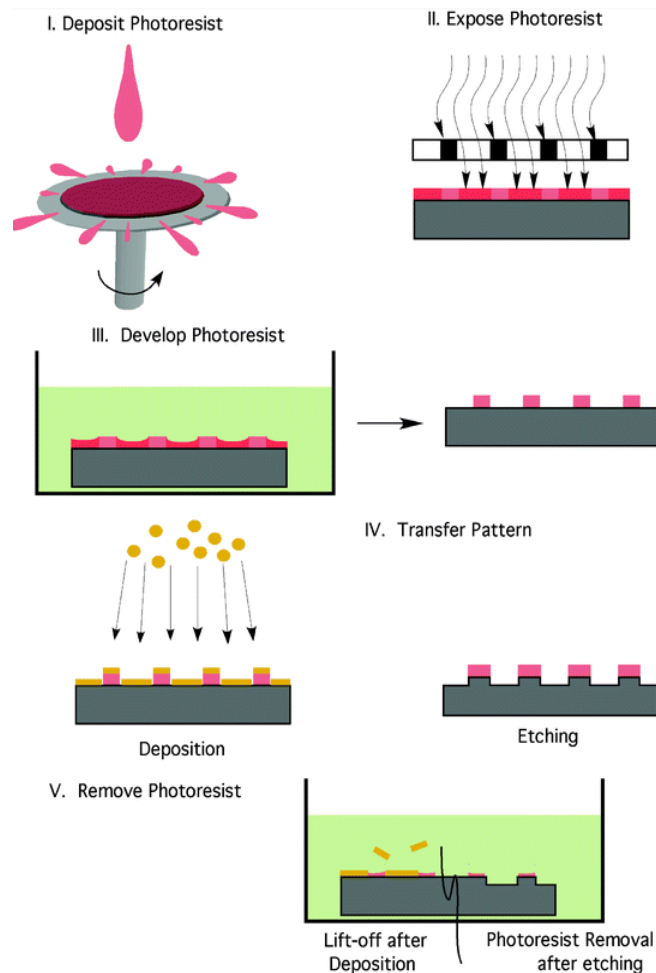


Figure 3: Photolithography process [10, p. 671]

Due to the fast-evolving needs of the IC and MEMS industry, many other variations of photolithography have been developed to comply with the growing needs. Grayscale lithography is one of these alterations, with this method the photomask is modified with pixels varying in size so that the transparent part of the mask can partially block the light. This allows us to cure the photoresist at different depths making 3D structures possible [10].

In order to achieve smaller features X-ray lithography makes use of the smaller wavelengths (up to 0,7 nm) to realise smaller geometries, allowing feature widths of 50 nm. One of the challenges in this method is to make masks that can guarantee the feature width of 50 nm. Because of the 1:1 transfer of the mask the accuracy of the production process is of great importance [10].

Other techniques to produce MEMS are: physical vapour deposition, Electrochemical deposition LIGA and printing [11]. Another technique that will be looked into in this thesis is blade coating. By definition coating is the displacement of gas at a solid interface by a liquid layer. The blade coating technique uses a blade that floats a predetermined distance above the surface. This creates a narrow gap. Ink is placed in front of the blade, the blade is then moved across the substrate forcing the liquid through the moving gap. Theoretically this leaves a layer behind with the same thickness as the gap between the blade and the substrate called the wet layer, reality shows that the wet layer is only 60-70% the thickness of the gap height. This is due to surface tension of the ink and other rheological properties, another factor is the speed of the blade during the process [12]. In the lab a doctor blade was used (See Figure 4). The final layer thickness is directly proportional to the wet layer thickness and the vol% of material dissolved in the solvent [12]. In order to deposit thicker dry layers higher vol% is needed.

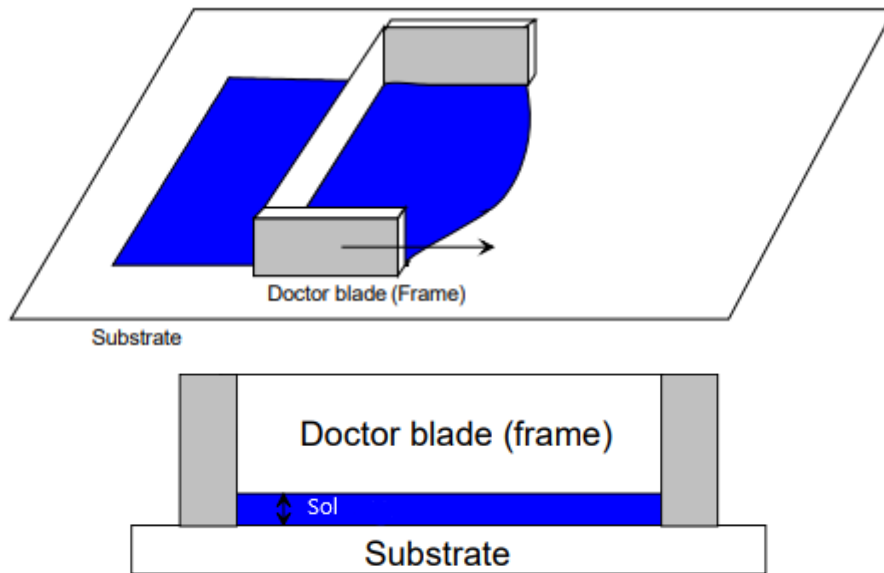


Figure 4: Visualisation of blade coating [12, p. 90]

## 2.2. Printing MEMS

The method to deposit the structural material of the MEMS that will be used in this thesis is screen printing. The screen printing process can be described using Figure 5. The layer upon which the MEMS is built, i.e. the substrate, is placed inside the screen printer. A first layer is printed using a mesh, over which the ink is rolled out. Certain areas in this mesh are covered, leaving the desired pattern behind. This is repeated several times using different materials. In order to make freestanding structures a sacrificial layer is needed, which is removed after the printing process allowing us to make more complex structures [13].

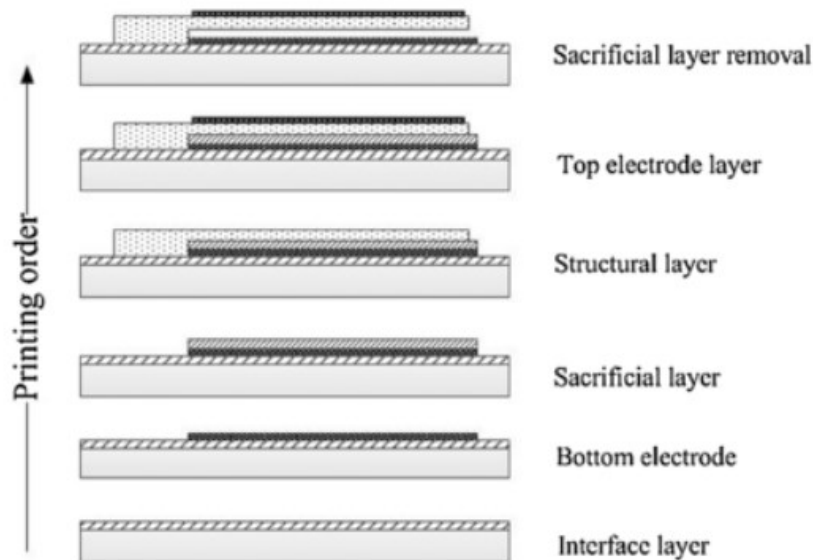


Figure 5: An example of a screen printed MEMS with sacrificial layer [13, p. 80]



Inkjet printing a MEMS is done similarly to the abovementioned screen printing. Instead of using a mesh to spread the ink, an inkjet head is used to deposit ink at the desired locations. The feature width of inkjet printing is 50–80  $\mu\text{m}$ , compared to 20  $\mu\text{m}$  for screen printing. The thickness of the deposited layer when inkjet printing is used is noticeably smaller than with screen printing. With screen printing the thickness can range from to 6-20  $\mu\text{m}$  [14], [15]. For this master’s thesis, screen printing is more feasible because of the desired printing thickness, which would take a lot more passes with an inkjet printer to achieve the same thickness than with the screen printing process.

In screen printing there are close to 50 variables that influence the printing process. Parameters regarding the printing system itself such as the printing speed, the angle of the squeegee and its geometry, distance between the screen and the substrate, material of the mesh, thread thickness and mesh count all have an impact on the printed sample [16]. The ink itself also has a great impact on the printed product. Rheological properties such as viscosity, thixotropy, viscoelasticity and creep-recovery have an effect on the final structure deposited onto the substrate [17]. For this thesis, the following relevant properties are discussed: screen properties, rheological ink properties, stacking of multiple layers and properties of freestanding cantilevers.

### 2.3. Influence of the screen properties

Screen printing relies on the process of a mesh that is loaded with an ink. The mesh will lower onto a substrate and a squeegee will wipe over the screen leaving the desired pattern behind. That is the basic principle of screen printing. As stated in the paragraph above this technique was chosen because of a thicker layer thickness. The layer thickness of a print is dependent on several parameters, it is obvious that the amount of ink left on the substrate is directly linked to the layer thickness [18].

It is possible to make a function of the deposited layer thickness in relation to the mesh and ink parameters. [18] states that the theoretical ink volume, which is the volume of ink that sits in the mesh before anything is printed can be described by the following formula:

$$TIV = 2D_{compressed} - \pi \frac{D^2 TPM_{stretched} \sqrt{1 + TPM_{stretched}^2 D_{compressed}^2}}{2} \quad (1)$$

With  $D_{compressed}$  the diameter of the mesh thread on the knuckles of the mesh (height of the mesh),  $D$  the normal diameter of the thread,  $TPM$  threads per micron (often written as TPI, threads per inch or TPC, threads per centimetre i.e., mesh count). Note that if a stencil is used to add thickness to the layer an extra 1  $\mu\text{m}$  of stencil will add 1  $\mu\text{m}$  of ink deposit, because the mesh is not involved here [18].

Of the ink that sits in the mesh roughly 70% gets deposited onto the substrate. Knowing this, the only thing left is to use the vol% of the solvent that will evaporate and use that to calculate the amount of material that is left [18].

Formula (1) states that higher mesh counts (greater TPM) will allow less ink to pass through the screen because of smaller gaps between the threads. We can see a practical example showing this effect in Figure 9. In order to deposit as much ink as possible a low TPM screen with an optimised wire diameter that maximises the relation between  $D_{\text{compressed}}$  and  $D$ .

#### 2.4. Influence of the rheological ink properties

To better understand the effects of rheological properties we need to look at the separate steps of the printing process. These are: the flood stroke, the squeegee stroke, mesh lifting up from the substrate, levelling and slumping. The ideal situations for each of these steps are [18]:

The flood stroke gives a good coverage of ink over the mesh without dripping from beneath the mesh.

The squeegee stroke fills the mesh and the image area whilst using a pressure as low as possible to ensure a long squeegee life.

The mesh gets lifted out of the ink with minimum effort and a low snap-off distance (distance between bottom of mesh and top of substrate during the squeegee stroke).

Levelling of the ink takes place as fast as possible; this ensures that there are no mesh marks left behind.

Very little slumping so the print resembles the design as close as possible.

Note that the properties needed for levelling and slumping contradict each other, a high viscosity ink will have minimum slump but there is a possibility that the mesh marks will be visible.

Otherwise, a low viscosity ink will leave no mesh marks but will have significant slumping.

However, [18] states that even high viscosity inks should have minimal impact on the levelling process. They also say that to print thin lines a non-Newtonian ink with high viscosity is needed.

Due to the high viscosity a high squeegee pressure and bigger snap-off distance is needed. The ink should also shear thin. Shear is the interaction between imaginary layers of ink on top of each other if the squeegee slides over it. The ink that is in contact with the mesh is stationary and the ink at the squeegee moves at the same pace as the squeegee, the ink in between moves at an intermediate speed [18]. The formula to calculate shear is shown in equation (2), where  $V$  is the velocity and  $H$  the thickness of the fluid layer. Figure 6 gives a visualisation.

$$\text{Shear} = \frac{V}{H} \quad (2)$$

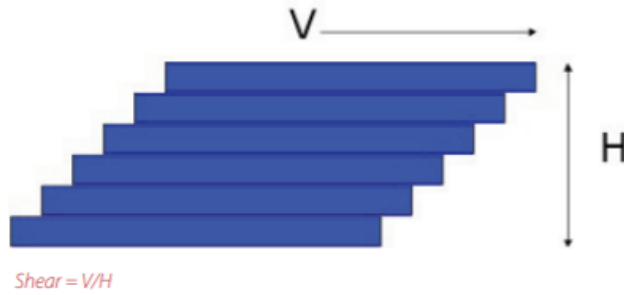


Figure 6: A visualisation of shear [18, p. 26]

With non-Newtonian fluids, the viscosity is tied to the shear, in the different steps the shear and thus the viscosity will be different. For printing a shear thinning ink is needed. This means that the viscosity gets lower when the shear is higher. For a typical shear thinning ink the relation between viscosity and shear is shown in Figure 7. However, it takes time for the ink to change viscosity, this is called time-dependency. For example, after the squeegee stroke it could take 10 seconds for the ink to return to the slump viscosity, this means that a thin line will have already expanded from 75  $\mu\text{m}$  to 100  $\mu\text{m}$  or even higher [18].

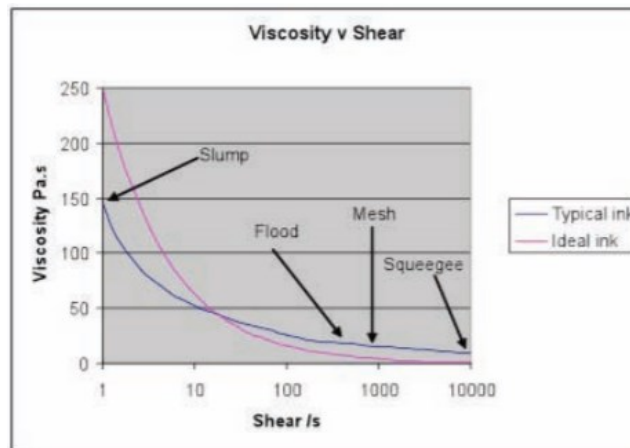


Figure 7: Relation of viscosity and shear of a typical shear-thinning ink, as shear rises the viscosity decreases, allowing the ink to pass through the screen mesh [18, p. 27]

Another property of the ink is viscoelasticity: this needs to be as low as possible because it stops the ink from flowing, instead, it will stretch and eventually return to its original shape [18]. This parameter can be described as the Elasto-Capillary Number  $E_c$ , given by the following formula:

$$E_c = \frac{\lambda\gamma}{\eta R} \quad (3)$$

Where  $\lambda$  is the relaxation time,  $\gamma$  the shear,  $\eta$  the viscosity and  $R$  the radius of the fluid bridge. It is measured by applying a sudden stretch to a droplet of fluid which is confined between two plates. This creates a bridge of fluid between the two plates of which the properties are measured [19].

The viscosity is linearly tied to the amount of solvent in the ink, adding more solvent in relation to solids will make the ink less viscous. When the ink is viscous the horizontal spread is less and therefore deposit thicker layers onto the substrate. The relation between viscosity and wt% is shown in Figure 8. In Figure 9 we can also see the effect of adding more solvent (lower viscosity) on the layer thickness [16].

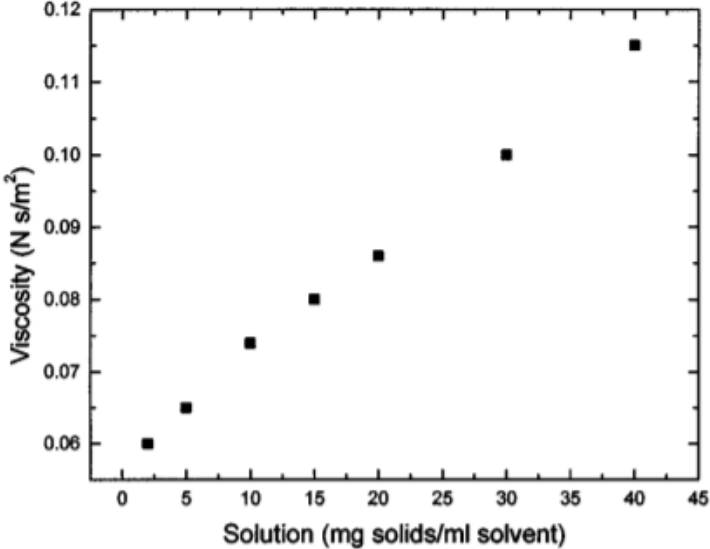


Figure 8: Relation between viscosity and wt% of the ink, higher solid contents lead to higher viscosity [16, p. 770]

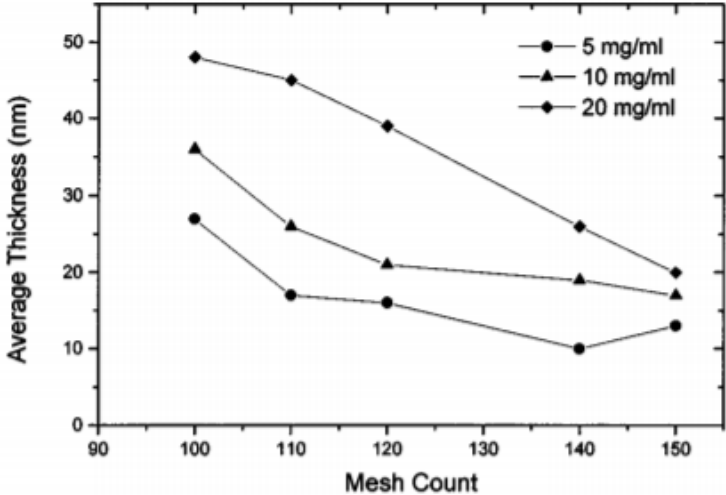


Figure 9: Effect of mesh count (TPC) on the thickness of the deposited layer. Higher mesh counts cause thinner layer deposition as does lower solid contents in the ink [16, p. 771]

Line widths above 150  $\mu\text{m}$  screen printed in silver ink are perfectly documented and feasible, however going below these widths introduces ink spread of up to 100%. Factors such as surface tension, roughness and wettability of the ink may influence line resolution.

In [20] several inks are analysed and selected to find solutions to these problems and to achieve line widths of down to 75  $\mu\text{m}$ . The structural material in this paper [20] needs to be conductive, it also needs to be compatible with the polymer substrates: PMMA, Pc, PET and COC. Curing times and temperatures for the conductive ink could form a problem for the polymer substrates.

In the abovementioned study [20], 7 silver inks were first printed in several lines with widths ranging from 75-150  $\mu\text{m}$ . The screen used was stainless steel of mesh 400 TPI with a wire diameter of 23  $\mu\text{m}$  and 10  $\mu\text{m}$  emulsion. The observed spread factor for lines thinner than 75  $\mu\text{m}$  was 1,5-2. To lessen the spread of the ink two options are proposed: increasing the hydrophobicity of the substrate or making the screen openings smaller than the design requirements to compensate for the ink spreading. The latter was tested in this study by making a screen with lines ranging from 35 to 75  $\mu\text{m}$  in steps of 5  $\mu\text{m}$ , the screen used was a 500 TPI mesh with wire diameter of 18  $\mu\text{m}$  and 10  $\mu\text{m}$  of emulsion. After analysing the 7 inks, only 3 seemed suitable for the testing phase. These inks are shown in Table 3 [20] along with the printing duration and the consumption per substrate.

*Table 3: Selected inks for thin line printing test [20]*

| Ink reference | Substrate | No. Of substrates | Printing duration | Ink consumption/substrate |
|---------------|-----------|-------------------|-------------------|---------------------------|
| Ag ink_A      | PC        | 30                | 35 min.           | 0,14 g                    |
| Ag ink_B      | PC        | 30                | 35 min.           | 0,15 g                    |
| Ag ink_C      | PMMA      | 30                | 40 min.           | 0,12 g                    |

Because the ink is exposed to the air during the printing process which takes around 35 minutes the solvent will evaporate, and the viscosity will change [20]. This change was measured and is shown in Table 4. This change in viscosity will have an influence on the properties of the samples that were printed near the end of the experiment. The first two prints of each sample were ignored to allow the ink to establish good wetting and rolling characteristics on the screen. The results are shown in Figure 10.

*Table 4: Change of viscosity after the printing process. Due to solvent evaporating when the ink is exposed to air, the viscosity of the ink rises [20]*

| Ink reference | Ink viscosity at 5 RPM, cP |        |          |
|---------------|----------------------------|--------|----------|
|               | Before                     | After  | % change |
| Ag ink_A      | 15 570                     | 33 880 | 118      |
| Ag ink_B      | 28 160                     | 34 790 | 24       |
| Ag ink_C      | 11 930                     | 19 880 | 67       |

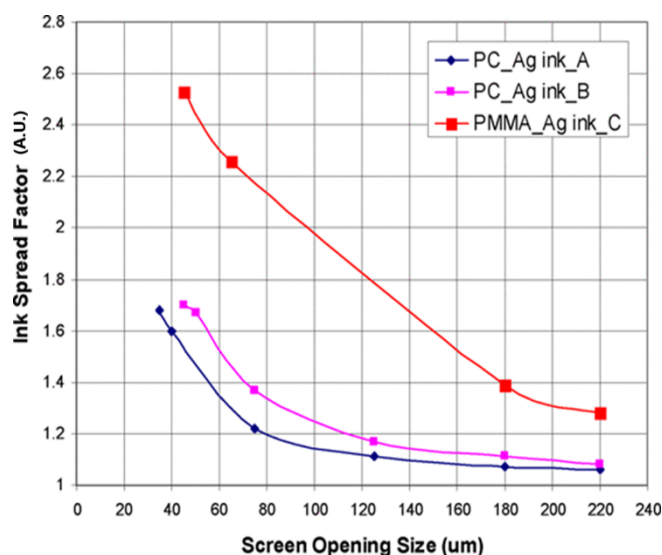


Figure 10: Results of thin line printing. Larger screen openings lead to less ink spread [20, p. 92]

It was found that the screen life was 20 prints and that the more viscous inks with low curing temperatures gave the best results. These results could be further improved by using a screen with finer wire mesh [20]. Dongpo C. et al. [17] also did a study regarding printing thickness and widths of silver pastes. They tested four different silver pastes which they printed in a silver grid to test the correlation between screen printing performance and rheological properties. The four silver particle inks used are shown in Table 5. As stated above the printing parameters also are of influence on the screen printing, Table 6 shows the settings of the screen printer used during the test [17].

Table 5: Properties of four silver pastes [17, p. 5323]

| Paste | Particle size | Main compositions    |                               |  |                          |
|-------|---------------|----------------------|-------------------------------|--|--------------------------|
|       |               | Metal                | Binder                        | Solvents   | Curing agent             |
| SM1   | ~100-150 nm   | ~87,3% Ag            | ~7,2% Bisphenol A epoxy resin | ~4,1% C <sub>10</sub> H <sub>20</sub> O <sub>4</sub>   | ~0,4% Modified imidazole |
| SM2   | ~2-8 μm       | ~56,6% Ag, ~25,5% Cu | ~3,1% Bisphenol A epoxy resin | ~4,1% C <sub>8</sub> H <sub>18</sub> O <sub>3</sub><br>~6,4% C <sub>7</sub> H <sub>8</sub> O               | ~0,3% Modified imidazole |
| SM3   | ~100-200 nm   | ~83,4% Ag            | ~2,7% Bisphenol A epoxy resin | ~4,1% C <sub>6</sub> H <sub>10</sub> O <sub>4</sub><br>~9,0% C <sub>7</sub> H <sub>12</sub> O <sub>4</sub> | ~0,2% Modified imidazole |
| SM4   | ~150-250 nm   | 91,7% Ag             | ~2,9% Bisphenol A epoxy resin | ~4,9% C <sub>8</sub> H <sub>10</sub> O <sub>2</sub>  | ~0,3% Modified imidazole |

Table 6: Parameters of the screen printer [17, p. 5323]

| Parameter                  | Value |
|----------------------------|-------|
| Snap-off distance (mm)     | 1,2   |
| Squeegee length (mm)       | 180   |
| Squeegee contact angle (°) | 70    |
| Squeegee pressure (Mpa)    | 0,3   |
| Scraper pressure (Mpa)     | 0,28  |
| Counter pressure (Mpa)     | 0,1   |
| Squeegee velocity (mm/s)   | 80    |
| Scraper velocity (mm/s)    | 120   |

The printed sample is a grid, using scanning electron microscopy (SEM) these grids are inspected on surface and cross-section deformities. The inks were characterised using several rheological analysing techniques with the Rheometer MCR302 (Anton Par Ltd, Germany). Properties such as viscosity, thixotropy and creep recovery were tested. The measurements are shown in Figure 11, Figure 12, Table 7 and Table 8 [17]. In Figure 13 the resulting widths and heights of the printed grids are shown. It can be concluded that ink SM4 is the best option in terms of slump. It has the highest loading of all tested inks, suggesting that this is a deciding factor.

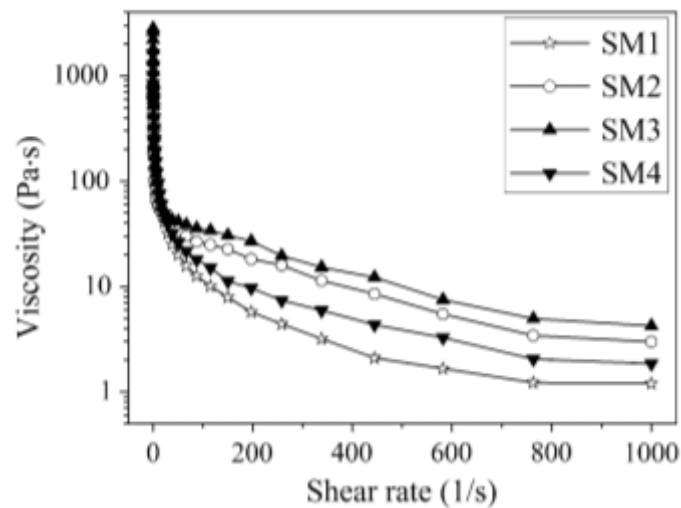


Figure 11: Viscosity in function of shear rate of the four inks. All inks show shear thinning properties which is desired for screen printing [17, p. 5326]

Table 7: Recovery rate and viscosity of the four different inks corresponding to different shear rates at steps in the printing process [17, p. 5327]

| Sample | 0,1/s (before squeegee stroke) | 1 000,0/s (squeegee stroke) | 0,1/s (after squeegee stroke) | Recover time (s) | Recovery level (%) |
|--------|--------------------------------|-----------------------------|-------------------------------|------------------|--------------------|
| SM1    | 987                            | 2                           | 400                           | 51               | 41                 |
| SM2    | 646                            | 6                           | 646                           | 134              | 100                |
| SM3    | 879                            | 6                           | 1 640                         | 20               | 92                 |
| SM4    | 1 196                          | 2                           | 153                           | 4                | 13                 |

Table 8: Creep compliance  $J_c$ , recovery compliance  $J_r$  and recovery ratio for the four kinds of pastes [17, p. 5328]

| Sample | $J_c$ (1/Pa) | $J_r$ (1/Pa) | $(J_c - J_r)$ (1/Pa) | $(J_c - J_r)/J_c$ (%) |
|--------|--------------|--------------|----------------------|-----------------------|
| SM1    | 7,98E-05     | 7,30E-05     | 6,80E-06             | 8,5                   |
| SM2    | 1,15E-02     | 1,11E-02     | 4,00E-04             | 3,5                   |
| SM3    | 6,36E-04     | 5,97E-04     | 3,90E-05             | 6,1                   |
| SM4    | 3,83E-06     | 2,60E-06     | 1,23E-06             | 32,1                  |

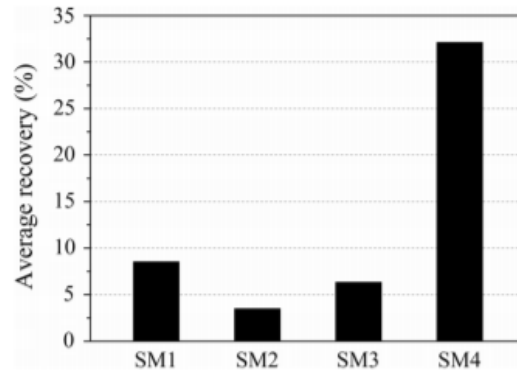


Figure 12: Recovery rates of the inks [17, p. 5329]

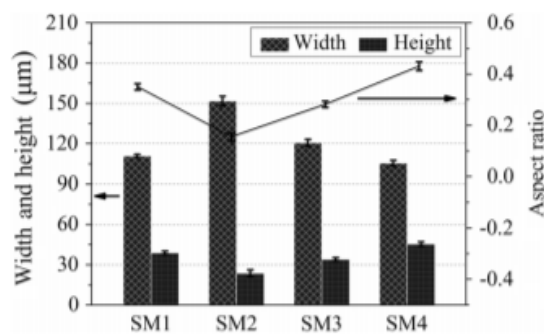


Figure 13: Widths and heights of the printed grids and their corresponding inks [17, p. 5326]

The substrate also has an influence on the print that gets left behind. In contradiction to popular belief, gravity does not have an impact on slumping, instead the surface tension of the substrate greatly impacts how much the deposited ink will spread. Other factors that determine the slump are shown in Table 9 [18]. To achieve small linewidths, a viscous ink that is shear thinning is needed. In combination with a substrate that has low surface tension, is porous and has a high equilibrium contact angle, thin lines could be possible.

Table 9: Parameters of the substrate that affect slump [18, p. 31]

| Parameter                              | Effect of high value   |
|--|------------------------|
| Surface tension                        | Fast spreading         |
| Initial contact angle or ink thickness | Fast spreading         |
| Equilibrium contact angle              | Slow (or no) spreading |
| Viscosity                              | Slow spreading         |
| Viscoelasticity                        | No effect              |
| Porosity of substrate                  | Slow spreading         |
| Evaporation                            | Slow spreading         |
| Freezing substrate                     | Slow spreading         |



## 2.5. Printing multiple stacked layers

Often MEMS have 3D-dimensions, to print this, it is required to stack layers of structural and sacrificial material on top of each other. The reference design has dimensions of over 100  $\mu\text{m}$  (Table 1) so stacking layers is inevitable. To see the effects of printing layers on top of each other, papers are reviewed. In [21] a cantilever structure is printed in glass ceramic using screen printing. With a length of 15 mm, width of 2 mm and a thickness of 50  $\mu\text{m}$  the cantilever requires stacked layers since the printing thickness is limited to a couple tenths of microns. The fact that the cantilever is made by multiple layers stacked on top of each other which has no major impact on the structural integrity of the MEMS proves that stacking layers is a possibility. The curing temperature of the sample was 850  $^{\circ}\text{C}$ .

Another paper [22] uses silver nanoparticle ink and an inkjet printer with a printing thickness of 450 nm and achieved a freestanding beam with a width of 90  $\mu\text{m}$ , length of 650  $\mu\text{m}$  and a thickness of 2,25  $\mu\text{m}$ , meaning that 5 layers were printed on top of each other. The beam was dried at 150  $^{\circ}\text{C}$  and annealed at 180  $^{\circ}\text{C}$ , it was experimentally found that the beam with the same width and length would collapse with a thickness lesser than 1,6  $\mu\text{m}$ . With the use of a nanoindentation measurement the Young's modulus of the structural material was calculated at 47,5 GPa (when cured at 120  $^{\circ}\text{C}$ ) which compared to the value of bulk silver (69-74 GPa) [23] is significantly lower. It was found however, that at higher sinter temperatures the grain size increases, and the strength of the material surged. The Young's modulus in function of the sintering temperature is shown in Figure 14. Stacked layers are a possibility, the post-treatment has a great influence on the properties of the structure. Higher sintering temperatures will lead to a stronger bond of the nanoparticles of the ink [23].

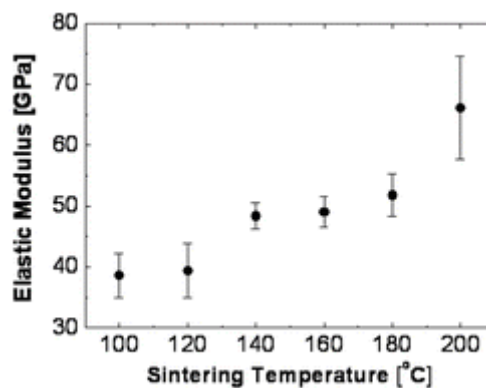


Figure 14: Young's modulus in function of the sintering temperature for nanoparticle ink. Young's modulus rises with sintering temperature [22, p. 5359]

## 2.6. Printed cantilevers

To test the possibilities of inks, the cantilever structure is a good option to test feasible dimensions and their corresponding strengths. The end goal of this master thesis is to optimise the production process of printed thermal actuator MEMS. If we look at other studies regarding this subject silver inks seems to be the most suitable structural material for this purpose. In Table 10 the inks, dimensions, sacrificial layer, Young's moduli, and cure temperatures of different cantilevers are shown.

Table 10: Cantilever dimensions and properties

| ink                        | Dimensions<br>(length*width*thickness) | Sacrificial<br>material                | Substrate            | Screen/inkjet | GPa          | Cure<br>temp.       | Reference |
|----------------------------|--|--|----------------------|---------------|--------------|---------------------|-----------|
| silver nanoparticle<br>ink | 650*90*2,25 $\mu\text{m}$              | PMMA                                   | oxidized Si<br>wafer | inkjet        | 47,5         | 180 °C              | [22]      |
| silver nanoparticle<br>ink | 550*100*1,8-2,2 $\mu\text{m}$          | PMMA                                   | oxidized Si<br>wafer | inkjet        | /            | 180 °C<br>30min     | [24]      |
| silver nanoparticle<br>ink | 200*100*3 $\mu\text{m}$                | PMMA                                   | glass                | inkjet        | 22 $\pm$ 1,5 | 150-400<br>°C 30min | [25]      |
| silver CRSN 2569<br>ink    | 5*2,5*0,015 mm                         | PVA film                               | PVA/PET              | screen        | /            | 160 °C<br>1h        | [26]      |
| ink ESL9912A               | 10*2*0,075 mm                          | Epoxy + S <sub>Cr</sub> O <sub>3</sub> | alumina              | screen        | 35           | 850 °C              | [27]      |
| ink ESL9912A               | 15*2*0,075 mm                          | Epoxy + S <sub>Cr</sub> O <sub>3</sub> | alumina              | screen        | 30           | 850 °C              | [27]      |
| ink ESL9912A               | 10*3*0,075 mm                          | Epoxy + S <sub>Cr</sub> O <sub>3</sub> | alumina              | screen        | 36           | 850 °C              | [27]      |
| ink ESL9912A               | 15*3*0,080 mm                          | Epoxy + S <sub>Cr</sub> O <sub>3</sub> | alumina              | screen        | 37           | 850 °C              | [27]      |

From the data above we can conclude that the ratios between the length, thickness and width of the cantilever plays a role in the structural integrity of the structure. It can also be seen that silver is the most common material used, especially for thermal applications, hence why silver is the material that will be used in this master's thesis.

## 2.7. Sacrificial layers and the interaction between the structural material

To create 3D structures with screen printing, a sacrificial layer is needed to make portions of the structural material freestanding. The sacrificial layer is used as support and is removed after the printing process. The interactions between the materials of the structural and sacrificial layers, as well as the processes that remove the sacrificial material could have impact on the properties of the MEMS. For this thesis, the impact of the printing process is studied for some materials which could be used as a sacrificial layer. Since the silver inks used need to be cured at 150 °C it is important that the material used is resistant to the elevated temperature.

### 2.7.1. Polystyrene sulfonate: polystyrene sulfonic acid (PEDOT:PSS)

PEDOT is a conductive polymer that has applications in organic light emitting diodes, organic photovoltaics etc. In order to process PEDOT to form a good film it is needed as a polyelectrolyte complex. The most effective anion for the process of forming films is PSS. Because of the ionic nature of this complex water is the most fitting solvent. Particles of the complex have sizes ranging from 10-500 nm. Due to the Coulomb interactions between the PEDOT and PSS ions viscosity can be as high as 1 Pa\*s with a wt% of 1%. This allows the ink to be deposited in layers with a thickness of up to several  $\mu\text{m}$  and small line widths can be achieved by inkjet printing [28]. In the table below the properties of some PEDOT inks are shown.

Table 11: Properties of the PEDOT ink [28]

| Trade name      | Solids content in water (w/w) (%) | PEDOT:PSS Ratio (w/w) | Viscosity at 20°C (mPas) | Average particle size | Conductivity (S/cm) |
|-----------------|-----------------------------------|-----------------------|--------------------------|-----------------------|---------------------|
| Clevios PH 500  | 1,1                               | 1: 2,5                | 25                       | 30                    | 500                 |
| Clevios PH 750  | 1,1                               | 1: 2,5                | 25                       | 30                    | 750                 |
| Clevios PH 1000 | 1,1                               | 1: 2,5                | 30                       | 30                    | 1000                |
| Clevios P       | 1,3                               | 1: 2,5                | 80                       | 90                    | 1                   |
| Clevios PH      | 1,3                               | 1: 2,5                | 25                       | 30                    | 0,3                 |

PEDOT could be used as a water-soluble sacrificial layer, the silver will not be etched by the removal process. PEDOT will easily dissolve in a water bath under mild sonication [29]. Heat treatments should not exceed 390 °C since PEDOT will start decomposing at this point [30]. Going over the melting point which is also above 300 °C might affect the ability of the solubility in water and will also have an effect on the silver print on top of it. The print might sink into the liquid PEDOT [31]. However, due to the low solid contents in the ink, the dry layer thickness will be very low. This makes PEDOT not a viable choice.

#### 2.7.2. Polymethyl methacrylate (PMMA)

There are several solvents to remove PMMA, in [25] PMMA ink with toluene as a solvent is removed by placing it in a chloroform bath for respectively 15, 10 and 5 minutes. After this the MEMS is dried by an N<sub>2</sub> gun. Due to the volatility of toluene the deposited PMMA show cracks and is not uniform. To achieve a uniform material the sample is placed in a vapor chamber with toluene vapours. This causes the PMMA to reflow or even partially melt, filling in the cracks and creating a smooth surface.

Dipping PMMA in acetone is also a viable option to dissolve the sacrificial layer [24]. When using acetone, the structure can be no longer immersed than 2 minutes, after this the acetone will start reacting with the silver [26].

PMMA will start decomposing weak head-to-head bonds at 150 °C, above 300 °C the molecular chains will break randomly. The solvent however has an impact on this temperature, it was seen that PMMA prepared in acetonitrile can withstand higher temperatures [32]. The melting point of PMMA lies between 140 °C and 160 °C [33]. Using inkjet printing a layer thickness of 2 µm is achievable.

#### 2.7.3. Polyethylene glycol (PEO)

PEO can be used as an ink when dissolved in water, a study [34] used 3 different samples using 1-, 1,5- and 2 g PEO dissolved in 10ml of distilled water. After 13-15 hours the mixture was a viscous gel that could be used for extrusion-based 3D printing. To test the printability of the PEO solution, lattices were designed with dimensions of 20\*20\*1 mm, the surface area of the printed samples was compared to the theoretical value (160,9 mm<sup>2</sup>). It was found that the mixtures with 1,5 g and 2 g PEO printed on a base plate of 50-70 °C with a printing speed between 0,5- and 1,5 mm/s gave the best results. The viscosity of the gels is shown in Figure 17.

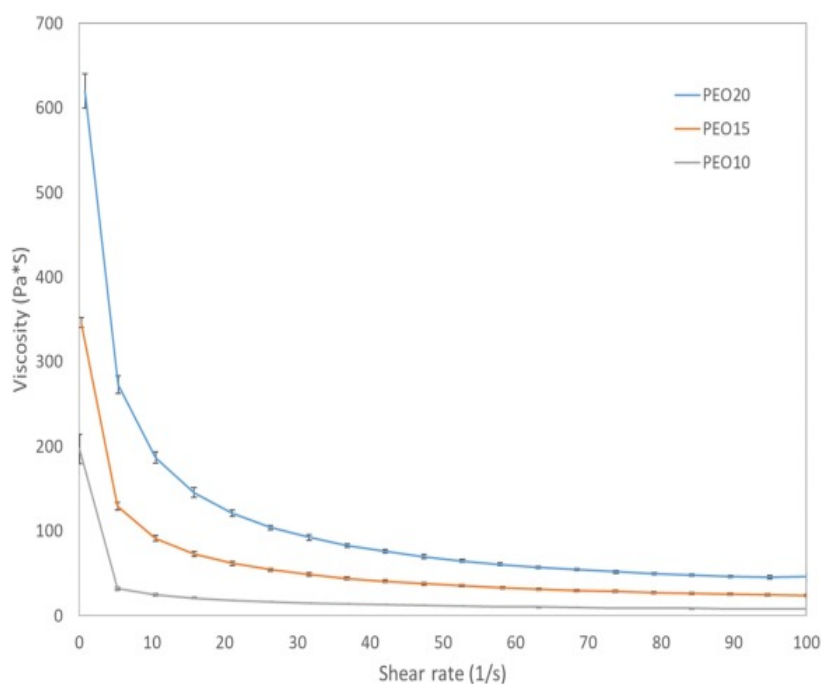


Figure 15: Viscosity of PEO gels at 25 °C (PEO 10, PEO 15 and PEO 20 with respectively 1, 1,5 and 2 g PEO in 10ml of distilled water). PEO inks show shear thinning properties which are desirable for screen printing [34, p. 4]

When curing the samples, it is important to keep in mind that the degrading temperature of PEO lies between 400 °C and 450 °C. However, during the curing process the melting point of PEO (64-66 °C) is exceeded [35]. This might cause problems to the structural layer on top.

#### 2.7.4. Polyvinylalcohol (PVA)

PVA can also be used as a sacrificial layer both as a film and as an ink, removing the material can be done by submerging it for 2 minutes in a water bath at 60 °C. This will have no effect on the silver [26]. PVA starts degrading at a temperature of 300 °C [36]. The melting point of PVA lies around 200 °C [37].

#### 2.7.5. Strontium carbonate (SrCO<sub>3</sub>)

An epoxy-type ink loaded with strontium carbonate particles could also be used as a sacrificial layer. It is soluble in a weak acidic solution [26]. There was however no information to be found about the composition of this ink.

#### 2.7.6. Overview of sacrificial materials

In Table 12 the solvent and degrading temperature of the different sacrificial materials are shown. These are important parameters to consider. If the melting or degrading point lies beneath the curing temperature (150 °C), the sacrificial layer may be affected by the high temperatures.

Table 12: Overview of the sacrificial materials

| Material          | Solvent              | Degrading temperature | Melting point |
|-------------------|----------------------|-----------------------|---------------|
| PEDOT             | Water                | 390 °C                | <300 °C       |
| PMMA              | Acetone              | 300 °C                | 140-160 °C    |
| PEO               | Water                | 400-450 °C            | 64-66 °C      |
| PVA               | Water                | 300 °C                | 200 °C        |
| SrCO <sub>3</sub> | Weak acidic solution | /                     | /             |

For this thesis it was chosen to investigate the use of PMMA and PVA as a sacrificial layer. PEDOT was eliminated because of the low wt% as can be seen in Table 11, the number of layers needed to be able to achieve a height of 100  $\mu\text{m}$  would be too high. PEO was eliminated due to its melting point being considerably lower than the curing temperature needed to cure the silver inks.

## 2.8.Characterization and properties of MEMS

### 2.8.1. Dimensions

After the print is made, it is needed to check the dimensions in order to compare it to the design and to spot possible defects in the structure. Parameters such as dimensions, roughness and straightness need to be known. This can be measured using several techniques such as: Scanning electron microscopy (SEM), transmission electron microscopy (TEM) or visual techniques [38]. Almudena R. [26] uses a Dektak XT™ Stimulus Surface Profiling System for the physical dimensions, which is also available in the IMO [38], it has a vertical resolution of 0,1 nm [39].

### 2.8.2. Electrical

The desired MEMS uses an electrical current to heat up the hot arm for the actuating motion. Therefore, the electrical resistance of the MEMS is an important factor [8].

Because of the porous nature of sintered silver particles, the conductivity of the printed material deviates from the bulk silver electrical resistivity [40]. Pores are electrical insulators, creating parallel current lines. They also reduce the volume of material where the current can flow through and force the current to make detours, making the electrical path longer, this being the main reason porous conductivity is lower than that of the bulk material.

In [41] the electrical conductivity under elevated heat of a 34 wt% silver nanoparticle ink with average particle size of 50 nm is tested. The experiments are done on a glass substrate with a  $3000 \times 103 \times 0,36 \mu\text{m}$  printed silver path which has been sintered at 523 K for 30 minutes. The material is heated using a laser sintering machine. In Figure 16 the results are shown.

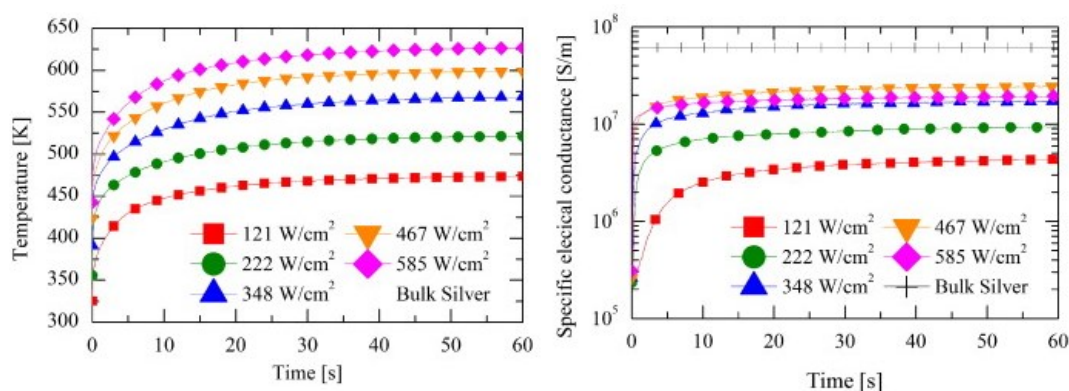


Figure 16: Relation between temperature and conductivity. As temperature rises so does conductivity, this is caused by further sintering of the nanoparticles [41, pp. 445-446]

It can be seen that the highest conductivity is achieved at  $\sim 600$  K which results in a conductivity of  $2,42\text{E}+07$  S/m which is 39,2% the conductivity of bulk silver. We also see that the conductivity increases with the temperature [41].

For the electrical characterisation, the four-wire technique can be used in combination with a precision Impedance Analyzer 4294A and an impedance probe kit. The calibration method for the electrical analysis is described in [42].

### 2.8.3. Mechanical

For the mechanical analysis Eun S. P. et al. [22] used a nanoindentation, the machine will use a sharp mechanically strong tip to apply a small force which is measured, the displacement of the tip that follows is also measured. The resulting load-displacement curve can be used to extract the values of stiffness and Young's modulus. The contact stiffness  $S$  is calculated by solving

$$S = \frac{dP}{dh|_{h=h_{max}}} \quad (4)$$

with  $P$  applied force and  $h$  tip displacement. The Young's modulus is found with:

$$Er = x = \frac{\sqrt{\pi}}{2\sqrt{A_c(h)}} \quad (5)$$

where  $A_c(h)$  is a contact area function depending on the indenter tip.

In [21] the Young's modulus is calculated with the data obtained by applying force with the stylus of a mechanical Tencor profilometer. It can apply a force between 5 and 100 mg and measures the displacement with an optical profilometer Altisurf 500 with a range of 3 mm and a resolution of 0,5  $\mu\text{m}$ . When the dimensions of the MEMS are known, the following formula is used to calculate the Young's modulus:

$$\delta = \frac{4L^3F}{Et^3\omega} \quad (6)$$

Where  $L$  is the length of the beam,  $F$  is applied force,  $t$  is the thickness,  $\omega$  is width and  $\delta$  the deflection at the tip of the cantilever.

In [27] is stated that the frequency of the first bending resonance is tied to the Young's modulus by the following formula:

$$f = \frac{1}{2\pi} \sqrt{\frac{Et^2}{0,96L^4\rho}} \quad (7)$$

With  $\rho$  the mass density,  $L$  the length of the cantilever and  $t$  the thickness. However, this formula can only be applied to the first natural frequency, for the second natural frequency another formula is needed [43]:

$$f = \frac{1}{2\pi} \sqrt{\frac{Et^2}{0,024717748L^4\rho}} \quad (8)$$

There is also a link between the yield strength and temperature [44]. At higher temperatures the yield strength will decrease until reaching zero at the melting point. This is something that needs to be monitored since the MEMS will be working at elevated temperatures. In Figure 17 a simulation of the relation between tensile strength and temperature of silver is shown.

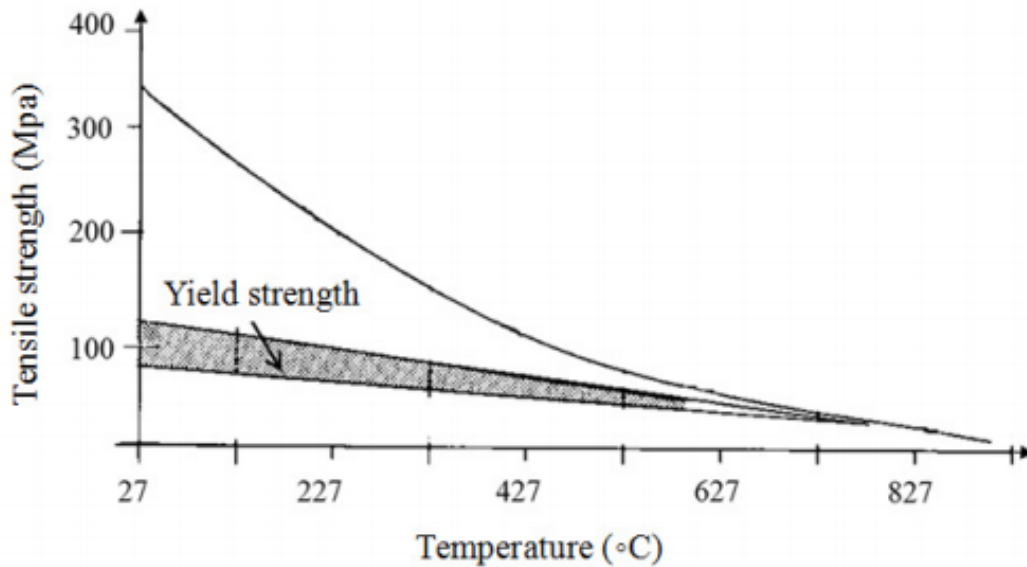


Figure 17: Relation between Tensile strength of silver and Temperature. The yield strength gradually decreases as the temperature rises until it reaches 0 at its melting point [44, p. 468]

#### 2.8.4. Displacement

For an actuator, the displacement is an important factor that needs to be characterised. For this application, the displacement is directly dependant on the thermal coefficient of expansion. For the peak-to-peak displacement of a structure a laser Doppler vibrometer could be used. Another option is visual techniques such as optical microscopy [38].

#### 2.8.5. Thermal conductivity

Because this paper researches a thermal actuator, properties such as thermal conductivity and thermal coefficient of expansion are also of great importance [8]. Because the structural material is the result of an ink that was deposited and cured, the thermal conductivity of the MEMS deviates from the bulk material. In nanoparticle ink the particles are sintered together and will form a thermal network as shown in Figure 18 [45]. In [40] it is stated that because the pores in the metal are so small (smaller than 1 mm), conductive heat transfer through gas or liquid trapped inside the structure is negligible. However, when the gas or liquid can move between pores, heat transport becomes a possibility. Radiative heat transfer between cells becomes more important as temperatures rise according to [40], factors that have an impact on this are: pore size, pore shape, relative density of the material and the temperature itself.

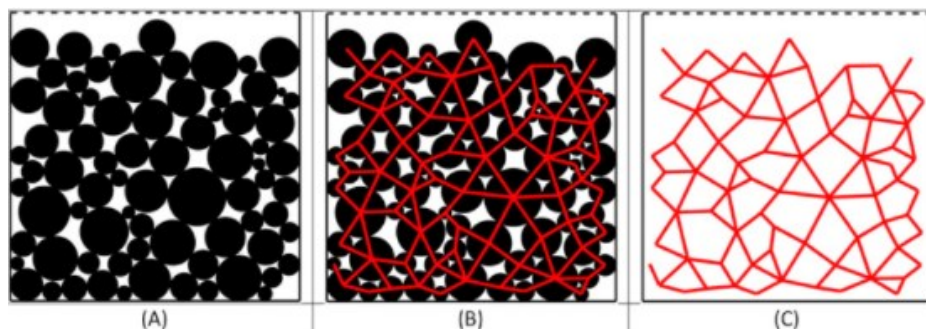


Figure 18: Visualisation of the thermal network in a porous material [45, p. 109]



Polansky J. et al. [45] used simulations of these networks to calculate the conductivity of sintered bronze particles (particles ranging from 10-100  $\mu\text{m}$ ), they found that their theoretical values differed 17% of the measured mean which was  $21,9 \pm 3,4 \text{ W/mK}$ , compared to bulk bronze which is  $85 \text{ W/mK}$  we see that sintered structures show lower thermal conductivity.

In the IMO these characteristics can be measured using infrared cameras, climate rooms and an oven with a conductivity measuring setup [38].

#### 2.8.6. Thermal expansion

As said earlier, the MEMS will gain its displacement from thermal expansion of primarily the hot arm. If the temperature comes near the melting point of the porous structure, trapped gas bubbles can artificially increase the thermal coefficient of expansion, however, when these temperatures are far below the melting point of the silver, the strength of the material will cause the effect of the expansion of the gas to be negligible. Therefore, the thermal expansion of the bulk material should be the same as that of the porous equivalent [40]. For silver, the fractional expansion per degree is  $18^{-6}/^{\circ}\text{C}$  [46].

#### 2.8.7. Thermoelectrical

The heat in the MEMS will be generated by applying a voltage to the anchors of the MEMS.

When a voltage is applied to the MEMS a current will flow through it. The power dissipated in the heater is given by [47]:

$$P = I^2R \quad (9)$$

Where P is the dissipated power, I the current and R the resistance of the path that the current takes. This resistance is given by [47]:

$$R = \frac{R_s L}{w} \quad (10)$$

With  $R_s$  sheet resistance, L length and w width of the electrical conductor. Sheet resistance is given by [47]:

$$R_s = \frac{\rho}{t} \quad (11)$$

Where  $\rho$  is the electrical resistivity of the material and t the thickness of the layer.  $R_s$  and t can be measured, using these values to find  $\rho$  and combining formula (11) and (10) allow us to calculate the resistance of a given sample:

$$R = \frac{\rho L}{A} \quad (12)$$

When the voltage is applied, ultimately a steady state temperature is reached. At this point the dissipated power will be equal to the heat dissipation by convection, conduction and radiation combined [47]. The characteristics can be measured by using an IR camera setup combined with the four or two wire method.



## 2.9. Conclusions from literature

### 2.9.1. Structural material

Silver seems to be the best material choice, its printability by both inkjet and screen printing is great. There is also a wide range of inks available. Since it is also conductive it is ideal for the use in a thermal actuator MEMS. Because the thickness of the reference design is 100  $\mu\text{m}$ , inkjet printing is not feasible due to its thin layer deposition [14], [15]. Blade coating does not allow the deposition of complex features and therefore screen printing is the best option to print the structural layer [12]. For screen printing, when choosing an ink, it is important to look at different factors such as dimensions of the desired pattern, thickness of the print and rheological properties of the ink [18]. Together these parameters in combination with the screen will determine the quality of the print. To test two extremes, the silver microflake ink Dupont ME602 [48] and the LOCTITE ECI1011 [49] nanoparticle ink were selected.

### 2.9.2. Sacrificial material

PMMA and PVA are materials that are considered for the sacrificial layer. As can be seen in Table 12, the melting and degradation point are not under 150  $^{\circ}\text{C}$ , which is the curing temperature the printed samples are dried at. PVA is soluble in water which does not have any impact on the integrity of the silver structure [26]. When using PMMA however, the silver can be no longer immersed in the acetone than 2 minutes [26]. If the silver is immersed longer it might react with the acetone.

### 2.9.3. Characterisation

Properties such as the dimensions, electrical conductivity, thermal conductivity, displacement, and joule-effect are all important factors for the intended purpose of the print as a thermal actuator. They will all be measured using the available equipment at IMO. Applying a current through the print will generate heat in the material. This will cause the material to cure further and decreases its electrical resistivity [41]. Due to the effect of curing on the properties of the inks, samples cured at varying curing temperatures will be tested.

## 3. Method

The first step is to find an appropriate sacrificial layer. Three inks will be tested: water based PEO, water based PVA, and acetone based PMMA. When a sacrificial material is found that can withstand the printing and curing process and is still soluble afterwards, the next step is to select an ink for the structural material. Two different silver inks were tested, the LOCTITE ECI1011 nanoparticle ink and the DUPONT ME602 microflake ink. The inks will be tested for their resistivity, strength, thermal conductivity, slump, and their heat generation due to the joule effect. The ink needs to be able to support a freestanding structure of at least the dimensions of the reference design and it needs to generate enough heat to achieve a deflection within the desired limits due to thermal expansion of the hot arm. Lastly, a MEMS design is printed and characterised to demonstrate the process.

### 3.1. Substrate

#### 3.1.1. Glass

The anchors and sacrificial layer are printed on top of glass, all samples use glass as the starting substrate. Since the influence of the anchors has no significant effect on the working of the MEMS no further tests were conducted.

### 3.2. Sacrificial layer

The sacrificial material is used to create the freestanding structure. In order to do this, it needs to comply to the following criteria: be soluble in a solvent that does not affect the silver ink, withstand the elevated temperatures of the curing step with no consequences to solubility, and it needs to be easily printable via screen printing or blade coating. The roughness is also a factor that needs to be optimised, ideally it would be as low as possible.

#### 3.2.1. PEO

The PEO ink was prepared using powder with an average molecular weight (mw) of 600 000. A solution of 6 wt% was made by adding the PEO powder to deionised water at 80 °C, it was stirred for 30 minutes at this temperature and afterwards stirred at 60 °C for another 30 minutes (Figure 19). It was screen printed on a glass substrate using a 100 TPC and 40 µm wire diameter mesh, squeegee pressure of 2 bar and 100 mm/s stroke speed. The same PEO ink was also used to prepare samples which were blade coated onto a glass substrate with a wet layer thickness of 100 µm.



Figure 19: Stirring setup (left) and screen printer (right)

### 3.2.2. PVA

Several PVA inks were prepared, in appendix C the method of preparation and printing parameters are shown for each ink and sample. All the PVA inks are also water based. The substrate of these prints is a glass plate which has been cleaned by putting it in a sonication bath for 10 minutes in isopropanol and then for 10 minutes in acetone. Afterwards they were dried using clean wipes.

In order to flatten the texture of the screen printed samples, they were put in the oven at different temperatures: 180 and 200 °C. Because the PVA is heated to a temperature above the glass transition temperature it starts to flow again, reducing the roughness [50].

The PVA inks were also used to blade coat, a doctor blade was used to do this. The blade coated samples were then cured using different techniques: one batch was cured directly at 150 °C for 5 minutes the other batch was first cured at 80 °C for 2 minutes and then at 150 °C for 5 minutes. In order to have a straight line to align the anchors to, a cut with a scalpel was made and the excess PVA was removed.

### 3.2.3. PMMA

An ink of 20 wt% PMMA in acetone was prepared by adding PMMA powder (120 000 mw) to acetone and stirring it for 4 days at room temperature. The ink was blade coated with a wet layer thickness of 200 µm. A silver print was also put into acetone and a roughness measurement was taken before and after it was put into the solvent to look for corrosion of the silver layer.

## 3.3. Structural layer

The two tested inks are a silver nanoparticle ink: ECI1011, and a silver micro flake ink: Dupont ME602. For each ink the following parameters were measured: the slump, behaviour of multiple layers on top of each other, influence of curing temperatures, the strength of printed freestanding beams, thermal conductivity and electrical conductivity. These properties are then analysed in order to select the best option for the production of the MEMS.

The in-plane thermal conductivity was measured using the parallel thermal conductance method (PTC method), see appendix E for a more detailed explanation of the test setup. The samples used for these measurements were squares of 38\*38 mm and 10 layers thick printed, for each ink 3 samples were made: one sample was cured at 120 °C, one at 150 °C and the last at 180 °C. They were cured for 5 minutes in between layers and 10 minutes after the final layer. The same samples were used to perform a van der Pauw sheet resistance measurement (Figure 20) see [51] for the specifics.

In order to test the slump at different thicknesses and widths of prints, the screen shown in Figure 21 was designed. The dimensions of the printed samples will be measured using the DektakXT Profilometer (Figure 20). The same samples were also used to measure the joule-effect in the prints. A current was applied while the temperature was monitored using a FLIR-camera. To calibrate the FLIR device, a hotplate was set to 50 °C, a glass plate and a beam of both inks were put on top of the hotplate. Since the emissivity coefficient ( $\epsilon$ ) of glass is known to be around 0,9 [52] the camera was calibrated using the glass. Then  $\epsilon$  of both inks was searched knowing that the temperature that should be read by the camera is 50 °C.

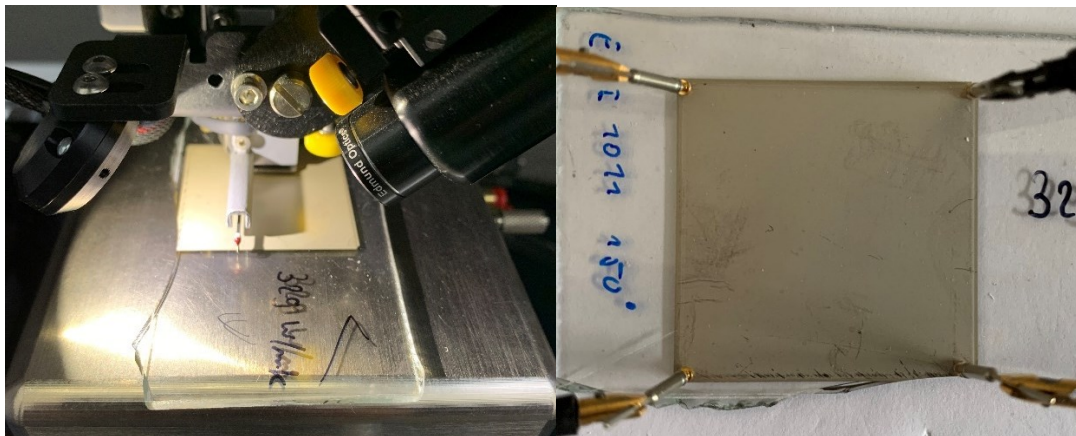


Figure 20: DektakXT profilometer (left) and van der Pauw measurement (right)

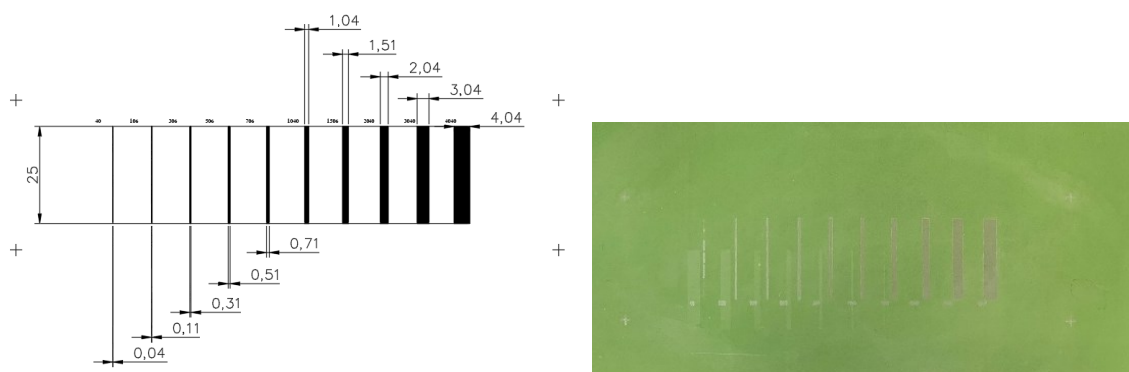


Figure 21: Design of screen for printing Beams/lines 165 TPC 31  $\mu\text{m}$  (units in mm) (left) and actual screen (right)

Using the temperatures measured by the FLIR camera, the expected deflection of the MEMS was simulated. It was assumed that only the hot arm was affected by the current. The elongation of the hot arm due to thermal expansion was then calculated using formula (13) [53]. With the thermal coefficient of expansion for bulk silver  $\alpha = 18E-06$  [46] and 20 °C as starting temperature.

$$\Delta x = L_0 \alpha (\Delta T) \tag{13}$$

The elongation was then used to simulate the deflection of the MEMS. This was done by making a simplified model in Autocad Inventor and constraining the dimensions of all parts of the MEMS (Figure 1) whilst changing the hot arm length. The geometry of the MEMS would adapt to the new hot arm length and the deflection could be measured.

For the nanoparticle ink the effect of sintering at different temperatures between depositing layers is tested. A sample was made using a 165 TPC mesh with a wire diameter of 31  $\mu\text{m}$ , squeegee pressure was 2 bar and stroke speed 100 mm/s. The sample consisted of four layers. the printing process is shown in Figure 23. To see the interaction between layers a SEM image in cross-section was made.

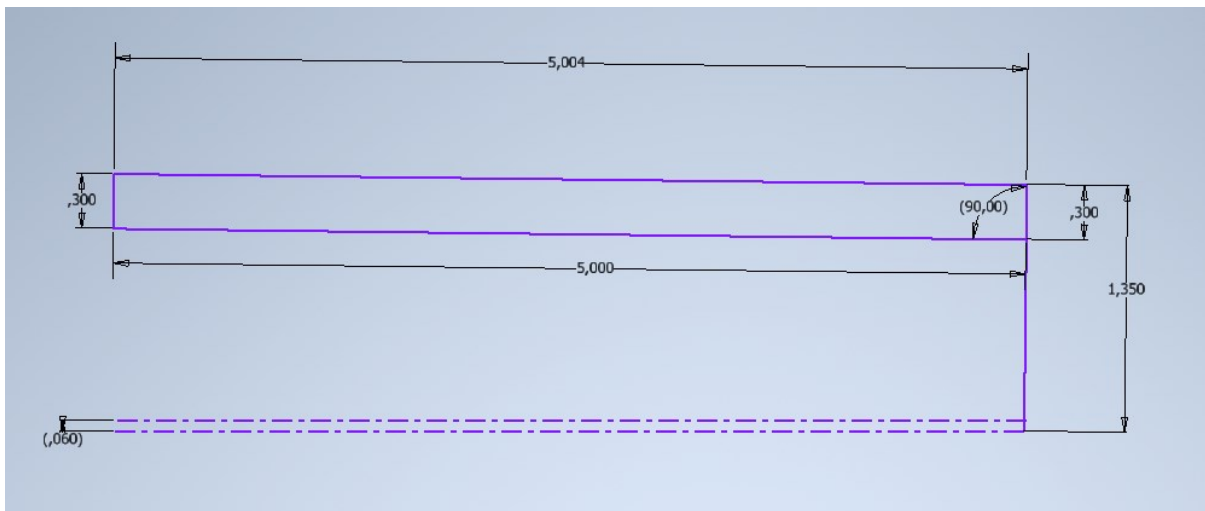


Figure 22: Simplified model of the reference design in Inventor. Distance between the two dotted lines is the deflection (units in mm)

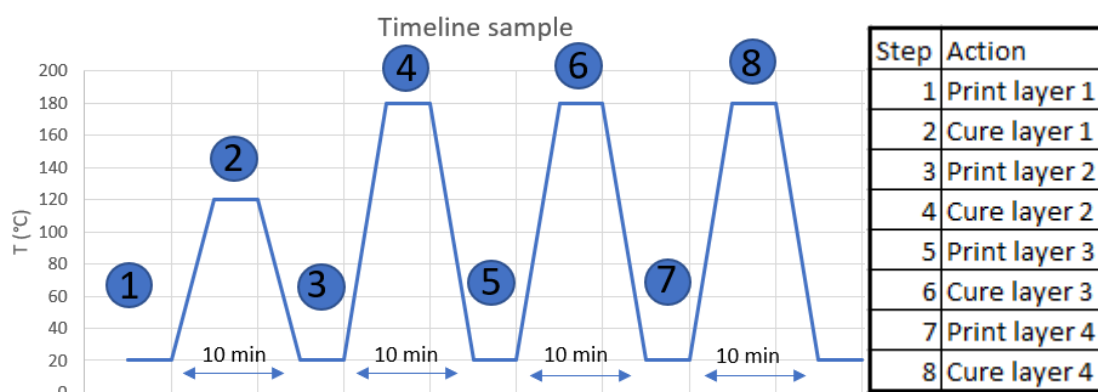


Figure 23: Printing process of the sample for layer interaction (ECI1011, 165 TPC mesh, wire diameter of 31  $\mu\text{m}$ , squeegee pressure 2 bar, stroke speed 100 mm/s)

### 3.3.1. PVA as a substrate

Because the structural layer is printed on top of the sacrificial layer, PVA can also be seen as a substrate. Both silver inks were printed on top of screen printed and blade coated PVA samples in order to check the printability of the silver on PVA. The stacks made are shown in appendix D. The silver lines on top are printed in 4 mm wide lines which were 30 mm long with a 165 TPC 35  $\mu\text{m}$  wire diameter mesh. In order to align the sample, a construction was made on the printing bed where the sample was pressed against. This allowed to accurately print on top of the previous layer.

### 3.3.2. PEO as a substrate

In order to test the effects of exceeding the melting temperature during the curing step, a blade coated sample of PEO was used to print a silver beam on top. In between layers the sample was cured for 5 minutes at 150 °C.

## 3.4. Freestanding beam

### 3.4.1. Printing

To print the freestanding beams the screen from Figure 21 is used. For both inks, three samples of 3, 5 and 10 layers thick were printed on top of a blade coated PVA sample. The sample was cured for 2 minutes at 150 °C between each layer and the final curing step was 15 minutes at 150 °C.

### 3.4.2. Removal of the sacrificial layer

The printed PVA samples are submerged in hot water ( $\sim 80$  °C) to dissolve the PVA, some samples were also put in a sonication bath in an effort to speed up the process. The silver lines should detach from the PVA and float freely in the water, they were dried on a piece of clean wipe paper and then glued on top of a glass plate with one end, so that the other end is floating in the air.

### 3.4.3. Beam characteristics

The Young's modulus of the beams was measured by acquiring the natural frequency of the beam [27]. This was done by putting a speaker alongside the beam and playing a range of frequencies, the deflection of the beam was monitored using a camera. This allowed to calculate the Young's modulus using formula (7) and/or (8). To make this calculation the density of the printed inks was also needed. This was done by measuring the beams and calculating their volume. The weight of the beams was measured and thus the density could be calculated. The bending due to self-weight was also measured.

## 3.5. Printed MEMS

### 3.5.1. Printing

The MEMS were printed using the ECI1011 nanoparticle ink. A screen was designed (165 TPC 31  $\mu\text{m}$  wire diameter) to print multiple variations of the proposed MEMS design, based on earlier results the dimensions of the MEMS have been altered accordingly. Figure 24 shows the screen. The substrate was blade coated PVA with 25 wt% foil ink. To have perfect alignment between printing layers the samples were cured on the printing bed. Using a near infrared (NIR) sintering setup [57] with a lamp of 400W which was used at 70% with 2-second-long flashes, each sample was treated 9 times with this lamp. After this the samples were cured in the oven for 5 minutes

and then they were put into hot water of 80 °C. When the MEMS released from the PVA layer they were put on glass while they were still wet with only the anchors touching the glass. Then a clean-wipe was used to remove excess water which also affixed the MEMS to the glass plate. Another glass plate of the same thickness was used to support the free-standing structure while the MEMS dried.

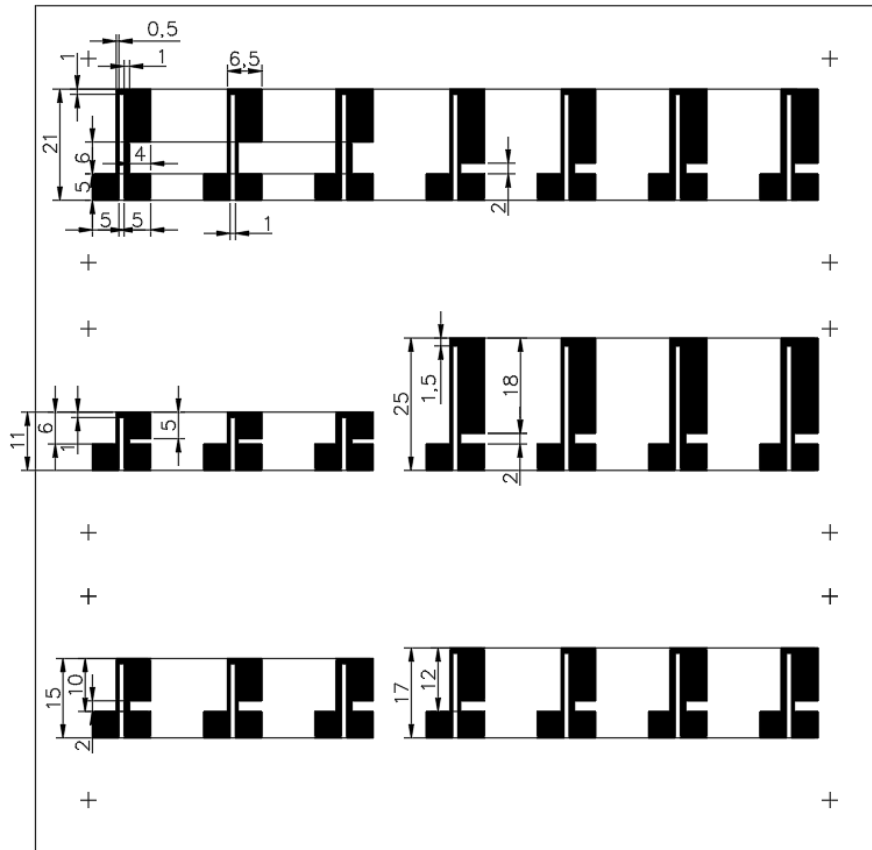


Figure 24: Screen design for MEMS designs (units in mm)

### 3.5.2. Characterisation

The electrical properties of the MEMS were measured using a multimeter and was measured from anchor to anchor. Two wires were attached to the anchors using silver adhesion epoxy. The displacement was measured using a microscope camera. Using a FLIR camera, the heating due to electrical current passing through the MEMS was also measured. It was also checked whether the beams would sag under self-weight.

## 4. Results & discussion

### 4.1. Sacrificial layer

The main goal of the sacrificial material is that it can dissolve after the printing process without having a negative impact on the structural layer. After dissolving it should leave the structural material freestanding. In this chapter the results of the sacrificial layer will be discussed and analysed. In 4.1.1. PEO, the results of the PEO sample to test the influence of the high cure temperature are shown. In 4.1.2. PVA the inks made with PVA are compared and characterised. In chapter 4.1.3. the PMMA ink that was made using acetone as a solvent is discussed. Lastly, chapter 4.1.4. gives an overview of the most important results for the sacrificial layer.

#### 4.1.1. PEO

The PEO ink of 6 wt% turned out to be too viscous to screen print. Using a squeegee pressure of 2 bar it could not be pushed through the mesh of 165 TPC and 31  $\mu\text{m}$  wire diameter. When the blade coating technique was tried, another problem occurred during the curing step. The melting point of PEO is around 60  $^{\circ}\text{C}$  [54] whilst the silver inks are cured at 150  $^{\circ}\text{C}$ , this caused the PEO to melt. Because it took more than 30 minutes for the PEO to harden again it was impossible to screen print correctly. The screen-life of the silver inks is 60 minutes, to print 10 layers of silver on top of the PEO layer it would take at least 5 hours, the properties of the silver ink will greatly change after being exposed to air for this amount of time [20]. The PEO layer also was not of an adequate strength to support the silver on top. Whilst measuring the roughness of the ink using the DektakXT Profilometer, the needle was pressed into the PEO with a force of only 1mg (see Figure 25). It is therefore certain, that with a squeegee pressure of 2 bar the print would be pressed into the PEO layer. Therefore, there was no further use of PEO in this research.

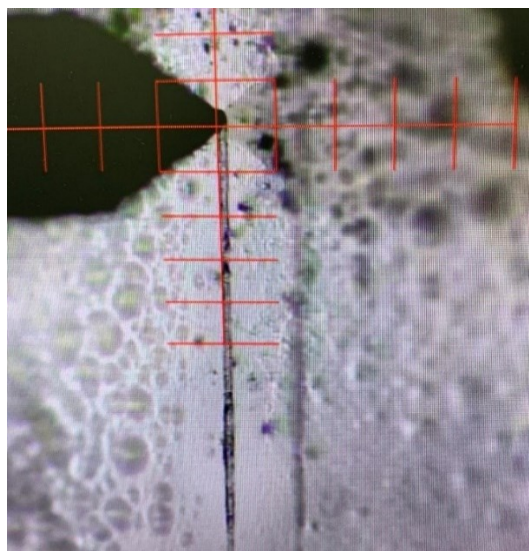


*Figure 25: Needle of profilometer pushed into PEO layer. The PEO layer cured at 150  $^{\circ}\text{C}$  was proven to be soft and not usable in the printing process*

#### 4.1.2. PVA

The PVA with a molecular weight 146 000-186 000, 99% hydrolysed seemed unfit to use, at 5 wt% it was not viscous enough and dripped through the mesh. At 10 wt% and 15 wt% the ink was too thick to fit through a mesh of 165 TPC and 31  $\mu\text{m}$  wire diameter, it is thought that due to high viscoelasticity the ink is not printable. The ink made from foil was of a too low viscosity at



10 wt% as it dripped through the mesh, after adding PVA until a mixture of 25 wt% was achieved the ink was viscous enough to be printed, see Figure 26 for the viscosity. Samples of 10 layers thick were printed using the 165 TPC 31  $\mu\text{m}$  wire diameter mesh and 100 TPC 40  $\mu\text{m}$  wire diameter mesh, the measurements of these samples can be seen in Table 13. From the viscosity measurement we can see that the ink is indeed shear-thinning which is the desired property for screen printing. The roughness of the print however, is not great. In an attempt to lower the roughness, they were put through the process as described in 3.2.2. The roughness of the samples after the treatment are shown in Table 14.

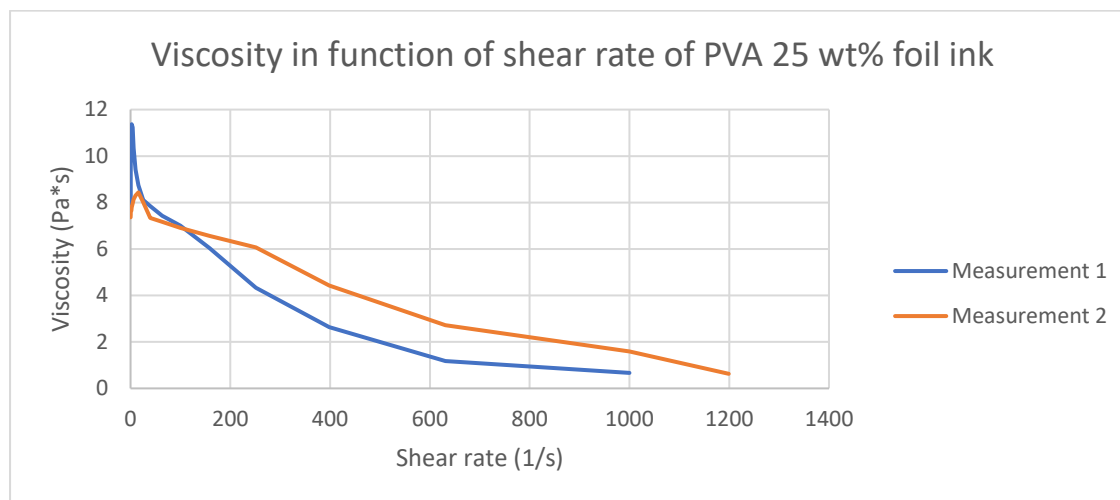


Figure 26: Viscosity of the PVA inks. The PVA 25 wt% ink shows shear thinning properties which is ideal for screen printing

Table 13: Measurements of screen printed samples with PVA 25 wt% foil ink. The roughness of these samples is too high. Three measurements with confidence interval of 95%

| Sample  | Ra (nm)             | Layer thickness ( $\mu\text{m}$ ) | #Printed layers | Mesh                     |
|---------|---------------------|-----------------------------------|-----------------|--------------------------|
| 12.03.A | 3014,1              | 23,6716                           | 10              | 165 TPC 31 $\mu\text{m}$ |
| 12.03.B | 5069,5 $\pm$ 1129,7 | 28,0897 $\pm$ 3,1741              | 10              | 100 TPC 40 $\mu\text{m}$ |

Table 14: Measurements after treatment to lower the roughness of screen printed samples of PVA 25 wt% foil ink. The treatment at 180  $^{\circ}\text{C}$  has lowered the roughness. However, it seems that the layer thickness was also greatly affected. Three measurements with confidence interval of 95%

| Sample  | Temp. and Time                | RA (nm)            | Layer thickness ( $\mu\text{m}$ ) |
|---------|-------------------------------|--------------------|-----------------------------------|
| 12.03.A | 180 $^{\circ}\text{C}$ 10 min | 1916,3             | 26,8616                           |
| 12.03.B | 200 $^{\circ}\text{C}$ 10 min | 1666,8 $\pm$ 338,8 | 23,6759 $\pm$ 2,4297              |

The treatment greatly reduced the roughness, from these measurements it could be concluded that the layer thickness has also been influenced. However, when looking at the SEM images of the print (Figure 27) the surface has the pattern of the mesh. This could be explicable due to the fact that the most ink is deposited under the threads [18]. The PVA ink is, however, of very low viscosity during the slump step (Figure 26). This should allow the PVA to flow and create a flat surface. The source of the mesh imprint is thought to be caused by the high squeegee pressure which presses the mesh into the PVA which was cured in the oven at 150  $^{\circ}\text{C}$ . Since this is close to the glass transition temperature of PVA it might have become soft. The measurements of Table 14

are therefore most likely taken at a different place where the average thickness was different than the original measurement, leading to a different value. Consequently, it is unsure if the treatment has any effect on the layer thickness whatsoever. Because the melting temperature of PVA is near 200 °C, another PVA sample that was cured at 200 °C partially melted and congealed again during the attempt to lower the roughness. The surface of the sample has also been discoloured and now has a yellow appearance as can be seen in Figure 28. When this sample was submerged in water in order to test if the ability to dissolve in water had been affected it became clear that the PVA could no longer dissolve easily in water, instead it started to crumble, which might destroy the silver layer if it were printed on top.

Screen printing multiple layers of PVA on top of each other also proved to be difficult, due to the sticky nature of PVA the deposited print often stuck to the screen during the snap-off step. This can be seen on the bottom sample in Figure 29. Due to all these difficulties the blade coating technique was tried. It gave the following results (see Table 15).

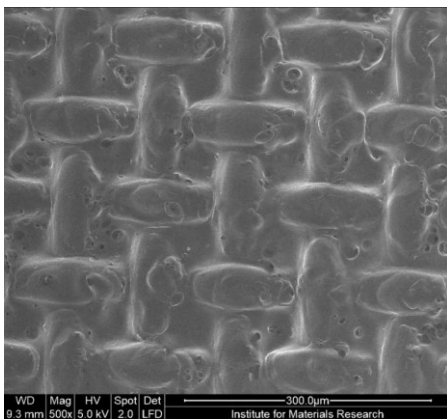


Figure 27: SEM-image of the surface after reducing the roughness at 200 °C of a screen printed sample PVA 25 wt% foil ink. The mesh is imprinted in the sample

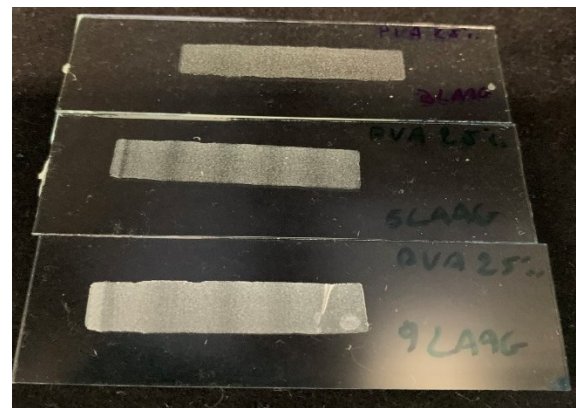


Figure 29: PVA 25 wt% foil ink sample of 3, 5 and 9 layers (from top to bottom). The sample of 9 layers stuck to the screen and came loose from the substrate, making it difficult to print a high number of layers



Figure 28: PVA 25 wt% foil sample after treatment at 200 °C. It has been discoloured and its solubility in water is affected

Table 15: Measurements of blade-coated PVA foil 25 wt% samples show very low roughness. Three measurements with confidence interval of 95%

| wet layer (µm) | ASH PVA (µm)   | Ra PVA (nm) |
|----------------|----------------|-------------|
| 100            | 11,1200±2,0822 | 112,87±27,3 |
| 200            | 29,9722±3,2878 | 73,43±10,7  |
| 300            | 38,8937±0,7301 | 45,79±15,1  |
| 400            | 47,5777±0,3767 | 66,17±23,9  |

The roughness of the blade coated PVA samples (PVA foil 25 wt%) is very low (Table 15). Which is ideal as a substrate to screen print the structural layer upon. The thickness of the layers also increases as the wet layer thickness increases, although the link is not linear. The next step was to cut away excess PVA with a scalpel. When looking at the profile of the cut sample it can be seen in Figure 30 that the cutting has caused the layer to detach from the glass near the cut and stick up. This was solved by putting the sample back in the oven at 150 °C for 5 minutes. As seen in Figure 31 this causes the PVA to affix itself back onto the glass.

PVA inks of other compositions were also tested. The blade coated samples made with the 17 wt% solution of PVA web had air bubbles on the surface and were not usable as a sacrificial layer (Figure 32). The blade coated samples made with the 27 000 molecular weight PVA powder were also very flat. Table 16 shows the ASH and roughness.

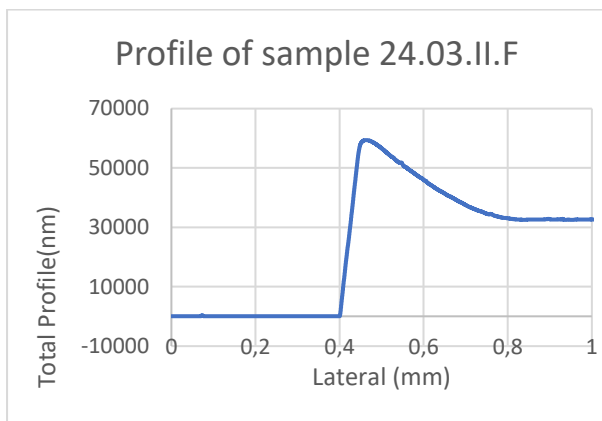


Figure 30: Profile of PVA foil 25 wt% sample shows that it has detached from the surface when cut by a scalpel

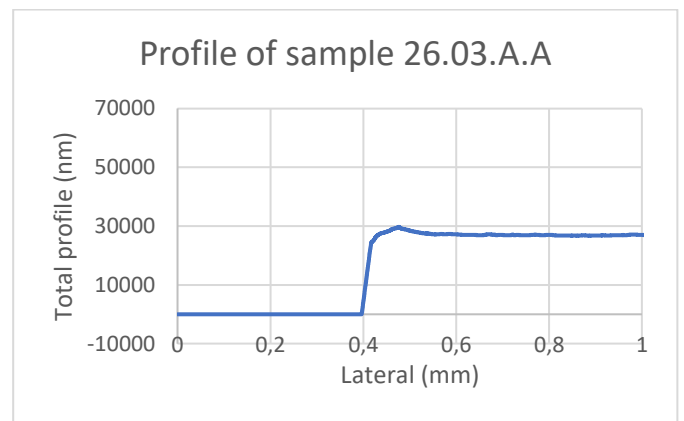


Figure 31: Profile of PVA foil 25 wt% sample after oven treatment shows that the layer affixes itself back onto the substrate after 10 min. at 150 °C in the oven



Figure 32: Rough surface of blade coated samples from PVA web 17 wt% ink, unusable as a substrate

Table 16: ASH and roughness of 27 000 mw PVA 20 wt% blade coated samples with low roughness. Three measurements with confidence interval of 95%

| Wet layer ( $\mu\text{m}$ ) | ASH ( $\mu\text{m}$ ) | Ra (nm)       |
|-----------------------------|-----------------------|---------------|
| 100                         | 12,176 $\pm$ 0,166    | 2,1 $\pm$ 3,0 |
| 150                         | 32,094 $\pm$ 1,817    | 3,0 $\pm$ 6,6 |
| 200                         | 21,502 $\pm$ 0,368    | 0,7 $\pm$ 0,2 |

The roughness measurements in Table 16, however, are not accurate. The lowest roughness that can be measured by the DektakXT Profilometer is 6 nm (with 2  $\mu\text{m}$  needle tip ISO4288). The real roughness value is thus somewhere below 6 nm. The thickness of the layers seems to have a maximum, the layer deposited with a 200  $\mu\text{m}$  wet layer is thinner than the layer deposited with a 150  $\mu\text{m}$  wet layer thickness. In order to achieve thicker layers multiple blade coating steps are needed. In contrast to the PVA foil ink, the 27 000 mw PVA ink could not easily be peeled of the glass. Instead, it was scraped off.

It was also observed that the PVA inks were only usable for two days after making the solution. After a couple of days, the ink would start to mold. The only solution to this problem was to put the ink directly after the stirring step into an air-tight container. However, once the container was opened and the ink was used, the mold would start to grow, presumably due to organic contamination. Another effect that was observed was that the viscosity of the prepared PVA inks would rise after the production. After one week the whole container of PVA (25 wt% foil) would clump together into one mass of gel. Urushizaki F. et al. [55] describe a possible explanation for this phenomenon, they state that the more thawing cycles the PVA solution experiences the more crosslinking occurs, increasing the viscosity. The PVA also swells over time, which will increase the viscosity as well. In [56] is stated that the change in properties of high wt% PVA solutions is the result of the formation of new polar interactions between molecules.

#### 4.1.3. PMMA

The PMMA ink of 20 wt% with acetone was too volatile to be used for screen printing, the surface of the ink almost immediately solidifies when in contact to air, leaving solid PMMA behind. If this ink were to be used on a screen it would clog the screen. When blade coating the ink, it became clear that due to the ink solidifying so fast it was difficult to apply an untouched surface. The ink would solidify at the place it was deposited on the substrate and on the doctor blade, when moving the blade, the already solid PMMA would leave a trail behind on the deposited layer.

The silver that was dipped into acetone for 10 minutes went from a roughness of Ra 607 $\pm$ 324 nm before to Ra 469 $\pm$ 230 nm after (Three measurements with 95% confidence interval). A paired sample T-test determined the difference of the two roughness values to be non-significant ( $p=0,1628$ ) therefore it is not certain whether the acetone influences the silver.

#### 4.1.4. Overview of results of the sacrificial layer

PEO was not selected because of its low melting point. The silver ink would be too long on the screen to wait for the melted PEO to harden. The melted PEO could also possibly affect the shape of the structural material. The PMMA ink was too volatile, thus leaving PVA as the best option for the sacrificial layer. The roughness of the blade coated samples made from the 25 wt% foil ink was very low (Table 15) making it a great substrate to print upon. The layer thickness can be controlled by varying the wet layer thickness. However, there seems to be a maximum wet layer thickness, once this value is exceeded the dry layer thickness will decrease. In order to achieve thicker dry layers, multiple blade coating steps are required. The 25 wt% ink made from PVA foil dissolved the fastest, under 15 minutes the ink would dissolve in water of 80 °C, therefore this ink is used as the sacrificial layer for the MEMS printing process. Another important detail is that all the PVA inks should be used as quickly as possible after they were produced. The rheological properties of the ink change over time and the ink can also start to mold due to contaminations.

#### 4.2. Structural layer

It was expected that the fine lines in the reference design could lead to problems. In Figure 33 and Figure 34 the spread of the two inks is shown for different sample widths and thicknesses. These samples are printed on blade coated PVA (20 wt% 27 000 mw). The relative slump rises at thinner mesh openings and higher numbers of layers printed. The thinnest line printed was with the 106  $\mu\text{m}$  mesh opening. The lines with a mesh opening of 40  $\mu\text{m}$  did not print at all with the microflake ink, the opening of the mesh might be too small for the particles to fit through. The lines of 40  $\mu\text{m}$  printed with the nanoparticle ink did not have straight edges. Because the mesh opening was only 1 square between the wires of the mesh, the printed beam was a dotted line (Figure 35). This is attributable to the fact that the viscosity of the ECI1011 ink is relatively high at low shear rates. This problem could be solved by choosing a smaller wire diameter of the mesh and/or lower TPC.

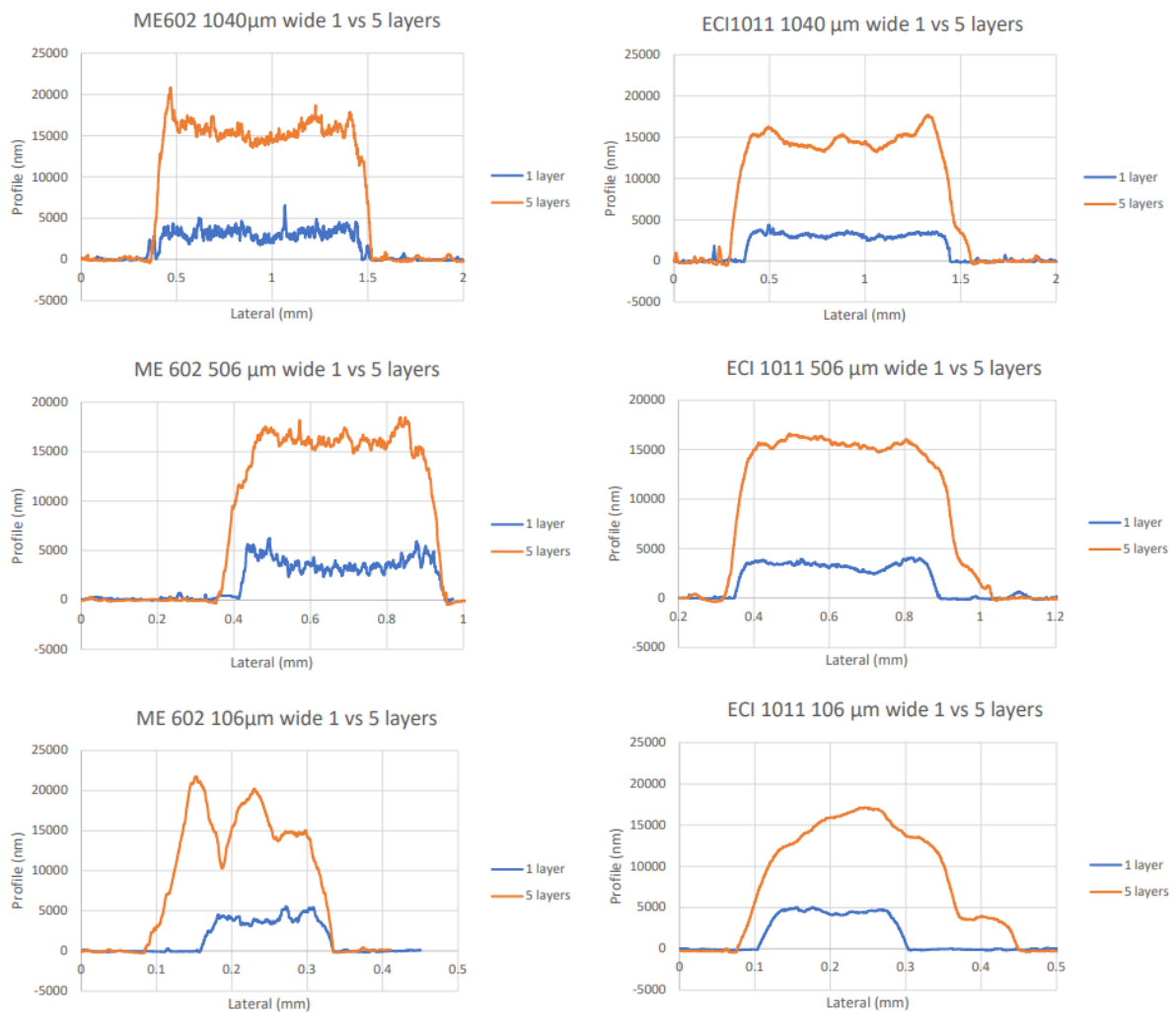


Figure 33: Slump of the inks increases with number of layers printed and smaller screen opening

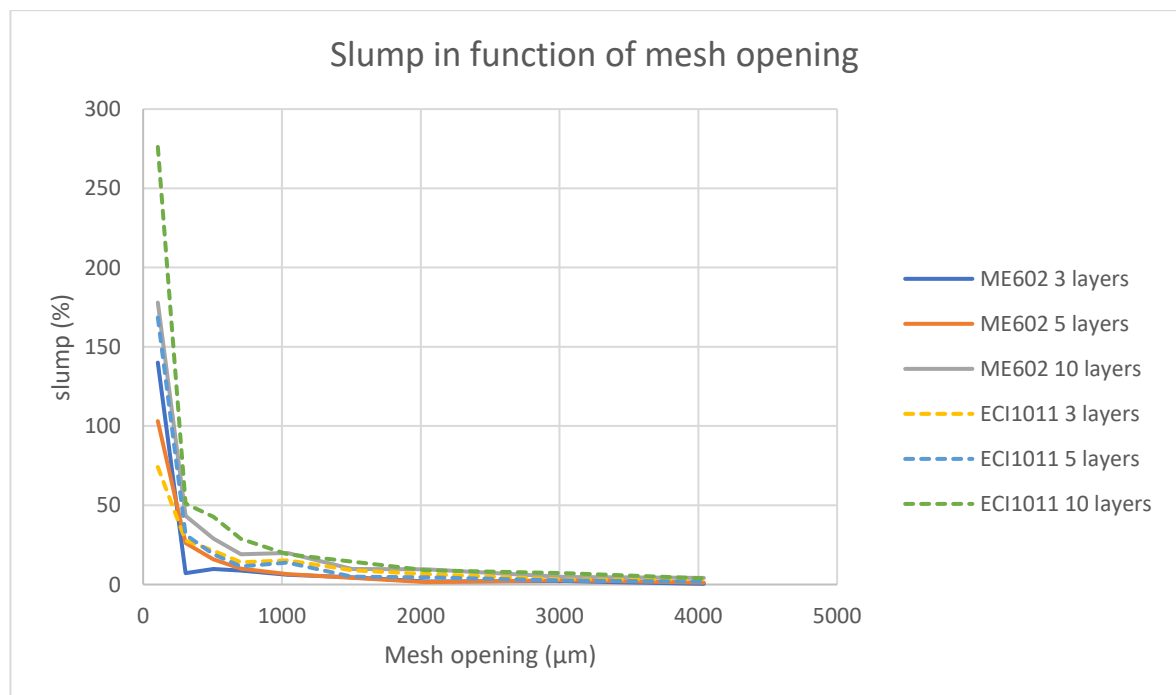


Figure 34: Slump decreases as line width and screen opening increases



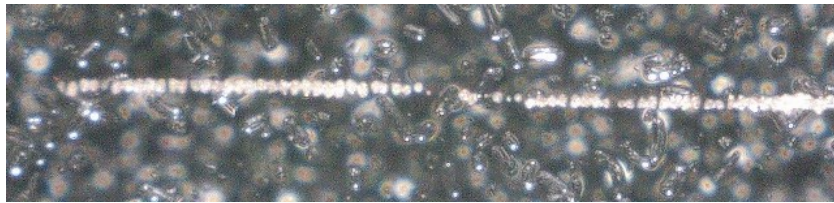


Figure 35: Printed line with 40 μm mesh opening (ECI1011) was not continuous

Before making conclusions based on Figure 33 and Figure 34 it needs to be mentioned that the alignment for one of the layers in the samples of the ECI1011 ink was off by approx. 50 μm as can be seen in the most lower-right graph in Figure 33. Regardless of this it can be said that the thinner lines will spread a lot more compared to the wide lines as can be seen in Figure 34. The spread of the ECI1011 ink is the most, even when disregarding the extra 50 μm spread due to the misalignment. However, the difference between the two inks is not significantly large.

The sheet resistivity and thermal conductivity of both inks was measured for samples which had been cured at different temperatures, the measurements are shown in Table 17 and Table 18. As can be seen in these tables the thermal conductivity rises with the curing temperature for both inks. For the ME602 ink the thermal conductivity is noticeably larger compared to the ECI1011 ink. This is a bit counterintuitive since the porosity of the nanoparticle ink (ECI1011) should be a lot lower than the microflake ink (ME602). A possible explanation is that the microflake particles, in comparison to the nanoparticles are larger. Therefore, the thermal resistivity between the interfaces of flakes is less common in the path than the thin joints of the nanoparticles. Despite the joints between nanoparticles having a higher conductivity, because they occur so frequently the cumulative resistance is higher than in the microflake ink.

By increasing the curing temperature, the electrical resistivity of the ECI1011 ink remains approximately the same whilst the ME602 decreases in resistivity. The resistivity of the ECI is a factor of 5 smaller compared to the ME602 for the samples cured at 180 °C, when looking at formula (9) this means it will generate far less heat with the same dimensions. The heat conductivity of bulk silver is 415-422 W/mK and the resistivity is 1,58-1,81E-10 Ωm [23]. Both inks have values lower than bulk silver, this can be explained by the porosity of the structure and impurities left by the solvent.

Table 17: Sheet resistance decrease was associated with higher curing temperatures. Eight measurements with confidence interval of 95%

| Curing temp | Sheetresistance (mΩ/□) |             | Thickness (μm) |        | Resistivity (Ωm) |          |
|-------------|------------------------|-------------|----------------|--------|------------------|----------|
|             | ECI1011                | ME602       | ECI1011        | ME602  | ECI1011          | ME602    |
| 120 °C      | 2,76±0,09              | 150,45±1,56 | 33,089         | 31,434 | 9,13E-08         | 4,73E-06 |
| 150 °C      | 2,03±0,03              | 28,4±1,35   | 39,410         | 41,081 | 8,00E-08         | 1,17E-06 |
| 180 °C      | 2,20±0,01              | 20,3±0,01   | 37,565         | 41,081 | 8,26E-08         | 8,36E-07 |

Table 18: In-plane thermal conductivity saw an increase as curing temperature increases

| Curing temperature | Thermal conductivity (W/mK) |        |
|--------------------|-----------------------------|--------|
|                    | ECI1011                     | ME602  |
| 120 °C             | 83,42                       | 101,37 |
| 180 °C             | 95,18                       | 135,80 |

The emissivity of the ME602 was determined to 0,51 and of the ECI1011 to 0,11. The temperature of the beams was measured when applying a current of 0,5-4 A (see Figure 36). The dimensions for the ECI1011 beam are 1,6\*6,6\*0,016 mm and for the ME602 3,2\*8,7\*0,014 mm. Due to the beam of ECI1011 of 3040  $\mu\text{m}$  wide breaking during the test, the measurements were done again with a beam of 1506  $\mu\text{m}$  wide. It is therefore not possible to compare the two beams in terms of heat generation due to the different dimensions. Nevertheless, the beam of ECI1011 of 1506  $\mu\text{m}$  wide is only half as wide so according to formula (12) its resistance is doubled. Despite the smaller dimensions the ECI1011 generates less heat than the ME602. The first time a current was applied the temperatures were higher compared to the second pass. This was seen in both inks, with the effect being stronger in the ME602 microflake ink. The highest temperature that was achieved when the beams were stabilized was 190  $^{\circ}\text{C}$  for the ME602 and 172  $^{\circ}\text{C}$  for the ECI1011, both at 4 A. At currents higher than 4 A the ME602 beam would burnout, for the ECI1011 the maximum current was 6 A. There were no FLIR measurements made above 4 A because the cables used could not withstand the current for prolonged periods. Assuming that only the hot arm (Figure 1) expands due to the temperature increase and the same temperatures can be realised in the reference design, the following deflections were simulated (Table 19). The maximum deflection is half the deflection that was simulated by the Nitte Meenakshi institute of Technology (appendix A); however, the operating temperature is also a factor 2 lower. The voltage applied to the beam could not be accurately measured due to losses in the cables and adhesion ink. They can be calculated however, using the resistance (cured at 180  $^{\circ}\text{C}$ ) of the beams and the current (4 A). The resistance for the beam of ME602 ink was calculated at 0,1662  $\Omega$ , the beam of ECI1011 ink has a resistance of 0,0299  $\Omega$ . The voltage drop over the ME602 beam is 0,66 V at 4 A and for the ECI1011 0,09 V. The ME602 voltage drop is within the desired limits of the reference design. The voltage drop for the ECI1011 is very low due to its low resistivity, this voltage drop is however not coherent with the heat generation. If we use the same resistivity values as above to calculate the resistance of the hot arm of the reference design, the resistance of the ME602 and ECI1011 is 0,4180  $\Omega$  and 0,0413  $\Omega$  respectively. This is roughly double the resistance of the tested samples, meaning that the heat generation could also double, matching the simulated values in Appendix A. It is thought however, that the material will burn out before reaching 900 K.

*Table 19: Simulated deflection of the MEMS rises with temperature*

| Temperature            | Hot arm length ( $\mu\text{m}$ ) | Deflection of MEMS ( $\mu\text{m}$ ) |
|------------------------|----------------------------------|--------------------------------------|
| 60 $^{\circ}\text{C}$  | 5003,6                           | 59,924                               |
| 120 $^{\circ}\text{C}$ | 5009,0                           | 149,52                               |
| 170 $^{\circ}\text{C}$ | 5013,5                           | 223,94                               |



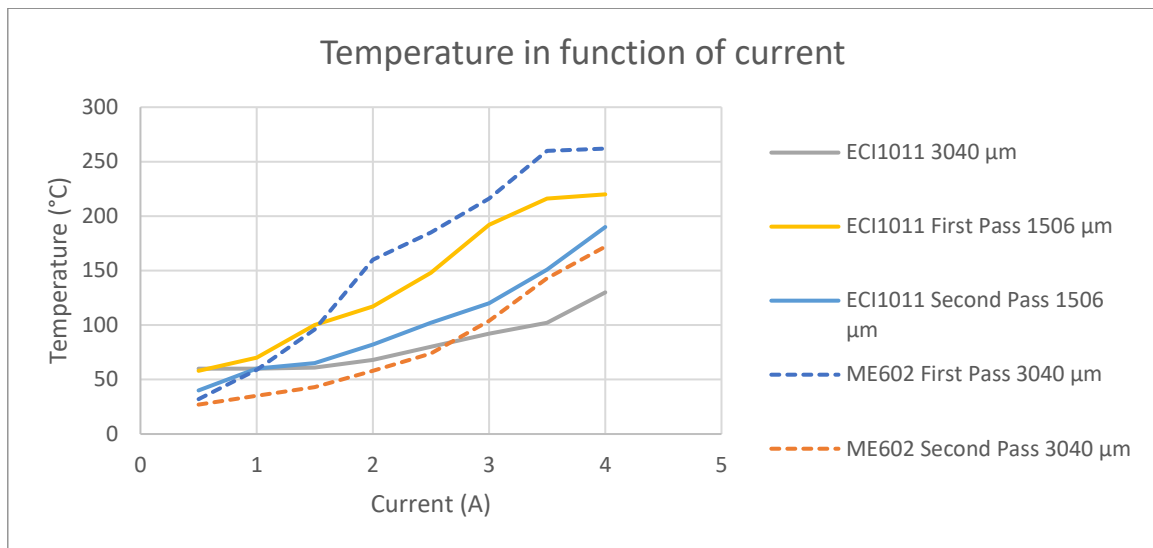


Figure 36: Temperature of beams increases with current, however the properties of the beams change as a second measurement reveals lower stable temperatures

The resistances for the beams were  $0,1662 \Omega$  for the ME602 and  $0,0299 \Omega$  for the ECI1011. Using these values in formula (9) makes us reconsider the measurements made on the ECI1011 beam, since the resistance of the sample is a factor 5 lower, the heat generation should also be significantly lower. When looking at Figure 37 it seems that the hottest parts are at the sides of the beam where the connection to the cable is made, here a silver conductor adhesion ink was applied, since the ECI1011 has relatively good heat conductivity it could be possible that the majority of the heat generation is originating from the adhesion ink and not the beam itself. The emissivity of the adhesion ink was determined to be 0,62. When measurements were made the adhesions temperature was always lower than the temperature of the beam. This leads to the conclusion that despite the low resistivity the ECI1011 ink does generate high temperatures.

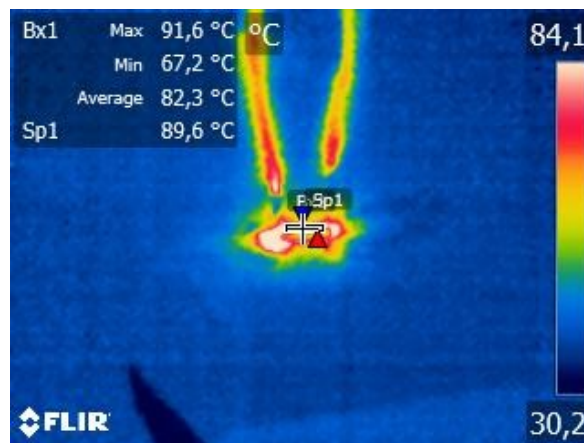


Figure 37: FLIR image of ECI1011 beam when a current of 1,5 A is applied suggests heat generates from adhesion applied on the beams

According to Biesmans I. and Reenaers D. [57] the emissivity decreases as silver nanoparticle ink sinters at higher temperatures. As seen in [41] and in the measurements of Figure 38 the ink cures further when a current is applied. Because the emissivity of both inks was determined on a sample that had been cured at  $150 \text{ }^\circ\text{C}$ , the change of emissivity due to the electrical current sintering the ink was not considered. Due to the emissivity decreasing, the real temperature is higher than what was measured.

To investigate what causes the change in behaviour as seen in Figure 36, a SEM image was made of the samples before and after a current was applied in Figure 38. For the ECI ink it can be seen that the small nanoparticles have ‘disappeared’, they have further sintered into larger particles, thus increasing electrical and thermal conductivity (Table 18). The ME602 has no change in particle size and no sintering occurs, however, there are more particles visible due to solvent vaporising. The increase in electrical and thermal conductivity (Table 18) is hypothesised to be caused by the vaporising solvent ‘pulling’ particles together, creating a denser structure.

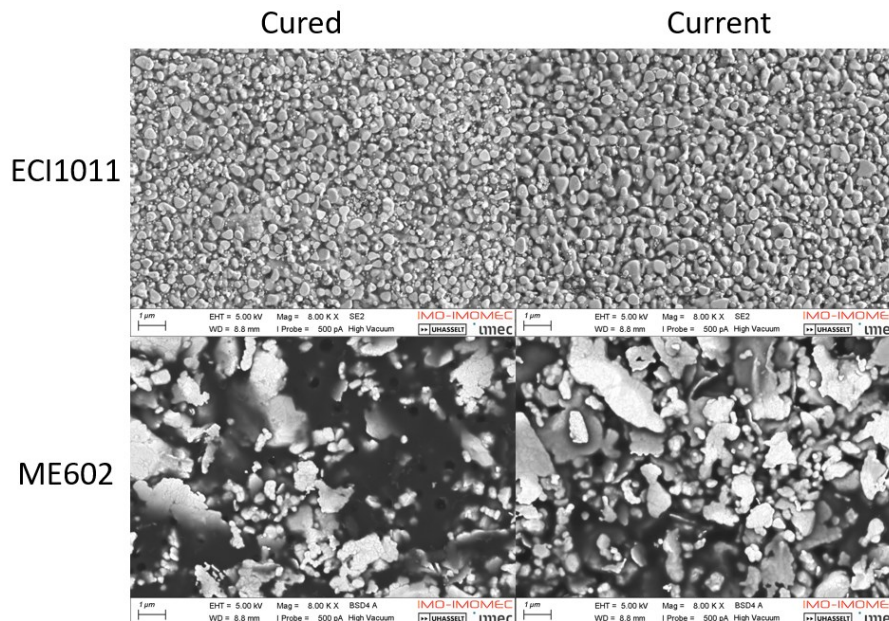


Figure 38: SEM images of the inks before and after a current was applied show that the ECI1011 nanoparticle ink has sintered further. The ME602 microflake ink seems denser due to solvent vaporising

In Figure 39 the cross-section of the sample prepared as described in 3.3.1 is shown. It can clearly be seen that there is an interface between layer 4 and 3. However, the interface between layer 3 and 2 is far less noticeable. Because the layers 2 and 1 have been 20 minutes longer in the oven compared to layer 4, the interface between the layers might have sintered due to the long cure time. It is therefore uncertain whether the uniform structure of layer 1 and 2 is due to the curing step at 120 °C or because it has been longer in the oven.

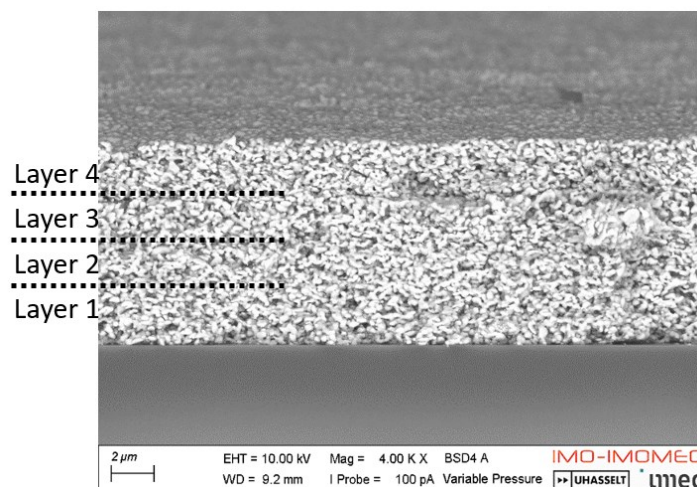


Figure 39: Interface between layer 4, 3 and 2 in the cross-section of sample (ECI1011) at which was prepared at different curing temperatures

#### 4.2.1. PVA

In sample 17.03.A (Appendix D) the ECI1011 ink was printed on top of the screen printed PVA samples (25 wt% PVA foil ink, 100 TPC mesh 40  $\mu\text{m}$  wire diameter). A cross section of the print can be seen in Figure 40. Because of the profile of the screen printed PVA (see Figure 27), the bottom of the silver print is very rough. At some places there is almost no PVA between the substrate and the silver, it can also be seen that cracks have formed at the tips of the PVA. These cracks will greatly impact the strength of the silver. Because of the downsides of screen printing, the blade coating technique will be used to apply the sacrificial layer. As we already know from the roughness measurements the blade coated samples are flat and show no erratic surface as can be seen in Figure 41.

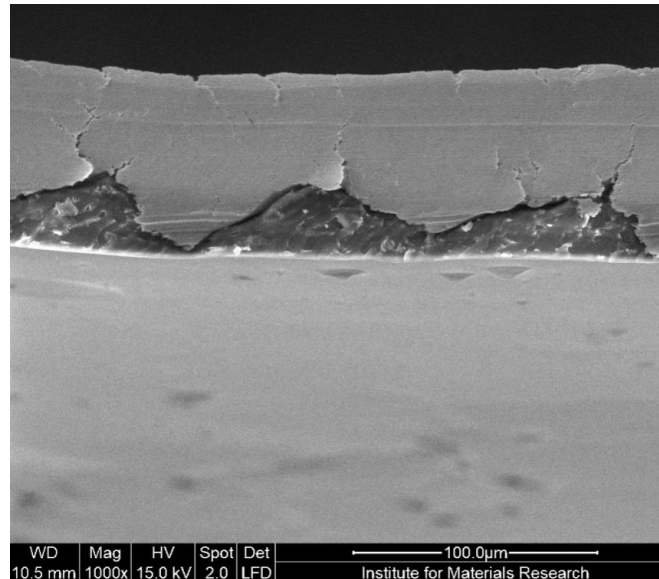


Figure 40: Cross-section of silver printed on top of screen printed PVA foil 25 wt% (17.03.A) shows that it causes the silver to form cracks

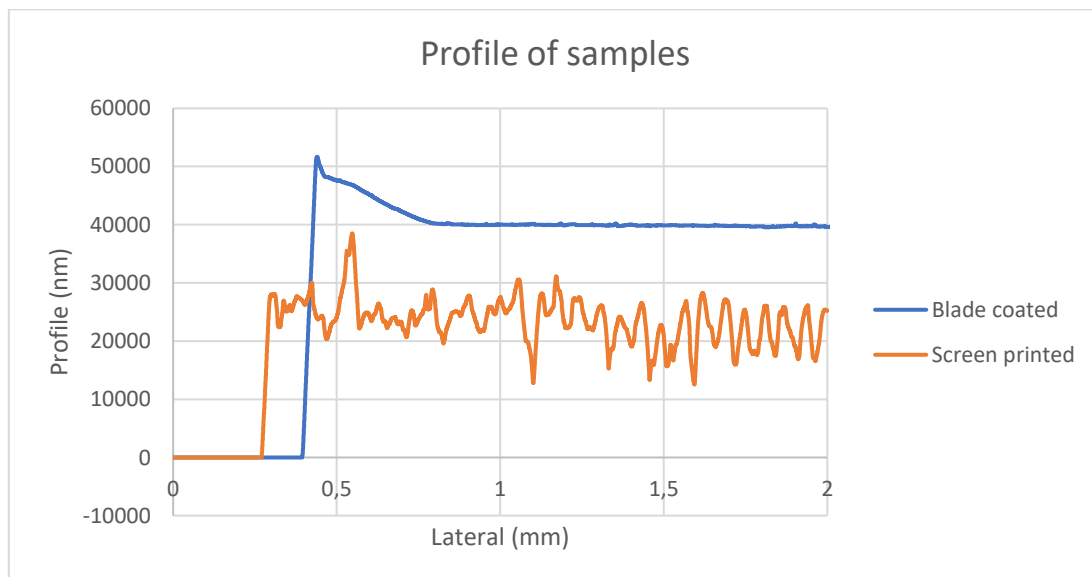


Figure 41: Comparison of the profiles of a blade coated and screen printed sample. It can clearly be seen that the blade coated sample is favoured as a substrate due to low roughness

#### 4.2.2. Overview of results of the structural layer

To achieve the desired measurements of the reference design, a factor to correct the slump should be taken into account when designing the mesh. Depending on the number of layers and the mesh opening the slump will change, more layers accord to more slump as does smaller mesh openings. The lines printed with the mesh opening of 106  $\mu\text{m}$  were approx. 300  $\mu\text{m}$  wide at 10 layers thick. To achieve an effective line width of 100  $\mu\text{m}$  at 10 layers thick, the mesh opening should be around 30  $\mu\text{m}$ . For this, a high (220 TPC 14,7  $\mu\text{m}$  wire diameter) TPC mesh is needed which could restrict the choice of ink to be used. Optimally the minimum feature width of the design would be more than 300  $\mu\text{m}$ , using a mesh opening of 106  $\mu\text{m}$  we can print the lines with both inks, which translates to a printed width of 300  $\mu\text{m}$ . This means that the thickness should be 33  $\mu\text{m}$  to have the same resistance value as in the reference design, which is approx. 10 printed layers.

Both inks show promising results regarding heat generation when a current is applied. Currents of 4 A heated the samples up to 190  $^{\circ}\text{C}$ . In Table 19 it was shown that for both inks deflections of up to 224  $\mu\text{m}$  could be achieved at a voltage of 2,04 V for the ME602 and 0,09 V for the ECI1011. This is not within the desired goals compared to the reference design. These goals are, however, infeasible due to the beams burning out at higher currents, making it impossible to achieve higher temperatures. It was also found that due to the heat generated by the joule-effect, the properties of the ink change. The electrical resistivity decreases, thermal conductivity increases. For the ECI1011 nanoparticle ink this was due to further sintering of the ink. For the ME602 it is hypothesised that the cause of these changes was that the solvent enclosed in the structure was vaporised, pulling together the particles.

The effect of different curing temperatures in between depositing layers nanoparticle ink was not clear due to limitations of the sample used. It can however be said that longer curing times (longer than recommended in the ink datasheets) do increase sintering rates.

### 4.3. Freestanding beam

The freestanding beam is the first experiment where the sacrificial layer is dissolved to release the structural layer from the glass substrate. The envisioned goal is to obtain a beam that perfectly retains its dimensions after it has released. Next, it is tested whether the beam can support its own weight, is conductive, and the Young's modulus is determined. These properties give more insight on the feasibility of the reference design. Firstly, problems that occurred during the printing of the beams are discussed. Then the removal process of the sacrificial layer is analysed. Afterwards the beam characteristics are shown and reviewed. In chapter 4.3.4. the key results are summarised.

#### 4.3.1. Printing

The only difficulty that occurred during the printing process was that the sample was not always correctly aligned to print the next layer. This can be avoided by using image recognition software in combination with a camera that can align the screen and the samples using a reference point on the sample and screen. Or by curing the samples on the curing bed so they do not need to be moved.

#### 4.3.2. Removal of the sacrificial layer

The silver lines printed on top of the PVA foil ink would release after approximately 15 minutes. The samples printed on top of the PVA ink made from the 27 000 molecular weight PVA powder would take a lot longer. The samples were put in water for 2 days and still needed to be cut loose from the substrate using a scalpel.

The samples of the Dupont ME602 ink which were put in hot water and in the sonication bath would curl up. This could possibly be caused by the energy added by the vibrations to the sample. Figure 42 shows a silver beam of ME602 which has curled up, presumably due to the vibrations. When putting the samples of Dupont ME602 ink in a cup of hot water they still curled up but not as much. When dried between two clean wipes with a weight on top the silver layer was flat again. Figure 43 shows the sample when the PVA was dissolved by submerging it in hot water.



*Figure 42: Releasing a sample of ME602 in a sonication bath causes curling of the beam*



*Figure 43: The release of a sample of ME602 in hot water with no deforming of the beam.*

The beams printed with ECI1011 would all curl up, this is caused by residual stress which builds up during the process. The deformities are worse with the nanoparticle ink because it is not as flexible as the microflake ink. The stress builds up during the curing process, the silver layers are cured and formed at 150-180 °C they settle onto the substrate at this elevated temperature. When the samples are cooled to room temperature the silver shrinks. However, it is constrained because it is fixed to the substrate. This causes stress to build up, when the sacrificial material is dissolved the constraint is removed and the beams curl due to the internal stress [58]. See Figure 44 for a visualisation [59], [60]. Note that the beam consists of multiple layers printed on top of each other, the top layer is the longest, here the most stress will occur, causing the beams to always curl up away from the substrate.



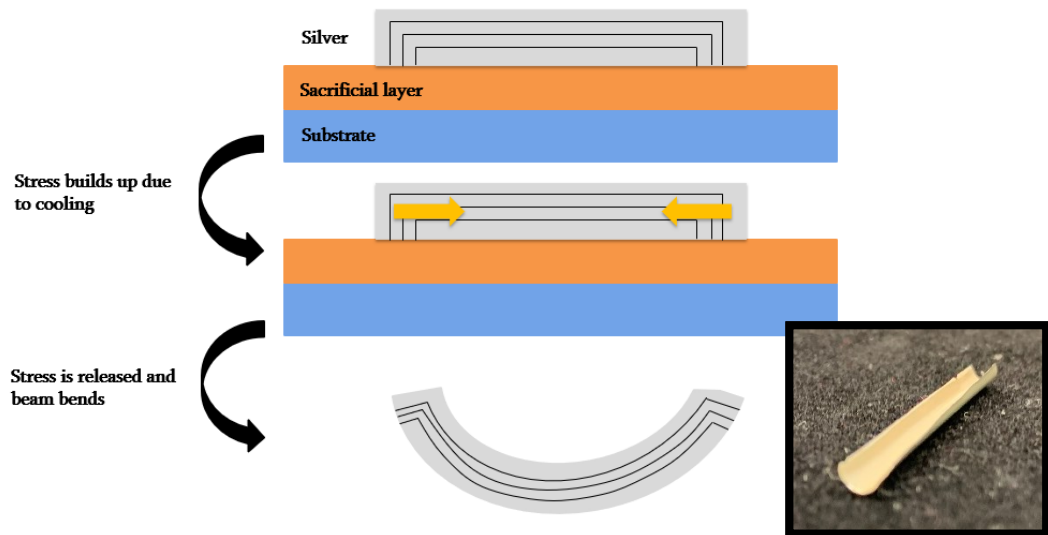


Figure 44: Bending of beam due to residual stress. The forming of the silver layer at high temperature in the oven causes stress to build up. This stress is released in the form of curling when the print is released from the sacrificial layer.

Sometimes the silver layer would release from the substrate before all the PVA was dissolved, this caused the beam to stick to the surface it was dried on. Upon closer inspection it was found that there was still PVA residue sticking to the released silver beams. To remove the residual PVA, the beams were transferred to a cup of clean water at 85 °C, and then dried again. It was found for both inks, especially for the ME602 that it was difficult to get the beams out of the water. The surface tension of water held the beams in its surface. The ME602 beams would sometimes even get trapped in water droplets that formed at the end of the tweezers that were used to pick up the beams.

#### 4.3.3. Beam characteristics

The density of the samples printed using the ECI1011 ink was calculated to be 6,788 kg/L and the ME602 ink was 2,755 kg/L (when cured for 10 min. at 150 °C). The density of bulk silver is 10,5 kg/L [23], again due to porosity and impurities the samples show lower density than bulk silver.

The Young's modulus was determined for both inks, Figure 45 shows the Young's modulus in function of the beam width for the Dupont ME602 ink, there is no apparent cohesion between the width of the beam and the Young's modulus. However there seems to be a connection between the Young's modulus and the number of printed layers. In Figure 46 the trend can be seen that for thinner beams the Young's modulus goes up. Since the Dupont ME602 ink is a microflake ink, no sintering occurs at temperatures under 800 °C [61], the flakes settle into each other as the solvent evaporates and gains its strength from the interactions between the surfaces of the flakes. A possible theory for the decrease in strength is that there occurs delamination between the layers causing the beam to lose its strength. This can be traceable to contaminations between the two layers, leading to gaps where they are not attached to each other. The Young's modulus at 10 layers thick was 6,34 GPa for the ME602.

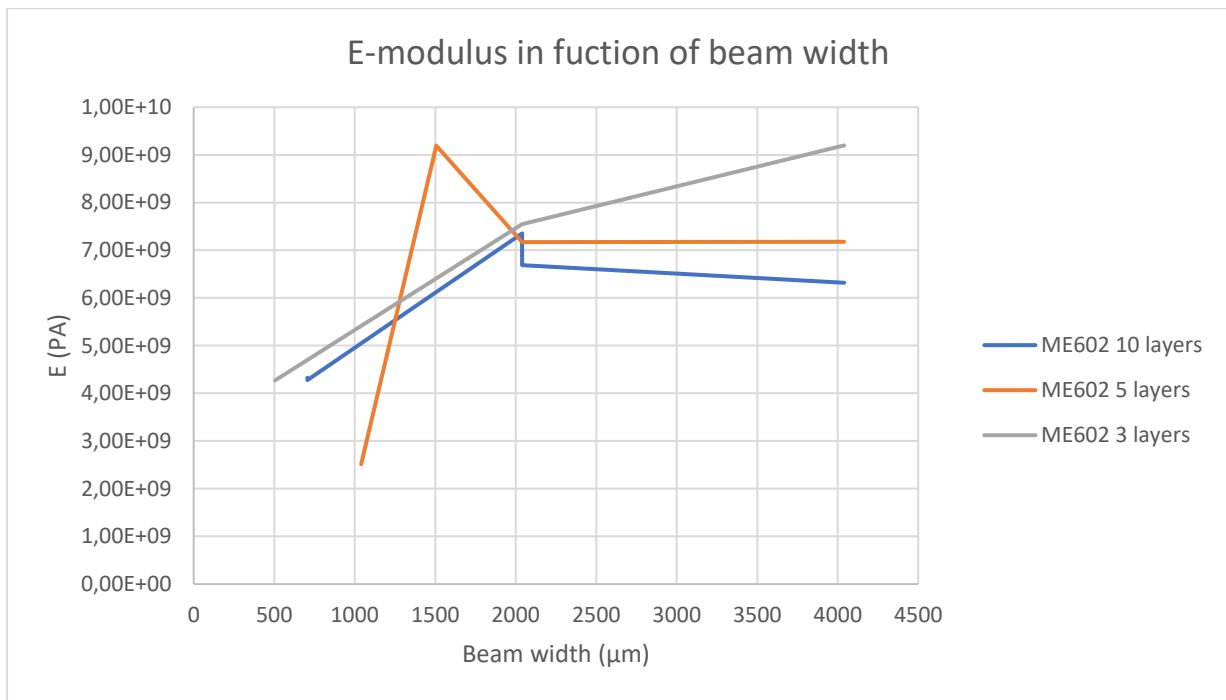


Figure 45: The Young's modulus has no direct correlation to beam width for Dupont ME602 [23]

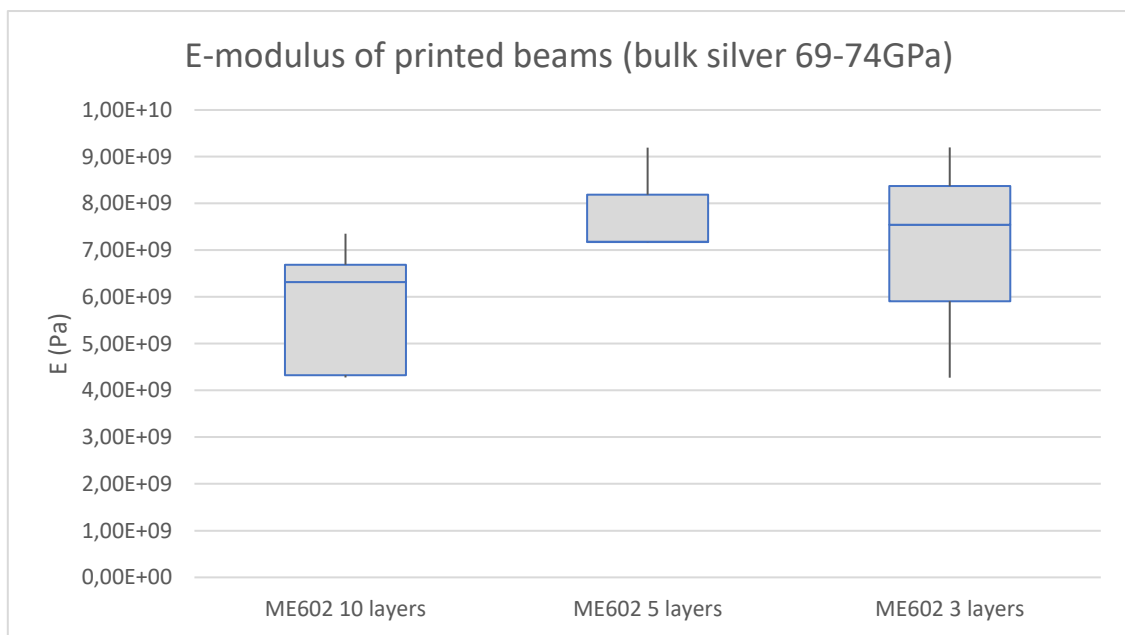


Figure 46: The Young's modulus of the printed beams for Dupont ME602 decreases with higher number of layers [23]

Because the printed beams of the ECI1011 ink all curled up into a U-shape during the release from the sacrificial layer the criteria for a perfect beam are not met. Therefore, most of the measurements were incorrect being higher than the value of bulk silver. One sample, however had no curling. A value of 34 GPa at 10 layers thick was measured for this beam, comparing this to literature [22], [27], makes it a possible estimation.

For this same reason, the bending under self-weight was no representative value. The beams of ECI were curled up into a U-shape whilst the samples made from the Dupont ME602 ink were deformed at the base by the glue applied. The glue would cause the beam to curl up into the glue or stick up or down due to the glue pulling or pushing it up or down.

The reference design (Figure 1) was simplified to a beam of 200  $\mu\text{m}$  wide (combining flexure and hot arm) and 100  $\mu\text{m}$  thick, using the Young's moduli found for both inks at 10 layers thick, the deflection was calculated at the tip of the beam at varying lengths (Figure 47). In this simplified model the cold arm is 4/5 of the length of the hot arm, the width stays 1 mm and its mass is a point load applied at the tip of the beam. We can see that the maximum length for the ME602 is around 9 mm and for the ECI1011 around 10,5 mm, longer dimensions will sag more than 100  $\mu\text{m}$ , which is the anchor height. This result confirms the usability of both inks for the reference design which has an overhang of 5 mm. Although the difference in Young's modulus is relatively large, due to the lower density of the ME602 the sag at the tip of the beams is not overwhelmingly great.

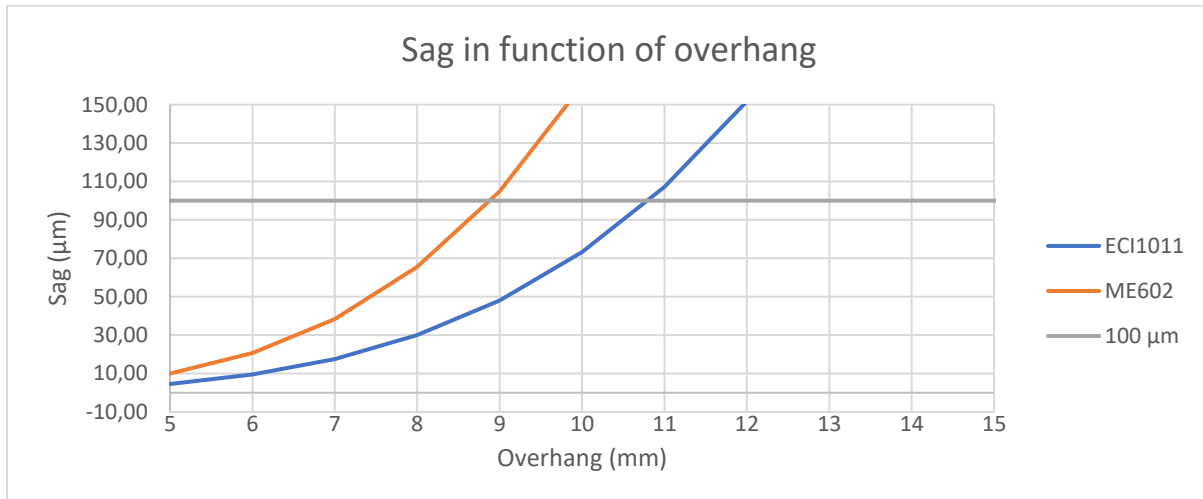


Figure 47: Simulated deflection in function of beam length (200  $\mu\text{m}$  width, 100  $\mu\text{m}$  thickness). Both inks can print long enough freestanding structures in comparison to the reference design

#### 4.3.4. Discussion of the results of the freestanding beam

The PVA 25 wt% foil ink is the best material for the sacrificial layer, it dissolves very quickly and does not need to be cut loose to release the print from the glass substrate. The ECI1011 ink is the strongest ink out of the two, although it is very brittle. However, due to its higher density the deflection due to self-weight of the ECI1011 ink is not significantly smaller (Figure 47). When handling the printed beams of ECI1011 with tweezers they often broke. The releasing process works as intended with the only downside being the curling due to residual stress in the beams. The aligning step of the anchors to the sacrificial layer proved to be difficult, this problem was bypassed by printing the whole structure on top of the sacrificial layer. Once the printed structure was then released it could be transferred to another substrate.

The solution to the residual stress in the beams (Figure 44) could be to print the beams directly onto a PVA film without a glass substrate. Since PVA is flexible, the stress that builds up due to the constrained sintering might be reduced or even entirely eliminated. The problem of the ECI1011 ink breaking can be solved by printing with the anchors directly onto desired end-product. This eliminates the transfer step, however, it takes away the option to print onto PVA film to void the residual stresses.



## 4.4. Printed MEMS

To test the whole picture, a printed MEMS based on the reference design was made to see whether an actuation was possible. In chapter 4.1.1. problems that occurred during the printing process are discussed. In 4.2.2. Characterisation the properties of the MEMS are summarised and analysed.

### 4.4.1. Printing

The NIR sintering setup made it possible to accurately deposit each layer on top of each other. The samples could be cured on the printing bed without being moved. A downside of the NIR sintering was that due to the printing bed being reflective, the bottom of the samples was also heated. When the lamp was used above 70% power level, the bottom of the samples became so hot that the PVA beneath the silver burned. Causing the samples to stick to the glass, they could not be removed using hot water.

### 4.4.2. Characterisation

To see how the heat generation was distributed in the MEMS, a FLIR image was made. The MEMS used had a hot arm width of 1 mm, was 12 mm long and approx. 35  $\mu\text{m}$  thick. In Figure 48 it can be seen that the majority of the heat generation takes place in the hot arm. While the hot arm is around 380  $^{\circ}\text{C}$ , the cold arm is 80  $^{\circ}\text{C}$  warm, this causes the hot arm to expand more than the cold arm, leading to deflections. The deflection of the MEMS was observed. For this, another MEMS was used with a hot arm of 500  $\mu\text{m}$  wide, 20 mm long and 35  $\mu\text{m}$  thick (Figure 49). It was seen that the first time a current was applied the MEMS deformed greatly. This can be traced back to the electric sintering as discussed before, the hot arm will shrink and since the structure is not constrained it will deform randomly, in this case it curled upwards and moved a bit to the side. After the initial current caused the MEMS to sinter, deflections could be seen when a current was applied. At 3 A the horizontal deflection was about 100  $\mu\text{m}$ , however, the vertical deflection was around 1 mm. All the printed MEMS could support their self-weight, the sag was however fairly large for the largest MEMS being around 2 mm.

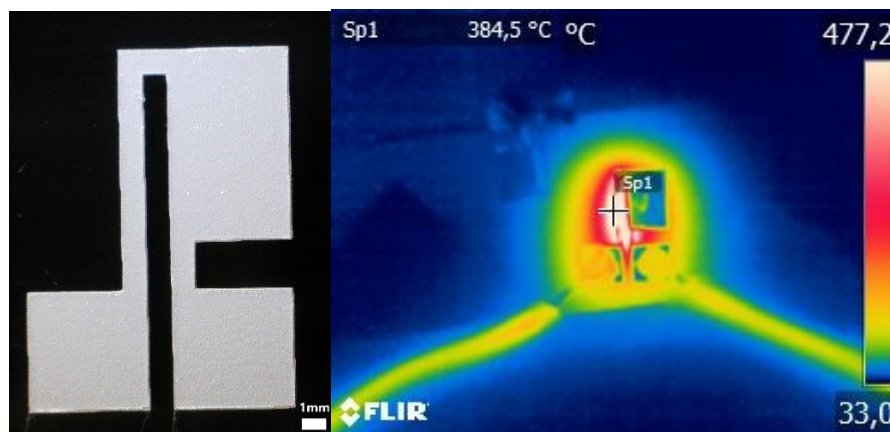
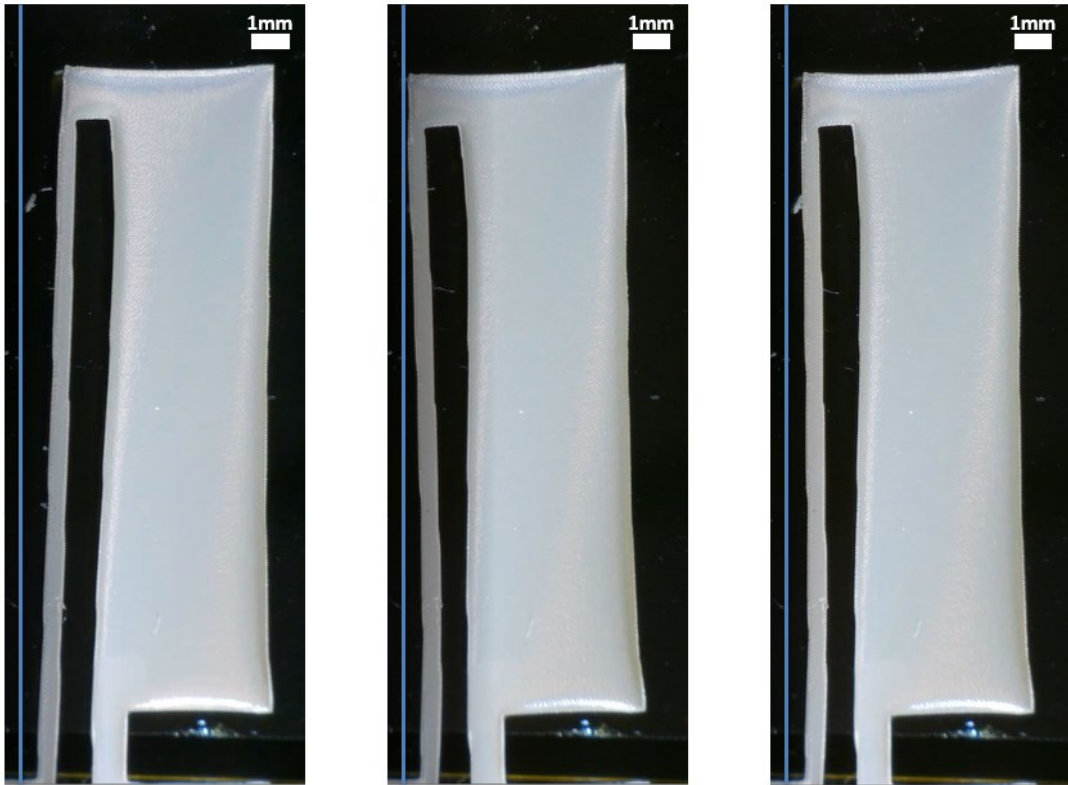


Figure 48: Printed mems (left) and heat generation at 4 A (right). The heat generation primarily takes place in the hot arm



**Before current**

**After 3 A**

**Deflection at 3 A**

*Figure 49: Applying a current to the MEMS for the first time will greatly deform it. Afterwards, applying current will lead to a deflection*



## 5. Conclusion

The goal of this thesis was to find a production process and materials to print/coat a thermal actuator MEMS, using the reference design as a guide. PEO and PMMA were dismissed as a sacrificial material. It was found that PEO cannot withstand the elevated temperatures during the curing step (Figure 25). The PEO layer will melt, greatly impacting the printed layers on top. PMMA was not chosen because of the volatility of the ink. PVA was found to be the most suitable material to use as a sacrificial layer, the PVA Avalon foil from Madeira in a 25 wt% solution in deionised water is easily applied on a glass substrate using blade coating (Table 15). With further optimisation the layer thickness of the deposited layer can be accurately controlled. Roughnesses as low as 46 nm (Ra) (Table 15) could be achieved. When put in water at 85 °C this sacrificial layer will dissolve under 15 minutes.

For the structural material both inks have shown promising results. As anticipated the inks show slump, meaning that the resulting print is larger than the mesh opening (Figure 34). This could be up to 300% for lines of 106 µm wide and 10 layers thick. In order to achieve the desired dimensions of the reference design the mesh opening must be adjusted. To achieve 100 µm linewidths a mesh of 220 TPC with a wire diameter of 14,7 µm and a mesh opening of 30 µm is recommended. Because of the high mesh count, the choice of inks usable on the mesh is greatly reduced. Therefore, it is proposed that the minimum feature width is raised to 300 µm, which will allow for a broader gamma of inks to be used.

From the thermal tests it was found that the ME602 ink generates the most heat (Figure 36), this is backed by the resistivity measurements which shows that the ME602 (2,57E-06 Ωm) is a factor of 5 more resistive to current than the ECI1011 ink (8,2643E-08 Ωm) (Table 17). The highest temperatures measured were 190 °C for the ME602 beam of 3,2\*8,7\*0,014 mm and 172 °C for the ECI1011 beam of 1,6\*6,6\*0,016 mm both at 4 A. The ECI1011, although had almost the same heat generation which cast doubt on the measured values. It was first thought that the adhesion used to affix the beam might generate heat (Figure 37). This suspicion was however debunked, after recalibrating the camera, it was found that the adhesion always was lower in temperature than the beam of ECI1011. The temperatures that were achieved could generate displacements of up to 224 µm in the reference design according to simulations (Table 19). These displacements are, however, not within the desired limits. The deflection could not be higher due to the beams of ME602 burning out at currents higher than 4 A, the ECI1011 ink might give better results as it was tested to currents of up to 6 A. In a later test, temperatures of 380°C at 4 A were achieved in a MEMS design printed using the ECI1011 ink (Figure 48). No FLIR measurements were made at currents above 4 A because the cables used to apply the currents could not withstand the heat for long periods of time.

The curing temperature also has an effect on thermal and electrical conductivity, higher and longer curing times will increase thermal conductivity and decrease electrical resistivity. However, the curing of a thermal actuator MEMS cannot accurately be controlled due to the high temperatures that occur because of the joule-effect during the working cycle of the MEMS.

The microflake ink has a considerably lower Young's modulus of 6,34 GPa for 10 printed layers compared to ECI1011 with 34 GPa with 10 layers. However, due to its lower density, the dimensions that can be realised for a freestanding structure do not differ much from the more rigid ECI1011 ink (Figure 47). Using the same ratios for the components (thickness constant at 100  $\mu\text{m}$ ) as in the reference design (Figure 1) the ME602 ink could support a MEMS of 9 mm freestanding length and the ECI1011 one of 10,5 mm, both with sag less than 100  $\mu\text{m}$ .

These measurements make both inks viable options to use as the structural material. There are, however, some drawbacks to both inks. The ECI1011 was very brittle and broke very easily, for the ME602 was observed that it had elastic behaviour. This is not ideal for the MEMS if the displacement is meant to exert a force.

Overall, it can be said that the reference design is not feasible to create using screen printing techniques. The minimum feature width is too small to be printed, the achievable deflection of the MEMS is also only half of what was simulated in the reference design (Table 2). The temperatures realised in practice are not near the simulated temperature of 900 K and are also deemed impossible due to the material burning out at in the hot arm. The highest temperature measured was  $\sim 650$  K.

A proof of concept was made (Figure 49). There are however still problems that need to be solved. Internal stresses caused the MEMS to deform upon release of the sacrificial layer. Electric sintering causes the freestanding structure to deform even further. This has a major impact on the deflection that can be realised as the MEMS does not move in the horizontal plane alone, as was intended. Deflections in the vertical plane of 1 mm were observed, whilst the deflection in the horizontal plane was only approx. 100  $\mu\text{m}$ . Further research is needed to develop methods to prevent the MEMS from deforming during the releasing process and the initial appliance of current.

## 6. Recommendations

### 6.1. Recommendations for future research

From the measurements of the blade coated PVA samples it could be stated that there is a correlation between the wet layer thickness and the dry layer thickness. There seems to be a maximum value of wet layer thickness, once this value is exceeded, the dry layer thickness no longer increases. A model could be designed to predict the dry layer thickness in function of wet layer thickness and ink composition.

The exact strength of the ECI1011 ink could not be determined, the tested samples were also only cured at one temperature. It is thought that curing temperatures will also have an impact on the strength of the print as well as current passing through. The change of properties due to the current could be tested by letting the printed sample go through a working cycle and testing the parameters afterwards. Tensile testing of samples might offer more insight to the change of these parameters. The maximum heat/current that can be realised in the structural material before burning out in relation to the dimensions also needs to be characterised.

Another problem that needs solving is the curling due to stress in the structures, the exact cause of the stress building up needs to be found to find a solution. Drying the layers without sintering them in between layer depositions, and afterwards curing the whole print might form a solution to this problem. A different factor that deformed the structure was the first appliance of current, a method needs to be found to minimise the deformation in this step. This would greatly improve the quality of the produced MEMS.

Although the dimensions of freestanding structures that could be realised using the ME602 ink met the criteria, it was observed that the printed beams showed elastic behaviour. This is not a desired property, the beams printed with ECI1011 ink were also very brittle and broke easily. The ECI1006 ink could form a solution. It is a microparticle ink with properties in between the ECI1011 and ME602 ink. Lastly the dimensions of the MEMS itself can also be altered to vary the systems displacement, strength, and other properties.

## 6.2. Recommendations for industrialisation

In this chapter a short proposal is made to transfer the experiments into an industrial setting.

A flow chart of the process can be seen in Figure 50. Roll-to-roll blade or knife coating is a proven technique, it can be used to efficiently coat the sacrificial layer on top of a substrate of choice. It is then immediately dried in an oven. After the sacrificial layer is applied and cured an optional step is to cut and peel away the area for the anchors. The substrate with sacrificial layer applied is then put into a screen printer. Using cameras and software the screen can be aligned with the substrate and the depositing of structural material can start. Between each layer the substrate needs to be taken out of the printer and cured in an oven. This can be done by using grippers or a conveyor belt. Once the desired number of layers is printed the batch is cured one last time before being put in hot water to dissolve the sacrificial layer. Because the printed layers are so thin and fragile this needs to happen very slowly as to cause no sudden movements in the MEMS which might break it. To ensure that the sacrificial layer does dissolve a constant stream of new hot water is needed. This also needs to happen with as little turbulence as possible to avoid breaking of the structural material. When the sacrificial layer is dissolved, and the MEMS have released from the substrate, the first problems occur. Due to the brittle and/or fragile nature of the printed MEMS, automation becomes almost impossible. It is therefore proposed that from now on the rest is done by manual labour i.e. the transfer from water to the drying stage and from drying to the intended substrate.

A NIR sintering setup could be used, eliminating the cameras and software needed to align the sample as it does not need to be moved to cure. However, the last curing step still needs to happen in an oven.

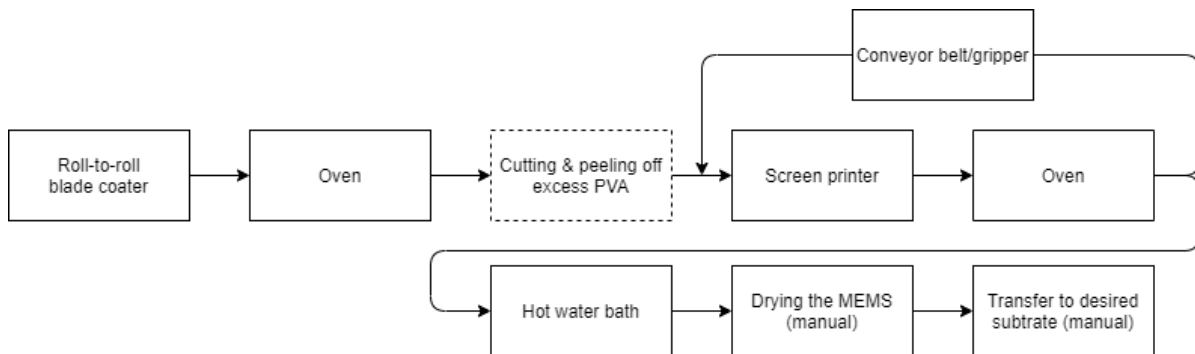


Figure 50: Flowchart of the automated printing process

## References

- [1] Prime Faraday Partnership, An Introduction to MEMS, Loughborough: Loughborough University, 2002.
- [2] “What is MEMS technology?,” MEMS-exchange.org, [Online]. Available: <https://www.mems-exchange.org/MEMS/what-is.html>. [Accessed 10 September 2020].
- [3] A. Madni and L. Wan, “Microelectromechanical systems (MEMS): an overview of the current state-of-the-art,” in *IEEE Aerospace Conference Proceedings*, Snowmass, CO, USA, 1998.
- [4] L. Swangoo, P. Sangiun and C. Dong-Il, “The surface/bulk Micromachining (SBM) process: A new Method for fabricating released MEMS in single Crystal silicon,” *Journal of Microelectromechanical Systems*, vol. 8, no. 4, pp. 409-416, 1998.
- [5] P. M. Nitatigour, “Mechanical sensors,” in *Micromanufacturing and Nanotechnology*, Berlin, Springer Berlin Heidelberg, 2006, pp. 107-130.
- [6] P. R. Kuppens, J. L. Herder and N. Tolou, “Permanent Stiffness reduction by thermal oxidation of silicon,” *IEEE journal of Microelectromechanical Systems*, vol. 28, no. 5, pp. 900-909, 2019.
- [7] Q. Liang, Y. ZhenChuan and Y. GuiZhen, “A CMOS compatible process for monolithic integration of high-aspect-ratio bulk silicon microstructures,” *Science China Information Sciences*, vol. 57, no. 8, pp. 1-7, 2014.
- [8] S. Veda, “pMEMS proposal,” Unpublished manuscript, Nitte Meenakshi Institute of Technology, India, 2020.
- [9] J. A. Dziuban and R. Walczak, “Etching Microwave Silicon [EMSi]-Microwave Enhanced Fast Deep Anisotropic Etching of Silicon for Micro-Electromechanical Systems [MEMS],” *Sensors and Materials*, vol. 13, no. 1, pp. 41-55, 2001.
- [10] R. H. Daniel, P. S. Nathan and M. G. A., “MEMS Lithography and Micromachining Techniques,” in *MEMS Materials and Processes Handbook*, Boston, MA, Springer, 2011, pp. 667-753.
- [11] P. A. David, S. Monika and Y. Yong-Kyu, “Additive Processes for Metals,” in *MEMS Materials and Processes Handbook*, Boston, MA, Springer, 2011, pp. 137-191.
- [12] B. A., M. M. and H. Schmidt, “Doctor Blade,” in *Sol-Gel Technologies for Glass Producers and Users*, Boston, MA, Springer, 2004, pp. 89-92.
- [13] Y. Wei, R. Torah, K. Yang, S. Beeby and J. Tudor, “Screen printing of a capacitive cantilever-based motion sensor on fabric using a novel sacrificial layer process for smart fabric applications,” *Measurement Science and Technology*, vol. 24, no. 7, pp. 75-104, 2013.



- [14] F. Zicarelli and A. Mesh, "Capability, limits and considerations for screen printing," [printedelectronics.com](https://www.printedelectronics.com), 8 November 2012. [Online]. Available: <https://www.printedelectronicsworld.com/articles/4885/capability-limits-and-considerations-for-screen-printing>. [Accessed 4 October 2020].
- [15] L. Jiantong, M. Lemme and M. Östling, "Ink-jet Printing of 2D Layered Materials," *ChemPhysChem*, vol. 15, no. 16, pp. 3427-3434, 2014.
- [16] G. Jabbour, R. Radspinner and N. Peyghambarian, "Screen printing for the fabrication of organic light-emitting devices," *IEEE Journal of Selected Topics in Quantum Electronics*, vol. 7, no. 5, pp. 769-773, 2001.
- [17] D. Chen, L. Zhao, H. Diao, W. Zhang and G. Wang, "Rheological properties and related screen-printing performance of low-temperature silver pastes for a-Si:H/c-Si heterojunction solar cells," *Journal of Materials Science. Materials in Electronics*, vol. 25, no. 12, pp. 5322-5330, 2014.
- [18] S. Abbott, *How to be a great screen printer*, Wantage: Macdermid Autotype Limited, 2008.
- [19] C. Clasen, P. M. Phillips, L. Palangetic and J. Vermant, "Dispensing of rheologically complex fluids: The map of misery," *AIChE Journal*, vol. 58, no. 10, pp. 3242-3255, 2012.
- [20] V. S. and Z. Wang, "Fine line screen printed electrodes for polymer microfluidics," in *2010 12th Electronics Packaging Technology Conference*, Singapore, 2010.
- [21] L. Riadh, D. Hélène, D. Isabelle and L. Claude, "Force Sensors Based on Screen-Printed Cantilevers," *IEEE Sensors Journal*, vol. 10, no. 6, pp. 1133-1137, 2010.
- [22] S. P. Eung, C. Yenhao, K. L. Tsu-Jae and S. Vivek, "A New Switching Device for Printed Electronics: Inkjet-Printed Microelectromechanical Relay," *Nano Lett.*, vol. 13, no. 11, p. 5355-5360, 2013.
- [23] AZOM, "Silver - Applications and Properties of Silver," AZO Materials, 21 July 2001. [Online]. Available: <https://www.azom.com/properties.aspx?ArticleID=600>. [Accessed 3 March 2021].
- [24] S. P. Eung, C. Yenhao, K. L. Tsu-Jae and S. V., "Inkjet-printed micro-electro-mechanical switches," in *2011 International Electron Devices Meeting*, Washington, DC, 2011.
- [25] E.W. Lam, H. Li and M. Schmidt, "Silver nanoparticle structures realized by digital surface micromachining," in *TRANSDUCERS 2009 - 2009 International Solid-State Sensors, Actuators and Microsystems Conference*, Denver, CO, 2009.
- [26] R. Almudena, F.-S. José, A.-A. Manuel, A. L.-V. Juan, F. C.-V. Luis and J. P. Alberto, "Improved manufacturing process for printed cantilevers by using water removable sacrificial substrate," *Sensors and Actuators A: Physical*, no. 235, pp. 171-181, 2015.

- [27] R. Lakhmi, "Determination of Young's Moduli for free-standing screenprinted thick film layers used in MEMS," in *20th workshop on micromachining, micro mechanics and micro systems*, Toulouse, 2009.
- [28] E. Andreas and L. Wilfried, "Solution-deposited PEDOT for transparent conductive applications," *MRS Bulletin*, vol. 36, no. 10, pp. 794-798, 2011.
- [29] K. Jong-Seon, H. Jeon, Y. Hae-Wook, B. Youn-Kyoung, H. K. Kyoung, W. K. Dae and J. Hee-Tae, "Generation of Monodisperse, Shape-Controlled Single and Hybrid Core-Shell Nanoparticles via a Simple One-Step Process," *Advanced functional materials*, vol. 24, no. 6, pp. 841-847, 2014.
- [30] V. Evangelos, S. Sotirios, P. Nikolaos, E. Konstantinos and A. C. Stelios, "Conductivity Degradation Study of PEDOT: PSS Films under Heat Treatment in Helium and Atmospheric Air," *Open Journal of Organic Polymer Materials*, vol. 2, no. 1, pp. 7-11, 2012.
- [31] "Poly(3,4-ethylenedioxythiophene)-poly(styrenesulfonate)," ChemicalBook, 2017. [Online]. Available: [https://www.chemicalbook.com/chemicalproductproperty\\_en\\_cb3165285.htm](https://www.chemicalbook.com/chemicalproductproperty_en_cb3165285.htm). [Accessed 1 May 2021].
- [32] R. V. Silvano, C. L. Patricia, L. P. Alessandra, A. H. J. Marco, G. N. Miguel and C. S. C. Carla, "Thermal Properties of Poly (Methyl Methacrylate)/Organomodified Montmorillonite Nanocomposites Obtained by in situ Photopolymerization," *Materials Research*, vol. 17, no. 1, pp. 265-270, 2014.
- [33] "POLY(METHYL METHACRYLATE) ISOTACTIC," ChemicalBook, 2017. [Online]. Available: [https://www.chemicalbook.com/ProductList\\_en.aspx?kwd=PMMA](https://www.chemicalbook.com/ProductList_en.aspx?kwd=PMMA). [Accessed 2 May 2021].
- [34] V. Laura, S. Dagmar, A. Osmo, K. Karin, H. Jyrki and L. Ivo, "3D-printability of aqueous poly(ethylene oxide) gels," *European Polymer Journal*, vol. 120, 2019.
- [35] "Poly(ethylene glycol)," ChemicalBook, 2017. [Online]. Available: [https://www.chemicalbook.com/ProductList\\_En.aspx?kwd=PEO](https://www.chemicalbook.com/ProductList_En.aspx?kwd=PEO). [Accessed 2 May 2021].
- [36] B. Holland and J. Hay, "The thermal degradation of poly(vinyl alcohol)," *Polymer*, vol. 42, no. 16, pp. 6775-6783, 2001.
- [37] "Polyvinyl alcohol," PubChem, [Online]. Available: <https://pubchem.ncbi.nlm.nih.gov/compound/Polyvinyl-alcohol#section=Boiling-Point>. [Accessed 2 May 2021].
- [38] UHasselt, "imo-imomec services," UHasselt, [Online]. Available: <https://www.uhasselt.be/UH/IMO-services/AMS/Algemeen>. [Accessed 10 March 2021].
- [39] "NanoFab Tool: Bruker Dektak XT Profilometer," NIST, 9 November 2020. [Online]. Available: <https://www.nist.gov/laboratories/tools-instruments/nanofab-tool-bruker-dektak-xt->

profilometer#:~:text=Specifications%2FCapabilities&text=Vertical%20resolution%3A%200.1%20nm.,span%20up%20to%20150%20mm.. [Accessed 26 May 2021].

- [40] R. Goodall and A. Mortensen, "24- porous metals," in *Physical Metallurgy (fifth edition)*, Elsevier, 2014, pp. 2399-2595.
- [41] L. Dae-Geon, K. Dong Keun, M. Yoon-jae and M. Seung-Jae, "Effect of temperature on electrical conductance of inkjet-printed silver nanoparticle ink during continuous wave laser sintering," *Thin Solid Films*, vol. 546, pp. 443-447, 2013.
- [42] R. Almudena, F.-S. José, A. Manuel, L.-V. Juan A., F. C.-V. Luis and J. P. Alberto, "Design and characterization of a low thermal drift capacitive humidity sensor by inkjet-printing," *Sensors and Actuators B: Chemical*, vol. 195, pp. 123-131, 2014.
- [43] "Free Vibration of a Cantilever Beam (Continuous System)," AMRITA, 2011. [Online]. Available: <https://vlab.amrita.edu/?sub=3&brch=175&sim=1080&cnt=1>. [Accessed 30 March 2021].
- [44] M. Fateri, J.-S. Hötter and A. Gebhardt, "Experimental and theoretical investigation of buckling," *Physics Procedia*, vol. 39, pp. 464-470, 2012.
- [45] J. Polansky, N. Jeffers and J. Punch, "A hybrid approach for predicting the effective thermal conductivity of sintered porous materials," *International Journal of Thermal Sciences*, vol. 148, pp. 106-130, 2020.
- [46] hyperphysics, "Thermal Expansion Coefficients at 20 C," hyperphysics, [Online]. Available: <http://hyperphysics.phy-astr.gsu.edu/hbase/Tables/thexp.html>. [Accessed 18 March 2021].
- [47] T. Shailendra Kumar, B. Someshekara and M. Krishna K., "Design and fabrication of screen printed microheater," *Microsystem Technologies*, vol. 24, pp. 3273-3281, 2018.
- [48] Dupont, "Dupont ME602 TDS," 2019. [Online]. Available: <https://www.dupont.com/content/dam/dupont/amer/us/en/products/ei-transformation/documents/ME602.pdf>. [Accessed 10 October 2020].
- [49] LOCTITE, "LOCTITE ECI1011 E&C," November 2016. [Online]. Available: <http://tds.henkel.com/tds5/Studio/ShowPDF/243%20NEW-EN?pid=ECI%201011%20EC&format=MTR&subformat=HYS&language=EN&plant=WERC S>. [Accessed 10 October 2020].
- [50] E. W. Lam, "Fabrication and Material Characterization of Silver Cantilevers via Direct Surface Micromachining," M.S. Thesis, Massachusetts Institute of Technology, Washington, 2008.
- [51] "Performing van der Pauw Sheet," 2012. [Online]. Available: [https://download.tek.com/document/S530\\_VanDerPauwSheetRstnce.pdf](https://download.tek.com/document/S530_VanDerPauwSheetRstnce.pdf). [Accessed 10 March 2021].

- [52] “Emissivity Coefficient Materials,” Engineering ToolBox, 2003. [Online]. Available: [https://www.engineeringtoolbox.com/emissivity-coefficients-d\\_447.html](https://www.engineeringtoolbox.com/emissivity-coefficients-d_447.html). [Accessed 11 May 2021].
- [53] “Linear Thermal Expansion,” Engineering ToolBox, 2008. [Online]. Available: [https://www.engineeringtoolbox.com/linear-thermal-expansion-d\\_1379.html](https://www.engineeringtoolbox.com/linear-thermal-expansion-d_1379.html). [Accessed 20 May 2021].
- [54] P. Sudeshna, Y. Munaiah, D. Piyush and N. Tharangattu, “Anisotropic Mechanical Responses of Poly(Ethylene Oxide)-Based Lithium Ions Containing Solid Polymer Electrolytes,” 2019. [Online]. Available: [https://www.researchgate.net/publication/336258671\\_Anisotropic\\_Mechanical\\_Responses\\_of\\_PolyEthylene\\_Oxide-Based\\_Lithium\\_Ions\\_Containing\\_Solid\\_Polymer\\_Electrolytes](https://www.researchgate.net/publication/336258671_Anisotropic_Mechanical_Responses_of_PolyEthylene_Oxide-Based_Lithium_Ions_Containing_Solid_Polymer_Electrolytes). [Accessed 28 March 2021].
- [55] F. Urushizaki, “Swelling and mechanical properties of poly(vinyl alcohol) hydrogels,” *International Journal of Pharmaceutics*, vol. 58, no. 2, pp. 135-142, 1990.
- [56] G. Han-Wen, Y. Rong-Jie, H. g Ji-Yu and Y. Lei, “Rheological behaviors of PVA/H<sub>2</sub>O solutions of high-polymer concentration,” *Journal of Applied Polymer Science*, vol. 116, no. 3, pp. 1459-1466, 2010.
- [57] I. Biesmans and D. Reenaers, “Optimaliseren van het sintergedrag voor printbare elektronica,” UHasselt, M.S. Thesis, Diepenbeek, 2017.
- [58] E. Olevsky, T. Tadesse Molla, H. Lund Frandsen, R. Bjørk, V. Esposito, D. Wei Ni, A. Ilyina and N. Pryds, “Sintering of Multilayered Porous Structures: Part I-Constitutive Models,” *Journal of the American Ceramic Society*, vol. 96, no. 8, pp. 2657-2665, 2013.
- [59] R. A. Coutu, R. S. LaFleur, J. P. K. Walton and L. A. Starman, “Thermal Management Using MEMS Bimorph Cantilever Beams,” *Experimental Mechanics*, no. 56, p. 1293–1303, 2016.
- [60] G. Cleas, “Study of surface-micromachined poly-silicon-germanium cantilevers,” M.S. Thesis, Eindhoven University of Technology, Eindhoven, 2005.
- [61] H. M. Cronin, S. Zlatka, M. Brown, M. Shkunov and S. R. P. Silva, “Photonic Curing of Low-Cost Aqueous Silver Flake Inks for Printed Conductors with Increased Yield,” *ACS Appl. Mater. Interfaces*, vol. 10, no. 25, p. 21398–21410, 2018.
- [62] D. Sougata, B. Joydeep and B. Santanu, “How does spacer length of imidazolium gemini surfactants control the fabrication of 2D-Langmuir films of silver-nanoparticles at the air–water interface?,” *Journal of Colloid and Interface Science*, vol. 430, pp. 85-92, 2014.



# Appendices

|   |    |
|---|----|
| Appendix A – Simulations of the reference design..... | 76 |
| Appendix B – ISO4288 .....                            | 79 |
| Appendix C – PVA parameters .....                     | 80 |
| Appendix D – Printed PVA stacks.....                  | 82 |
| Appendix E – PTC method.....                          | 83 |

# Appendix A – Simulations of the reference design

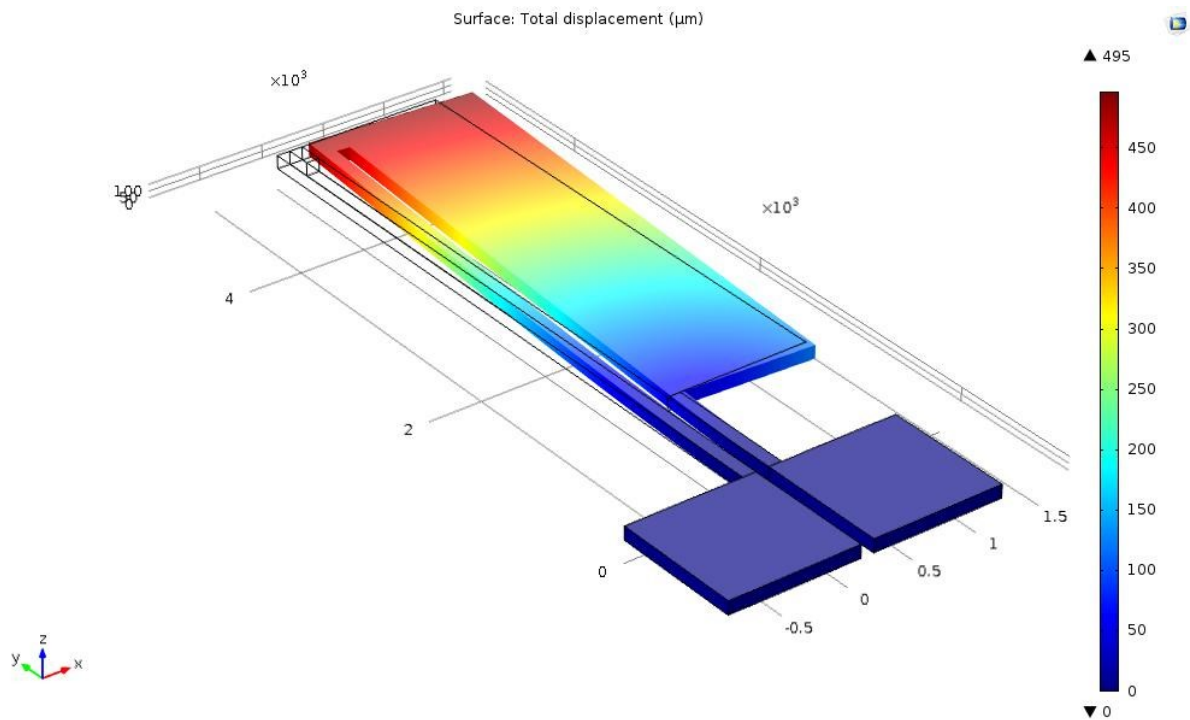


Fig 2.3: Variation in displacement along the length of the heat actuator

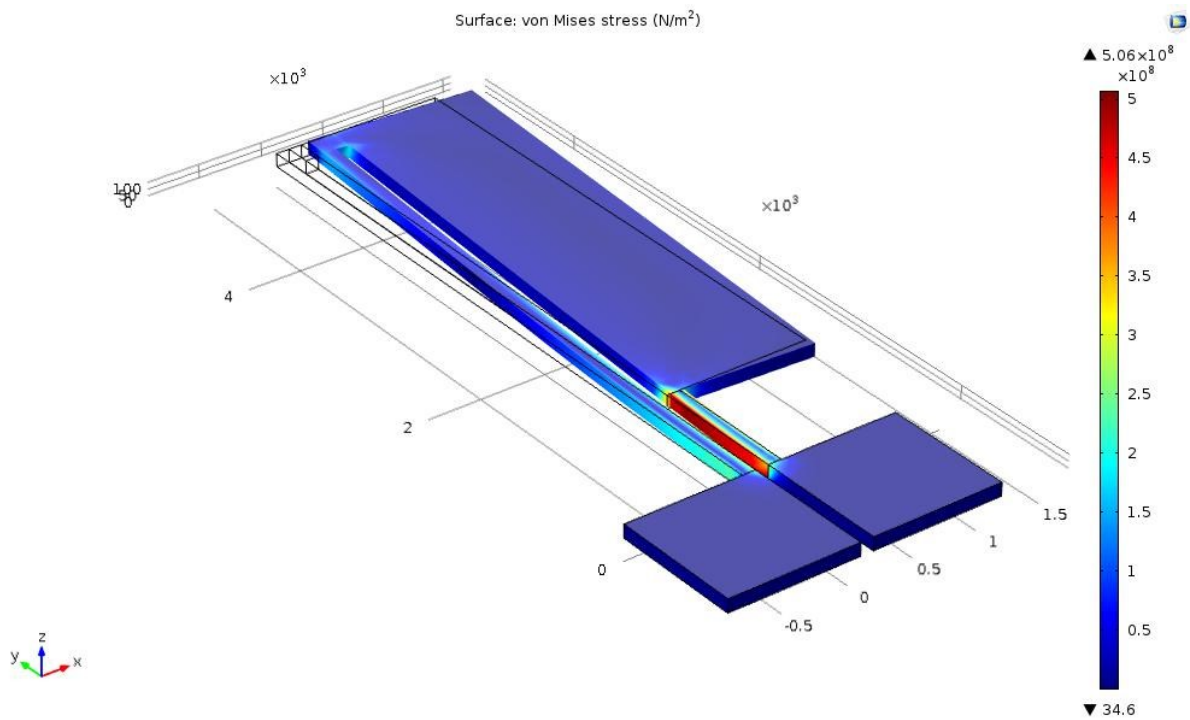


Fig 2.4: Stress distribution

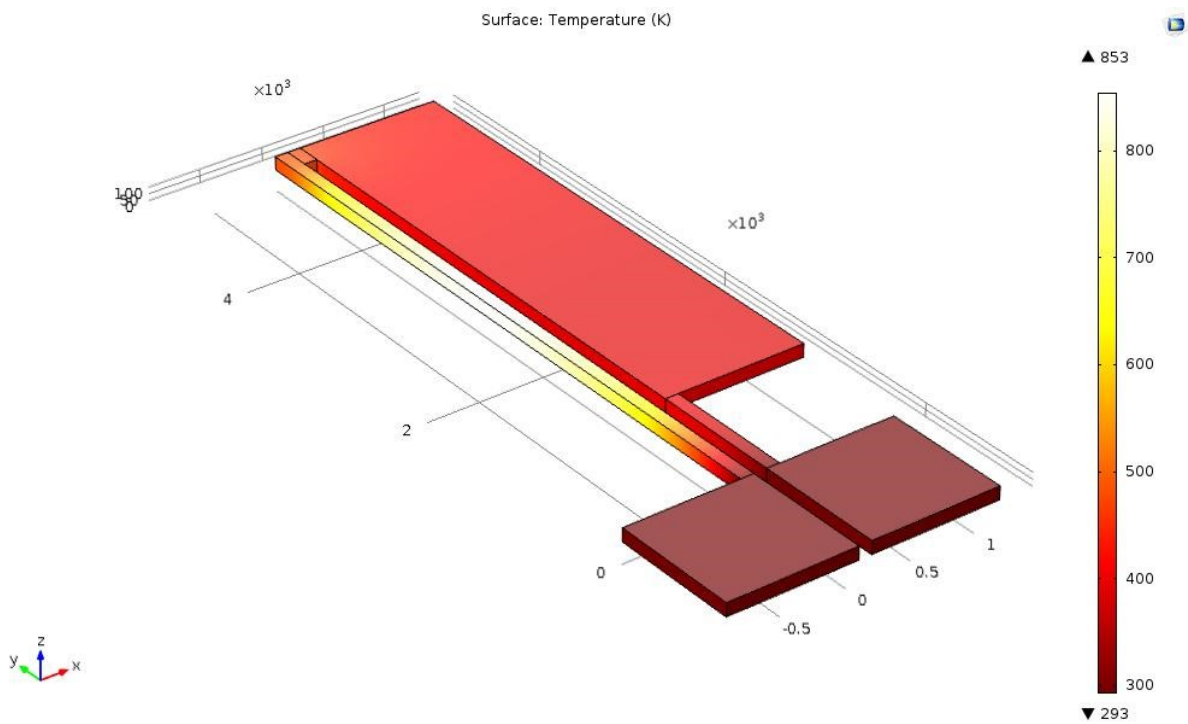
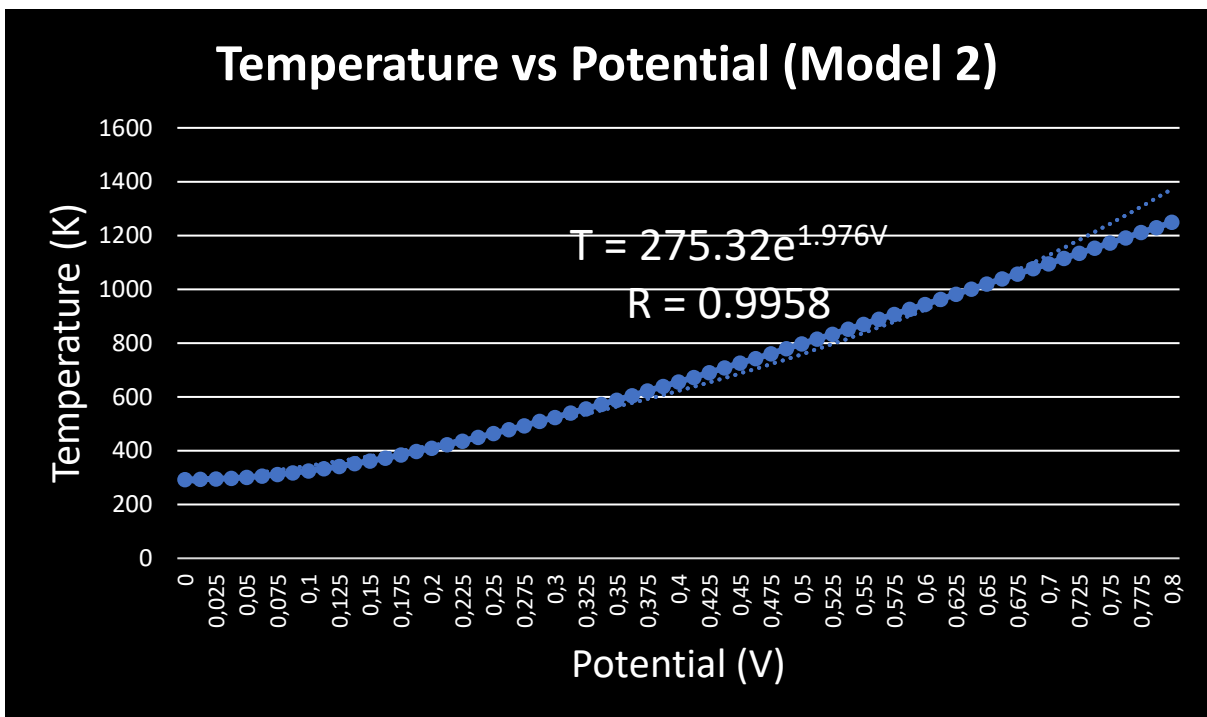
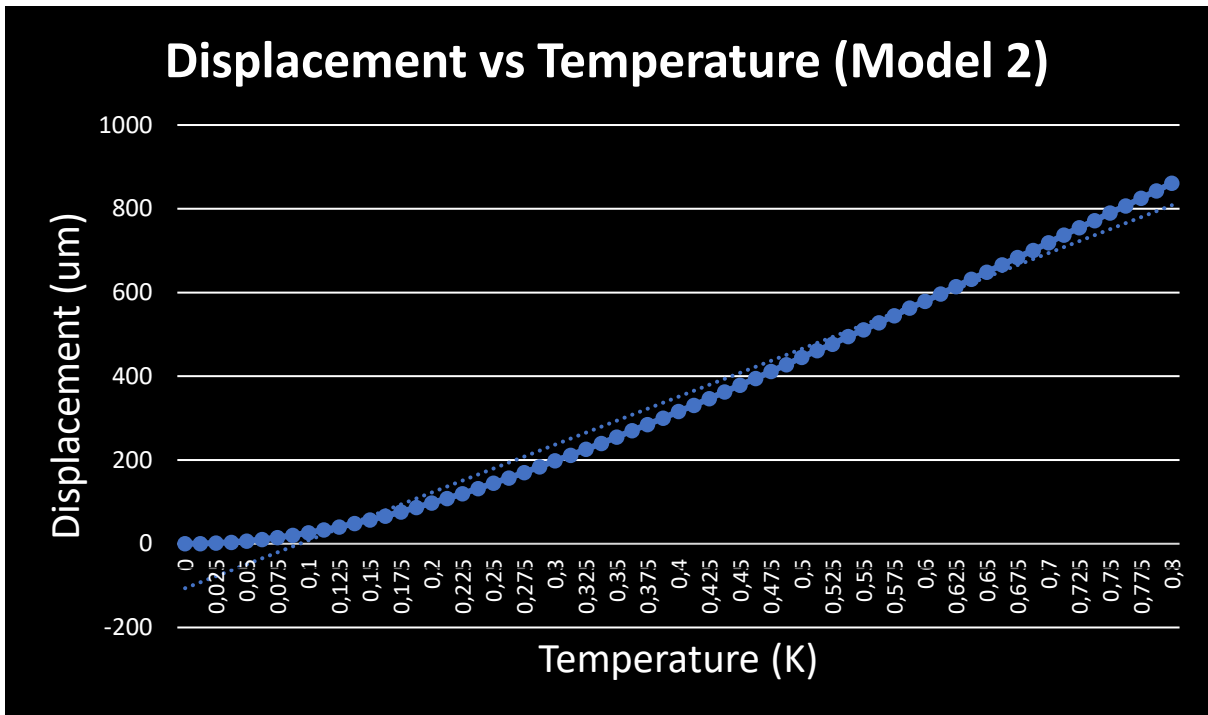


Fig 2.2: Study of temperature distribution on the application of electric potential of 0.538 V







Plot 2.2 : Graphical plot of the variation in Displacement with respect to Potential

# Appendix B – ISO4288

## Measuring condition: R-parameter ISO4288: '96

| Non-periodic profile    |       |                       |       | Periodic profile or RSm |       | Measuring Condition                                       |   |
|-------------------------|-------|-----------------------|-------|-------------------------|-------|---|---|
| Ra, Rq, Rsk, Rku or RΔq |       | Rz, Rv, Rp, Rc, or Rt |       | RSm (mm)                |       | Sampling length: $\ell r = \text{CutOff } \lambda c$ (mm) | Evaluation length $\ell n$ (mm) = $5 \times \ell r$ |
| Over>                   | Less≤ | Over>                 | Less≤ | Over>                   | Less≤ |   |   |
| 0.006                   | 0.02  | 0.025                 | 0.1   | 0.013                   | 0.04  | 0.08  | 0.4   |
| 0.02                    | 0.1   | 0.1                   | 0.5   | 0.04                    | 0.13  | 0.25  | 1.25  |
| 0.1                     | 2     | 0.5                   | 10    | 0.13                    | 0.4   | 0.8   | 4   |
| 2                       | 10    | 10                    | 50    | 0.4                     | 1.3   | 2.5   | 12.5  |
| 10                      | 80    | 50                    | 200   | 1.3                     | 4     | 8   | 40  |

## Measuring condition : P-parameter ISO4288: '96

| Stylus radius    | $\lambda s$       | $\lambda c$ | No. of $\ell p = n$ | S. length $\ell p$              | E. length $\ell n$ |
|------------------|-------------------|-------------|---------------------|---------------------------------|--------------------|
| 2 $\mu\text{m}$  | 2.5 $\mu\text{m}$ | -           | 1                   | Length of feature (Plane, Line) | Length of feature  |
| 5 $\mu\text{m}$  | 8 $\mu\text{m}$   |             |                     |                                 |                    |
| 10 $\mu\text{m}$ | 25 $\mu\text{m}$  |             |                     |                                 |                    |

## Measuring condition: W-parameter ISO1302: '02

| $\lambda c$                 | $\lambda f$                 | No. of $\ell w = m$ | S. length $\ell w$ | E. length $\ell n$ |
|-----------------------------|-----------------------------|---------------------|--------------------|--------------------|
| $\lambda c$ (for roughness) | $n\lambda c$ (n: specified) | m: specified        | $\lambda f$        | $m\lambda f$       |

## Appendix C – PVA parameters

| ink                  | solvent         | added substance                    | Stirring step 1  | Stirring step 2 | Step 3                        | Step 4              |
|----------------------|-----------------|------------------------------------|--|-----------------|-------------------------------|---------------------|
| PVA powder 5 wt%     | deionised water | PVA powder mw 146 000 – 186 000    | 30 min. at 80°C  | 30 min at 60°C  | /                             | /                   |
| PVA powder 10 wt%    | deionised water | PVA powder mw 146 000 – 186 000    | 30 min. at 80°C  | 30 min at 60°C  | /                             | /                   |
| PVA powder 15 wt%    | deionised water | PVA powder mw 146 000 – 186 000    | 30 min. at 80°C  | 30 min at 60°C  | /                             | /                   |
| PVA foil 25 wt%      | deionised water | PVA foil avalon ultra from madeira | 30 min. at 80°C  | 2h at 60°C      | Vacuum chamber - 0.8 bar      | Speedmixer sequence |
| PVA web 17 wt%       | deionised water | PVA web avalon plus from madeira   | 30 min. at 80°C  | 30 min at 60°C  | Vacuum chamber - 0.8 bar      | Speedmixer sequence |
| PVA 20% powder 27000 | deionised water | PVA powder mw 27 000               | 4 hours 80°C   | 8 hours 60°C    | /                             | /                   |
| sample name          | ink             | method used                        | parameters   |                 | sintering step between layers | Last sinter step    |
| /                    | 5% PVA powder   | Screen printing                    | 165 mesh; 60mm/s print speed; 2 bar squeegee pressure            |                 | /                             | /                   |
| /                    | 10% PVA powder  | Screen printing                    | 165 mesh; 60mm/s print speed; 2 bar squeegee pressure            |                 | /                             | /                   |
| /                    | 15% PVA powder  | Screen printing                    | 165 mesh; 60mm/s print speed; 2 bar squeegee pressure            |                 | /                             | /                   |
| 12.03.A              | PVA 25% foil    | Screen printing                    | 165 mesh; 60mm/s print speed; 2 bar squeegee pressure; 10 layers |                 | 5 min. at 150°C               | 10 min. at 150°C    |
| 12.03.B              | PVA 25% foil    | Screen printing                    | 100 mesh; 60mm/s print speed; 2 bar squeegee pressure; 10 layers |                 | 5 min. at 150°C               | 10 min. at 150°C    |
| 24.03.I.A            | PVA 25% foil    | blade coating                      | 100µm wet layer  |                 | 5 min. at 80°C                | 10 min. at 150°C    |
| 24.03.I.B            | PVA 25% foil    | blade coating                      | 100µm wet layer  |                 | 5 min. at 80°C                | 10 min. at 150°C    |
| 24.03.I.C            | PVA 25% foil    | blade coating                      | 100µm wet layer  |                 | 5 min. at 80°C                | 10 min. at 150°C    |
| 24.03.I.D            | PVA 25% foil    | blade coating                      | 100µm wet layer  |                 | 5 min. at 80°C                | 10 min. at 150°C    |
| 24.03.I.E            | PVA 25% foil    | blade coating                      | 100µm wet layer  |                 | 5 min. at 80°C                | 10 min. at 150°C    |
| 24.03.I.F            | PVA 25% foil    | blade coating                      | 100µm wet layer  |                 | 5 min. at 80°C                | 10 min. at 150°C    |
| 24.03.II.A           | PVA 25% foil    | blade coating                      | 200µm wet layer  |                 | 5 min. at 80°C                | 10 min. at 150°C    |

|              |                      |               |                  |                               |                  |
|--------------|----------------------|---------------|------------------|-------------------------------|------------------|
| 24.03.II.B   | PVA 25% foil         | blade coating | 200µm wet layer  | 5 min. at 80°C                | 10 min. at 150°C |
| 24.03.II.C   | PVA 25% foil         | blade coating | 200µm wet layer  | 5 min. at 80°C                | 10 min. at 150°C |
| 24.03.II.D   | PVA 25% foil         | blade coating | 200µm wet layer  | 5 min. at 80°C                | 10 min. at 150°C |
| 24.03.II.E   | PVA 25% foil         | blade coating | 200µm wet layer  | 5 min. at 80°C                | 10 min. at 150°C |
| 24.03.II.F   | PVA 25% foil         | blade coating | 200µm wet layer  | 5 min. at 80°C                | 10 min. at 150°C |
| 24.03.III.A  | PVA 25% foil         | blade coating | 300 µm wet layer | 5 min. at 80°C                | 10 min. at 150°C |
| 24.03.III.B  | PVA 25% foil         | blade coating | 300 µm wet layer | 5 min. at 80°C                | 10 min. at 150°C |
| 24.03.IIII.A | PVA 25% foil         | blade coating | 400 µm wet layer | 5 min. at 80°C                | 10 min. at 150°C |
| 24.03.IIII.B | PVA 25% foil         | blade coating | 400 µm wet layer | 5 min. at 80°C                | 10 min. at 150°C |
| Sample name  | ink                  | method used   | parameters       | sintering step between layers | Last sinter step |
| 15.04.A      | PVA 20% powder 27000 | Blade coating | 100 µm wet layer | 5 min at 80°C                 | 5 min 150°C      |
| 15.04.B      | PVA 20% powder 27000 | Blade coating | 100 µm wet layer | 5 min at 80°C                 | 5 min 150°C      |
| 15.04.C      | PVA 20% powder 27000 | Blade coating | 150 µm wet layer | 5 min at 80°C                 | 5 min 150°C      |
| 15.04.D      | PVA 20% powder 27000 | Blade coating | 150 µm wet layer | 5 min at 80°C                 | 5 min 150°C      |
| 15.04.E      | PVA 20% powder 27000 | Blade coating | 200 µm wet layer | 5 min at 80°C                 | 5 min 150°C      |
| 15.04.F      | PVA 20% powder 27000 | Blade coating | 200 µm wet layer | 5 min at 80°C                 | 5 min 150°C      |

## Appendix D – Printed PVA stacks

| Origin    | Sample    | Material 1         | Parameters 1  | Sinter 1                       | Material 2 | Parameters 2   | Sinter 2                         |
|-----------|-----------|--------------------|---|--------------------------------|------------|--|----------------------------------|
| /         | 17.03.A   | PVA foil<br>25 wt% | 100 mesh; 60mm/s;<br>2 bar squeegee<br>pressure; 5 layers | Hot air<br>gun; 5 min<br>150°C | ECI1011    | 165 mesh; 160 mm/s;<br>2 bar squeegee<br>pressure; 5 layers  | 2 min<br>150°C; 10<br>min. 150°C |
| /         | 17.03.B   | PVA foil<br>25 wt% | 100 mesh; 60mm/s;<br>2 bar squeegee<br>pressure; 3 layers | Hot air<br>gun; 5 min<br>150°C | ECI1011    | 165 mesh; 160 mm/s;<br>2 bar squeegee<br>pressure; 5 layers  | 2 min<br>150°C; 10<br>min. 150°C |
| /         | 17.03.C   | PVA foil<br>25 wt% | 100 mesh; 60mm/s;<br>2 bar squeegee<br>pressure; 9 layers | Hot air<br>gun; 5 min<br>150°C | ECI1011    | 165 mesh; 160 mm/s;<br>2 bar squeegee<br>pressure; 10 layers | 2 min<br>150°C; 10<br>min. 150°C |
| 24.03.I.A | 31.03.A   | PVA foil<br>25 wt% | 100 µm wet layer  | 80°C 5<br>min; 5 min<br>150°C  | ECI1011    | 165 mesh; 160 mm/s;<br>2 bar squeegee<br>pressure; 10 layers | 2 min<br>150°C; 10<br>min. 150°C |
| 24.03.I.B | 31.03.B   | PVA foil<br>25 wt% | 100 µm wet layer  | 80°C 5<br>min; 5 min<br>150°C  | ECI1011    | 165 mesh; 160 mm/s;<br>2 bar squeegee<br>pressure; 5 layers  | 2 min<br>150°C; 10<br>min. 150°C |
| 24.03.I.C | 31.03.C   | PVA foil<br>25 wt% | 100 µm wet layer  | 80°C 5<br>min; 5 min<br>150°C  | ECI1011    | 165 mesh; 160 mm/s;<br>2 bar squeegee<br>pressure; 10 layers | 2 min<br>150°C; 10<br>min. 150°C |
| 24.03.I.D | 31.03.D   | PVA foil<br>25 wt% | 100 µm wet layer  | 80°C 5<br>min; 5 min<br>150°C  | ME 602     | 165 mesh; 160 mm/s;<br>2 bar squeegee<br>pressure; 5 layers  | 2 min<br>150°C; 10<br>min. 150°C |
| 24.03.I.E | 31.03.E   | PVA foil<br>25 wt% | 100 µm wet layer  | 80°C 5<br>min; 5 min<br>150°C  | ME 602     | 165 mesh; 160 mm/s;<br>2 bar squeegee<br>pressure; 10 layers | 2 min<br>150°C; 10<br>min. 150°C |
| 24.03.I.F | 31.03.F   | PVA foil<br>25 wt% | 100 µm wet layer  | 80°C 5<br>min; 5 min<br>150°C  | ME 602     | 165 mesh; 160 mm/s;<br>2 bar squeegee<br>pressure; 10 layers | 2 min<br>150°C; 10<br>min. 150°C |
| 26.03.A.E | 13.04.I   | PVA 25<br>wt% foil | 200 µm wet layer  | 80°C 5<br>min; 5 min<br>150°C  | ME 602     | 165 mesh; 100 mm/s;<br>80N squeegee<br>pressure; 1 layer     | 10 min.<br>150°C                 |
| 26.03.A.D | 13.04.II  | PVA 25<br>wt% foil | 200 µm wet layer  | 80°C 5<br>min; 5 min<br>150°C  | ME 602     | 165 mesh; 100 mm/s;<br>80N squeegee<br>pressure; 5 layers    | 2 min<br>150°C; 10<br>min. 150°C |
| 26.03.A.C | 13.04.III | PVA 25<br>wt% foil | 200 µm wet layer  | 80°C 5<br>min; 5 min<br>150°C  | ECI1011    | 165 mesh; 100 mm/s;<br>80N squeegee<br>pressure; 1 layer     | 10 min.<br>150°C                 |
| 26.03.A.F | 13.04.IV  | PVA 25<br>wt% foil | 200 µm wet layer  | 80°C 5<br>min; 5 min<br>150°C  | ECI1011    | 165 mesh; 100 mm/s;<br>80N squeegee<br>pressure; 5 layers    | 2 min<br>150°C; 10<br>min. 150°C |

# Appendix E – PTC method

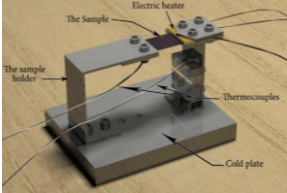


**Technical presentation** Dieter Reenaers  
Thermal conductivity measurement setup

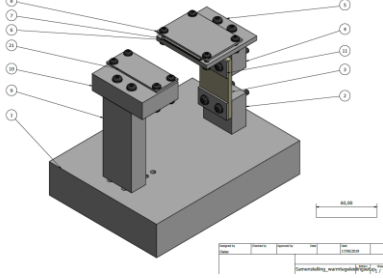
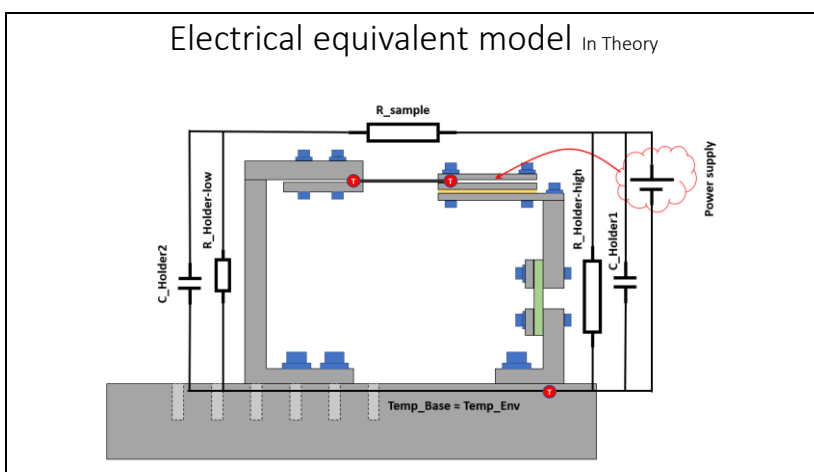
IMO-IMOMEC  
UHASSELT imec

But... We can't actually measure the *in-plane* thermal conductivity of that layer in order to find the best material

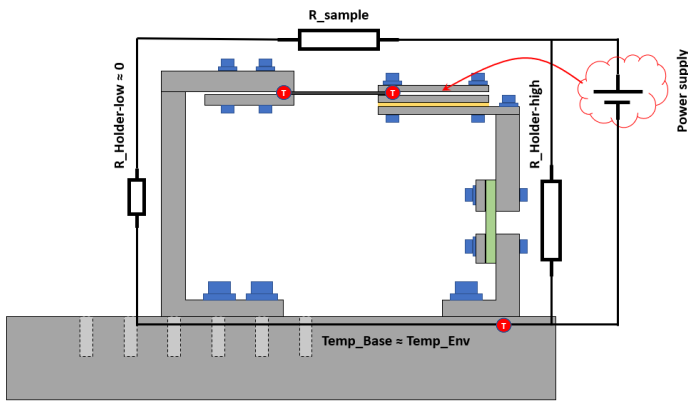
**Reference model from literature:**  
Technique: Parallel thermal conductance (PTC) method



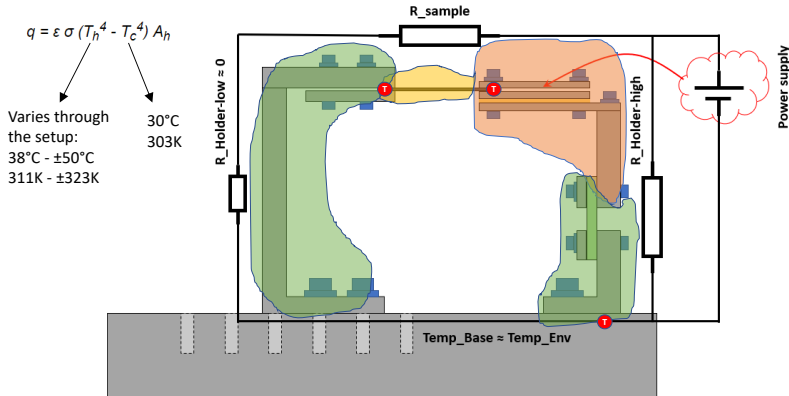
**Our design:**

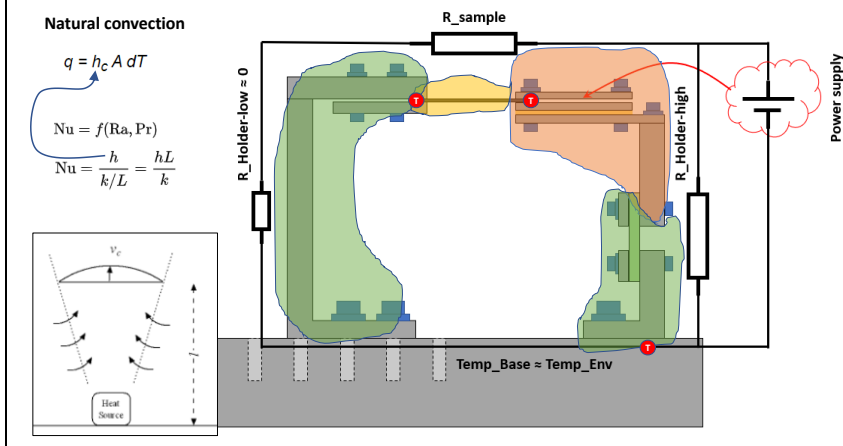
### Thermal equivalent model: steady state



### Thermal equivalent model: Radiative losses



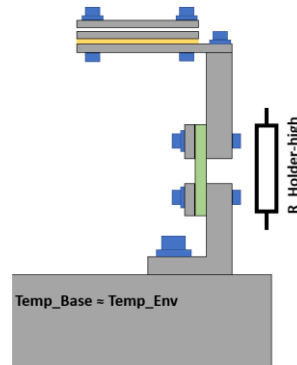
### Thermal equivalent model: Convective losses



## Working principle (Case 1: A316 Stainless steel)

### Excel workflow:

| 1. Estimation sample and Selection holder |   | Holder is OK! ✓                            |           |
|---|---|--|-----------|
| 1.1                                       | Estimation of bulk material conductivity (k)                          | Estimation material conductivity (k):      | 16 W/mK   |
| 1.2                                       | Dimensions of the sample  | Sample length                              | 0,029 m   |
|   |   | Sample thickness                           | 0,001 m   |
|   |   | Sample width                               | 0,05 m    |
| 1.1                                       | Thermal conductivity of the sample must be at least 1/10th of Rholder | Estimation thermal sample resistance (Rs): | 36,25 K/W |
| 1.2                                       | Selection of the holder   | PTFE                                       | 9,2 K/W   |



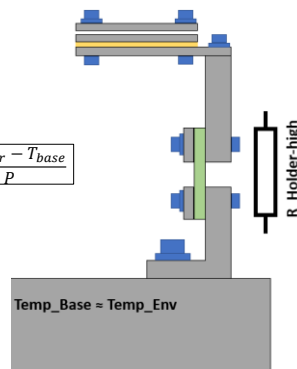
## Working principle (Case 1: A316 Stainless steel)

| 2. Calculation Thermal conductivity of the sample |  |         |
|---|--|---------|
| 2.1   | Reference measurement holder (no sample) |         |
|   | Power (heater)                           | 2,5 W   |
|   | Environment temp.                        | 30 °C   |
|   | Rholder equivalent                       | 9,2 K/W |
|   | Thheater                                 | 52,8 °C |
|   | Tbase                                    | 29,8 °C |

$$R_{Holder\ Equivalent} = \frac{T_{Heater} - T_{base}}{p}$$

### Rholder equivalent represents:

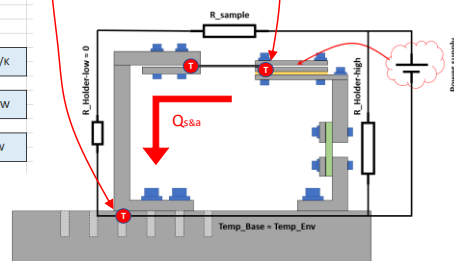
- The resistance of the holder
- The equivalent resistance of convectional losses inside the arm
- The equivalent resistance of radiational losses inside the arm



## Working principle (Case 1: A316 Stainless steel)

|     |                         |             |          |
|-----|-------------------------|-------------|----------|
| 2.2 | Measurement with sample | Thheater(s) | 49,11 °C |
|     |                         | Tbase(s)    | 30 °C    |

|     |                      |   |                      |          |     |
|-----|----------------------|---|----------------------|----------|-----|
| 2.3 | Rtot                 | $R_{tot} = \frac{T_h(s) - T_b(s)}{p}$                         | Rtot                 | 7,644    | K/W |
|     | Rsample & AluHolder  | $\frac{1}{R_{tot}} = \frac{1}{R_{h,eq}} + \frac{1}{R_{s\&a}}$ |                      |          |     |
|     |                      | $\frac{1}{R_{s\&a}} = \frac{1}{R_{tot}} - \frac{1}{R_{h,eq}}$ | $\frac{1}{R_{s\&a}}$ | 0,022126 | W/K |
|     |                      |   | Rs&a                 | 45,19589 | K/W |
| 2.4 | Power through sample | $Q_{s\&a} = \frac{T_h(s) - T_b(s)}{R_{s\&a}}$                 | Qs&a                 | 0,422826 | W   |



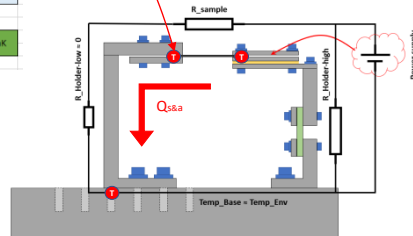


## Working principle (Case 1: A316 Stainless steel)

| 2.5 | Thermal conductivity of the sample   | After sample | 35.1 °C       |
|-----|--------------------------------------|--------------|---------------|
|     | $Q_s = Q_s a$                        |              |               |
|     | $R_s = \frac{T_h(e) - T_c(e)}{Q_s}$  | $R_s$        | 37,86427 K/W  |
|     | $k = \frac{l}{R_s \cdot A_{sample}}$ | $k$          | 15,31787 W/mK |

Goodfellow AISI 316:

Thermal conductivity @23°C: 16.3 W/mK



## Other tests:

|                     | Thermal conductivity (W/mK) according to specifications | Measured Thermal conductivity (W/mK) |
|---------------------|---|--------------------------------------|
| AISI316 Steel (1mm) | 16.3  | 15.32                                |
| Copper 99.9% (1mm)  | ±400  | 397.27                               |
| Graphite (15µm)     | ±1500   | 1410.4                               |
| Alu foil (15µm)     | ±235  | 270.1                                |

Holder not sufficient

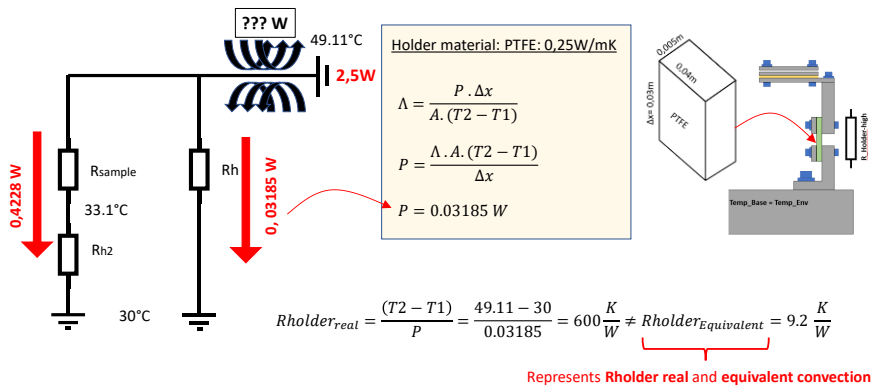
## How to increase the resolution (towards thinner films)

- Reduce the convective losses
- Introduce a PID temperature controller, measure power required for certain temp and keep temp constant

**Question: Are the convective losses significant?**

Answer: **Yes**, lets have a look at previous case (AISI316)

## Convection losses (Case 1: AISI316)



## Convective losses (Case 1: AISI316)

| Surfaces of convection |                       | Natural convection coefficient | Convective power losses |
|------------------------|-----------------------|--------------------------------|-------------------------|
| Surface                | Area                  | H (W/m <sup>2</sup> K)         | W                       |
| Top surface            | 0.0049 m <sup>2</sup> | 8                              | 0.74911                 |
| Bottom surface         | 0.0049 m <sup>2</sup> | 4                              | 0.374556                |
| Vertical surface       | 0.0032 m <sup>2</sup> | 7.2                            | 0.4403                  |

$$\text{Prandtl number } (Pr) = \frac{\mu \cdot C}{K}$$

$$\text{Grashof } (Gr) = \frac{L^3 \cdot \rho^2 \cdot g \cdot \Delta T \cdot \beta}{\mu^2}$$

$$\text{Rayleigh number } (Ra) = Pr \cdot Gr$$

Density  $\rho = 1.12043 \text{ kg/m}^3$   
 Viscosity  $\mu = 0.000190951 \text{ N}\cdot\text{s/m}^2$   
 Specific heat  $C = 1005.15 \text{ J/kg}\cdot\text{K}$   
 Thermal conductivity  $k = 0.02739 \text{ W/m}\cdot\text{K}$   
 Thermal expansion coefficient  $\beta = 0.0031711300 \text{ 1/K}$

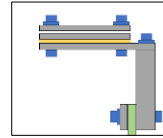
$$\text{Nusselt number } (Nu) = f(Ra, Pr)$$

Churchill & Chu correlation ( $Ra < 10^9$ )

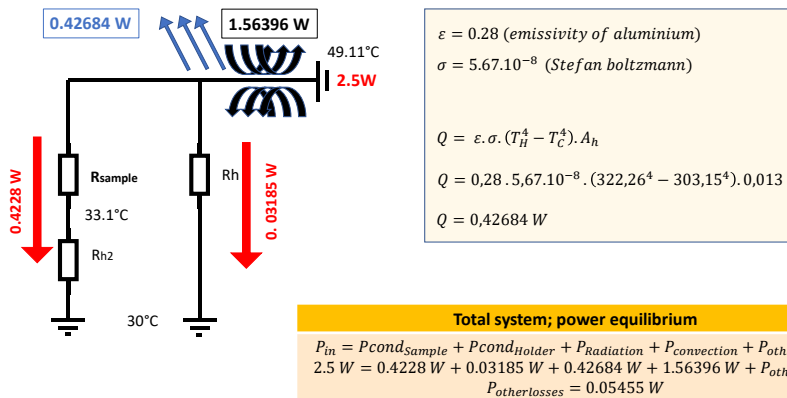
$$\text{Nusselt number } (Nu) = \frac{L \cdot h}{k}$$

1.56396 W

$$Q_{conv} = h \cdot A \cdot (T_{sample} - T_{env})$$



## Radiation losses (Case 1: AISI316)



## References

1: [www.wattagnet.com](http://www.wattagnet.com)

3: N. Alhazmi\*, M.S. Ismail, D.B. Ingham, K.J. Hughes, L. Ma, M. Pourkashanian; The in-plane thermal conductivity and the contact resistance of the components of the membrane electrode assembly in proton exchange membrane fuel cells; Journal of Power Sources 241 (2013) 136-145

4: [https://www.engineeringtoolbox.com/convective-heat-transfer-d\\_430.html](https://www.engineeringtoolbox.com/convective-heat-transfer-d_430.html)